**Title**
Understanding and Optimization of Field-Effect Transistor-Based Biological and Chemical Sensors



**Author**
Shoorideh, Kaveh

**Publication Date**
2016

Peer reviewed|Thesis/dissertation

University of California

Los Angeles

# Understanding and Optimization of Field-Effect Transistor-Based Biological and Chemical Sensors

A dissertation submitted in partial satisfaction
of the requirements for the degree
Doctor of Philosophy in Electrical Engineering

by

Kaveh Shoorideh

2016

# Abstract of the Dissertation

Understanding and Optimization of Field-Effect Transistor-Based Biological and Chemical Sensors

by

Kaveh Shoorideh
Doctor of Philosophy in Electrical Engineering
University of California, Los Angeles, 2016
Professor Chi On Chui, Chair

Over the past 15 years, biologically sensitive field-effect-transistors (bioFETs) employing a nanowire as their active element have become very popular. Each year, many experiments are reported that use nanowire bioFETs to detect and quantify new clinically relevant biomolecules.

This thesis aims to enhance our understanding of bioFETs in order to answer important practical questions regarding the operation and optimization of them.

We discuss the proper biasing of a bioFET in order to maximize sensitivity. Using electrostatic arguments and MATLAB simulations, we offer a recipe for biasing that applies to biomolecule detection using SOI-based FETs, including nanowire and nanoribbon bioFETs. In contrast to previous works, we take into account the two degree of freedom afforded by a solution-gate and a back-gate. We find that such a bioFET is best operated when the channel is fully depleted. This is in line with the findings of others regarding the biasing of bioFETs using a single gate. We also discuss the opportunity to tune an extra degree-of-freedom: the electric charge on the surface of bioFETs that could be brought by other chemical species, such as linker molecules, probe molecules, or surface groups. We show that an optimum value exists for this surface charge. The optimum amount of charge is that which minimizes the electric field at the solution/bioFET interface prior to analyte capture. We show that this optimum is a result of a minimum in Debye screening strength.

We study the electrostatics of a nanowire bioFET as we change the geometry of the nanowire. It is commonly accepted that nanowires with small diameters are more sensitive than larger nanowires because their surface-area-to-volume ratio is larger. We use analytical arguments to show that this analysis is incorrect. Using simulations, we show that analytes captured in concave regions and corners produce a stronger signal due to reduced Debye screening. All structures have such corners, but in small nanowires, these corners are a larger fraction of the entire surface, so the positive effect of the corner is more apparent, leading to higher sensitivity for smaller nanowires.

We discuss the necessity of solution electrodes in the operation of bioFETs. We show that without a solution electrode, the sample solution will capacitively couple to various FET terminals, resulting in an unpredictable bias point, and an unpredictable return path for the bioFET electric field. These effects could adversely affect the reproducibility of bioFET measurements. We use analytical arguments to show that a return path must exist for the electric fields that emanate from the biomolecules and enter the bioFET. We use simulations to show that the uncontrolled capacitive coupling between the sample solution and the bioFET terminals provides this path in the absence of a solution electrode. We also show that slight variations in the structure could affect this capacitive coupling and change the sensitivity in largely unpredictable and unexpected ways. We conclude that either a solution electrode must be present, or the sample solution must be coupled to a terminal using a controlled large capacitance in order to minimize the effect of variations. We also show that lack of a solution electrode can be a source of signal drift in experiments.

The dissertation of Kaveh Shoorideh is approved.

Robert Candler

Laurent Pilon

Wentai Liu

Chi On Chui, Committee Chair

University of California, Los Angeles

2016

*To my parents . . .*

*whose support did not waver during this endeavor.*

# Table of Contents

# List of Figures

# List of Tables

# Acknowledgments

My time in the PhD program has been longer than most. Naturally, I have more people to thank as well.

First and foremost, I must thank my parents. They provided the genetic material, the initial funding, and the much-needed TLC for the project that is me. They probably see this document as part of the return on their investment, and I made them wait for it for too long. Every year for the past 4 years I promised that it would be done next year. Any other investor would have pulled the plug, but they never withdrew their support. I am truly lucky and grateful.

I was also lucky to work with Professor Chi On Chui. I could not have asked for a better advisor. I found him intimidating early on, but in hindsight, I realize that I needed to be whipped into shape. He took the time to carefully learn my strengths and weaknesses, much more than any other advisor would. He did his best teach me how to take advantage of my strengths, and recognize and correct my weaknesses. He grilled me privately so I would find the flaws in my work, but he always supported me publicly. He was always the perfect facilitator; if there was something I needed, he made sure that I got it. He taught me how to conduct research properly so that my work has the most impact. In recent months, I have sometimes given advice to some younger graduate students, and suddenly noticed that I have begun to sound like him, which makes me really happy. These bits of research wisdom are equally important to me, if not more so, than the technical knowledge I have gained under his supervision. I have learned much, and hope to learn more from him in the years to come.

I would like to thank the other members of my dissertation committee, Professors Laurent Pilon, Wentai Liu, and Robert Candler, for their time and guidance. Their help was extremely valuable in strengthening the arguments presented in this thesis. I must also thank Professor Candler for allowing me to be his teaching assistant. It was a great opportunity to learn his amazing teaching methods. I hope to be able to replicate his style one day. I also thank Professor William Kaiser for generously agreeing to be on my qualifying exam committee despite his extremely busy schedule.

I acknowledge the awesomeness of the people who have come and gone through our lab: Kyeong-Sik, Kun-Huan, Hyung-Suk, Andrew, Greg, Jorge, Yufei, Dingkun, Cheng-Yi, Rowan, Wuran, Ablai, Raghav, and Xin. These people were helpful beyond measure in my progress towards my PhD, partly because of their academic support, and mainly because of their friendship. Many of my ideas were born out of brainstorming sessions with Andrew, and many were also shot down by him. We have many projects to (start) and finish together. I cannot thank Greg and Yufei enough for their help with fabrication. Yufei and Kyeong-Sik taught me almost everything I know about the practical side of biosensing. The torch has now passed to Wuran, who has been my eyes and hands in the past few months, and occasionally my brain as well. It was great fun creating the portable reader with Cheng-Yi and Rowan and learning as we went along. Outside of our group, discussions with Omeed, Asael, Jere, and others were like kids' games, both fun and educational.

I would like to give special thanks to Deeona Columbia and her team, for the miracles they performed for graduate students like myself who were often a day late and a dollar short. They saved me from banging my head against the wall more times than I care to count. The entire Electrical Engineering department staff are indispensable to the research and livelihood of the students, and I thank them all.

During my early years at UCLA, I worked with Professor Eli Yablonovitch. He taught me many valuable lessons, both academically and otherwise. Most important of all, he taught me to think outside the box, and to "kill my own babies". I am eternally grateful to him for teaching me so much in such a short time.

I am extremely lucky and grateful to have too many good friends to list. Properly acknowledging them would take an entire chapter, each. Piraj, Pamchal, Neda, Ka, Gholoom, Doki, Pooria, Omeed, Kiana-Bobby, Rommina, Anna, Mehrdad, and Yeganeh were like family to me. They cheered me through the bad times and distracted me from my work during the good. However, most of the distraction was kindly provided by Shahrzad, Sohaela, Narges, and Negar. Many people go through hell during their studies, and I never did, thanks to them. Special thanks go to Narges; as a fellow PhD student, she knew exactly what to say to stop me from falling into despair after the repeated failures that all PhD

students encounter. Special thanks go out to Negar, for pursuing my happiness as her own. Special thanks go to Niousha and Pamchal, for providing light during the darkest time of my life, and for their support during the writing of this thesis. They have my eternal love, gratitude, and admiration.



I gratefully acknowledge the funding provided for the work in this thesis by the Electrical Engineering department, the National Science Foundation (Grant 1128673), and SELFA, Inc.

# Vita

| | |
|---|---|
| 2005 | B.S. (Electrical Engineering), UCI, Irvine, California |
| 2005 | B.S. (Physics), UCI, Irvine, California |
| 2008 | M.S. (Electrical Engineering), UCLA, Los Angeles, California |

# Publications

Kaveh Shoorideh and Chi On Chui, "Understanding and Optimization of the Sensitivity of Nanoscale FET-Based Biosensors," presented in *The SPIE Conference on Nanoepitaxy: Materials and Devices VI*, San Diego, CA, August 17-21, 2014. (Invited Paper)

Kaveh Shoorideh and Chi On Chui, "On the Origin of Enhanced Sensitivity in Nanoscale FET-based Biosensors," *Proc. Nat. Acad. Sci. USA*, vol. 111, no. 14, pp. 5111-5116, 2014.

Kaveh Shoorideh and Chi On Chui, "Optimization of the Sensitivity of FET-Based Biosensors via Biasing and Surface Charge Engineering," *IEEE Trans. Electron Devices*, vol. 59, no. 11, pp. 3104-3110, 2012.

Chi On Chui, Kun-Huan Shih, and Kaveh Shoorideh, "Low Dissipation Nanoscale Transistor Physics and Operations," presented in *Proceedings of the 9th International Conference on Solid-State and Integrated Circuit Technology (ICSICT)*, Paper A1.3, pp. 29-32, Beijing, People's Republic of China, October 20-23, 2008. (Invited Paper)

# CHAPTER 1

# Introduction

## 1.1 Overview

It goes without saying that the ability to measure concentrations of vital proteins, RNA, and DNA in biological samples has great medical use. To this end, various detection techniques and sensor platforms have been developed to do exactly that. The most widely used technique of this sort is called enzyme-linked-immunosorbent assay (ELISA), which is mostly performed in medical diagnostic labs. Other techniques, such as amperometry, are used in glucose monitors and Abbott's i-STAT device. These sensor platforms, and many others, each have their strengths and weaknesses, the discussion of which is beyond the scope of this document.

The subject of this thesis is the understanding and optimization of a particular sensing technique that is sensitive to the electric charge on an analyte; an analyte is a particle of interest whose concentration is to be detected. The technique has no particular name, but the electronic device that embodies the technique, and its variants, are known by many names: ion sensitive field-effect transistor (ISFET), enzyme sensitive field-effect transistor (EnFET), chemically sensitive field-effect transistor (ChemFET), immunologically sensitive field-effect transistor (ImmunoFET), and most recently, biologically sensitive field-effect transistor (bioFET).

BioFETs, or FET-based biosensors, are devices that detect and quantify the concentration of biomolecules (DNA, RNA, proteins) in an aqueous (electrolytic) sample through their intrinsic electric charge. By detecting intrinsic charge, they eliminate the need for labeled reagents and repeated wash steps. Essentially, they are MOSFETs without the gate electrode; instead, the gate insulator is exposed to the sample that contains the target analytes

to be detected. These target analytes are captured (or spontaneously adsorb) onto the gate insulator, and the drain current of the FET will change in response to their electric field, much in the same way that it changes in response to the electric field emanating from the gate terminal in a regular MOSFET. A schematic diagram of a bioFET based on a nanowire structure is shown Fig. 1.1, and depicts its operating principle.

In order to confer specificity to the assay, the gate insulator (which is exposed to the sample-under-test) is commonly "functionalized" with appropriate capture probes. A capture probe is a molecule to which the target analyte specifically binds, hence is selectively "captured" by it. These probe molecules are commonly attached covalently to the gate insulator, via linker molecules that are 1-2 nm long. So, for example, in order to detect a particular antigen, an antibody can be covalently attached to the sensor, and to detect a DNA strand, its complementary strand can be used instead.

The operation of a bioFET can be summarized thus: one begins with a sensor, fully "functionalized" with a probe molecule of interest, and ready to capture analytes. The surface "coverage" of analytes on the sensor surface is zero at the beginning. A sample (e.g. blood, urine, saliva, etc.) is then introduced to the sensor surface. Analytes in the sample somehow make their way to the sensor surface where they bind, and increase the surface coverage. During the initial transient, as the coverage increases, the sensor's signal will also increase. During this time, some analytes will also detach from the sensor surface and return to the bulk of the solution. Finally, the solution bulk and the surface will reach equilibrium when the rate of attachment and detachment become equal. The sensor's signal, if devoid of artifacts, should also reach a steady state value. The initial transient signal contains information about the mass transfer rate to the surface, and the reaction rate at the surface. The steady state signal contains information only about the equilibrium state. Both should include information about the concentration of the analyte in the bulk of the sample, which is what we are interested in measuring.

In practice, the signal during the initial transient is affected by many unknown chemical processes that occur at the sensor surface, so extracting useful information from it is very difficult. However, the steady state signal is much less susceptible to artifacts (compared to

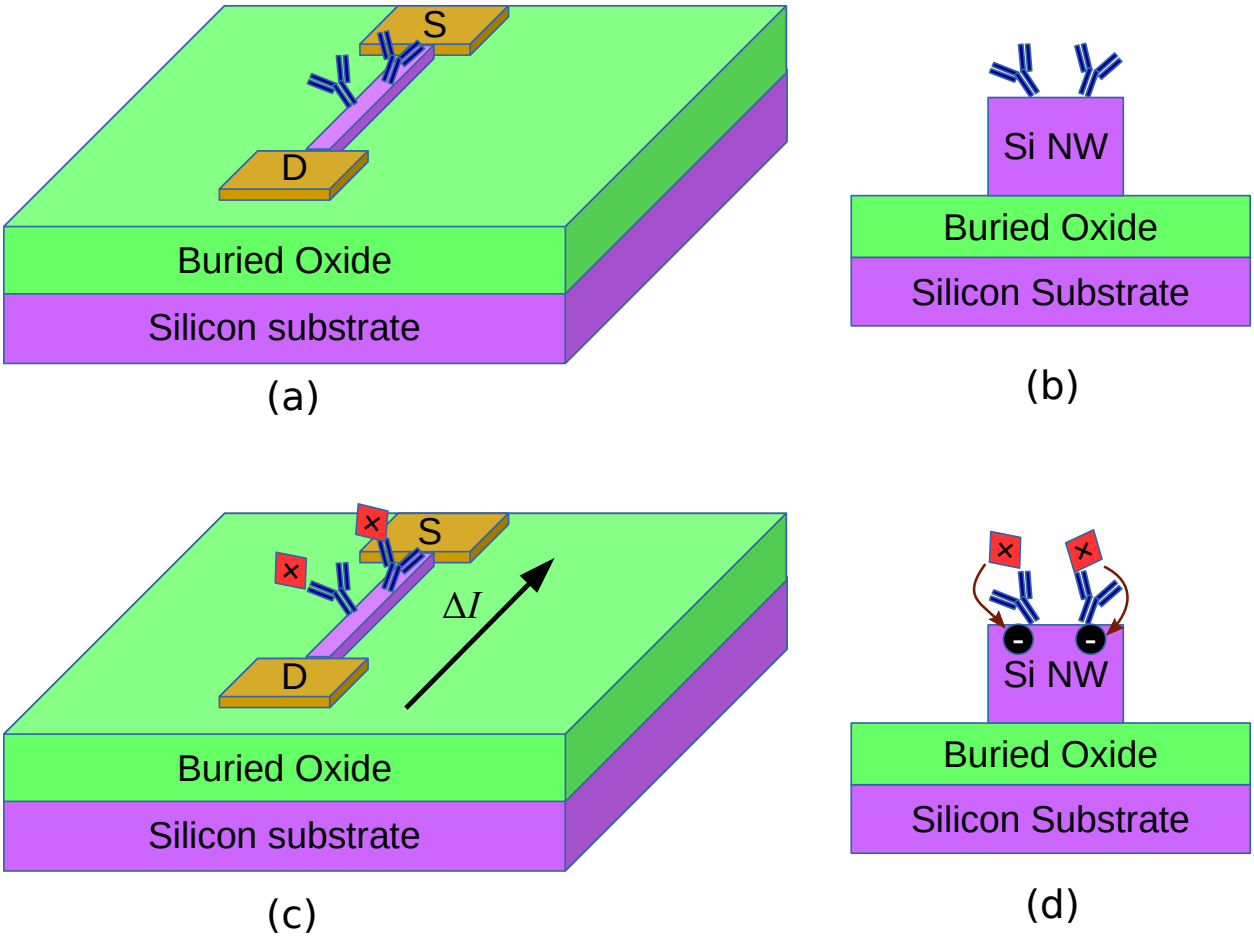


Figure 1.1: Schematic diagram of a nanowire bioFET. A 3D schematic is shown in (a), depicting the nanowire as a pink rectangle on the buried oxide; the gold-colored regions marked "S" and "D" represent the source and drain regions. The antibodies, colored in blue, are covalently attached to the sensor surface. A cross section of the bioFET is shown in (b). In (c), positively charged biomolecules, shown in red, are captured by the antibodies, causing the drain current to change. The cross section of (c) is depicted in (d), with the electric field emanating from the biomolecules as brown arrows, and the electrons that are induced in the bioFET as black circles. These induced electrons are responsible for the change in the drain current of the bioFET.

the transient), so most researchers wait for a steady-state before recording the signal. The signal never truly reaches a steady state; there is always "drift", which is defined as the change of the signal output as a function of time. However, if the drift is small compared to the magnitude of the signal, it can be ignored. In most cases (demonstrated in various research labs), the time it takes to reach steady-state is on the order of a few minutes [HL04, BSY06, SKR07, PLP10].

## 1.2 History

Many researchers trace the ancestor of the bioFET to the ISFET, which was invented by Bergveld in 1970 [Ber70]. I prefer to trace it further back to the glass electrode.

The sensing properties of glass membranes were discovered in 1909 [HK09]. It was found that if two solutions with different hydrogen ion activities (pH) were separated by a glass membrane, a potential difference would develop between the solutions that could be measured if each solution was contacted by its own reference electrode. This discovery was made into a practical instrument called the glass electrode, whose schematic diagram is shown in Fig. 1.2. It comprises a glass bulb, typically about 1mm thick, which contains a liquid sample of known pH that is contacted by an internal reference electrode. To measure the pH of an unknown sample, the sample is contacted by both a second reference electrode and the outer surface of the glass electrode's bulb. The potential that develops between the two reference electrodes is then recorded using a high input-impedance electrometer. It is quite common for the entire setup to be combined into one body for ease of use.

Initially, it was thought that the sensitivity of the glass electrode to pH was due to the fact that the glass could exchange sodium ions embedded in it with hydrogen ions in the solutions; this was called the ion-exchange theory [Eis62]. It was observed that an upper bound existed for the sensitivity, which was about 60mV per unit of pH. This number also appeared when the Nernst equation was applied to calculate the potential across *permeable* membranes (e.g. the ion permeable membranes in neurons) [BF01]. It was therefore concluded that ions penetrated into the glass to be "exchanged", and the Nernst equation was applied with

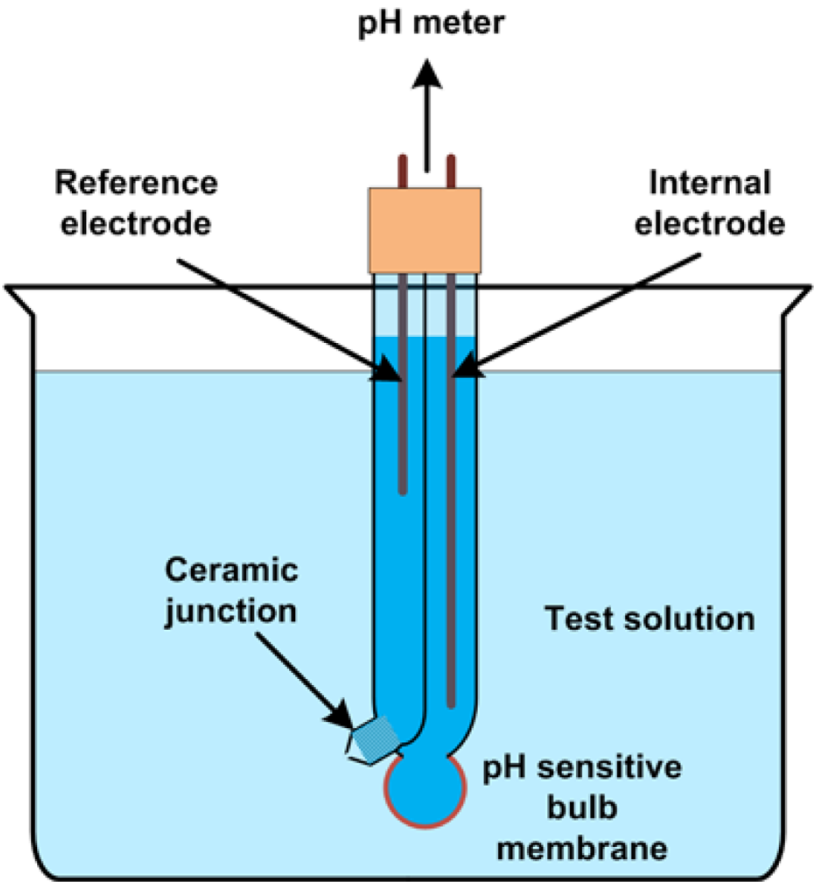


Figure 1.2: A schematic of a pH glass electrode, as described by Shinwari et al. [SZD10]. The pH of the sample solution creates a potential drop at the interface between the glass bulb and the sample solution. The internal electrode and the reference electrode measure this potential difference.

success.

This theory was incorrect, but produced correct results. It was shown many years later that the glass electrode responded nearly instantaneously to changes in pH, so much so that it was not possible to change the pH fast enough to observe a measurable delay in the electrode response [DD54]. This fact ran counter to the idea that ions that penetrated into the glass were responsible for its response. Also, it was argued that the exchange of singly charged sodium ions for singly charged hydrogen ions could not possibly lead to a potential difference [Sch10]. An alternative "site dissociation" theory was accepted instead, which explained the response of the glass electrode in terms of surface groups that could capture or release hydrogen ions [Bau85]. When hydrogen ions were abundant and the pH was low, these surface groups would bind hydrogen ions and become positive (or neutral, depending on the actual composition of the surface group). When the pH was high and hydrogen concentration was low, these groups would release hydrogen ions and become neutral (or negative). A "site-binding" model that was developed to model dissociation constants for various glasses [YLH74] was later adapted to describe the same process, but for biomolecules, in the context of various FET-based sensors [LAM05].

Concurrently with these modeling developments, it was found that the glass electrode suffered from interference from sodium ions, i.e., that changes in sodium concentration would create a signal where none was desired [Eis62]. It was also found that by changing the composition of the membrane, one could make the electrode sensitive to ions other than hydrogen, and tune its *selectivity* as well [Hin59]. An entire class of electrodes were born that were similar in operation to the pH glass electrode, but selective to other ions. These electrodes were called "ion-selective electrodes" (ISE). Just like glass electrodes, the potential at the ISE needed to be measured by a high input-impedance electrometer [PT70].

The ISE had one significant drawback: the requirement for a reference solution. The reference solution made the electrode susceptible to drying up and breakage. Instead, a wire can be coated with a the salt of its metal, and can still function as an ISE. This structure is called a "coated wire electrode" and was invented in 1971 [CF71]. This development highlights the fact that the reference solution is actually not required; the response comes simply from the

contact of the sensitive membrane with the sample-under-test. The coated wire electrode still needed to be connected to a high input-impedance electrometer for measurement.

Between 1970 and 1972, another important development occured: the ISFET was invented by Bergveld [Ber70, Ber72]. The schematic of Bergveld's ISFET is shown in Fig. 1.3. Bergveld sought to eliminate the "loading" caused by the wires that ran from the ISE to the electrometer's first amplifier stage. He did more than just bring the amplifier close to the ISE; he *integrated* them. The ISFET is a combination of an ISE and a FET; the gate oxide of the FET is covered with the membrane that confers selectivity in the ISE. The potential and electric field that appears at the surface of the ion sensitive/selective membrane directly and locally couples to the FET channel, changing the FET's drain current. Thus, the voltage signal from the ISE, which requires a high input-impedance electrometer for measurement, is locally converted into a current signal which could traverse relatively long wires without degradation and can be measured by less complicated instruments. Additionally, the ISFET proved more rugged than the ISE, which was quite important in applications where breakage of the glass in the ISE could pose serious hazards, such as in measuring the pH of food. Another potential benefit of the ISFET was its extreme miniaturization. However, this promise was not fulfilled, because a reference electrode is still necessary for its proper operation [Ber72], and it is not practical to make miniaturized reference electrodes that can operate for long periods of time [SV99]. Attempts were made to create reference ISFETs, also called ReFETs that were *not* sensitive to ions, and use them in lieu of reference electrodes. These attempts mostly resulted in failure, since it is very difficult to find surfaces that are completely inert [SV99].

A short time after the invention of the ISFET, Janata invented the immunoelectrode [Jan75]. An immunoelectrode is an electrode that is functionalized with an antibody, in order to detect an antigen. When the immunoelectrode and a reference electrode are placed in a solution, the potential measured between them would vary depending on the concentration of the antigen whose antibody is functionalized on the immunoelectrode. The source of this potential is the same as those obtained in ISEs and ISFETs. Unfortunately, Janata was not able to make his electrodes sensitive enough for them to become as useful as ISEs.

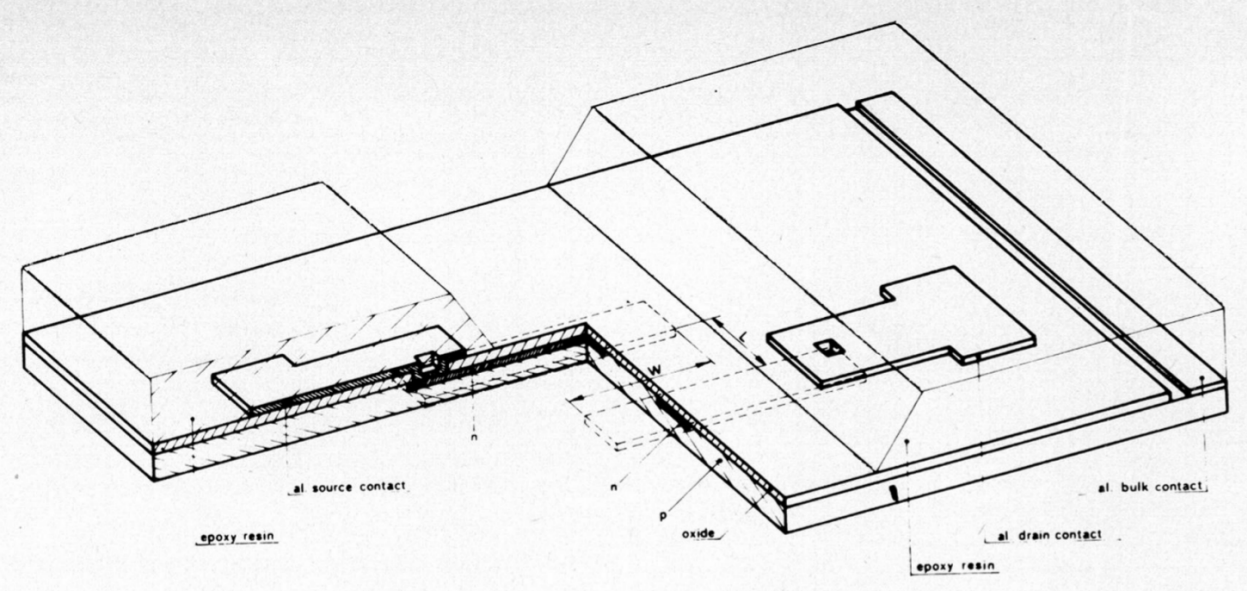


Figure 1.3: The first schematic of an ISFET ever drawn, taken from Bergveld's second ISFET paper published in 1972 [Ber72]. Note that the entire device is to be submerged in the sample to be tested.

Shortly after, in 1980, Schenk proposed the immunoFET, which integrated an immunoelectrode with an FET, just as Bergveld had done for pH measurement. The immunoFET was basically the first bioFET ever conceived. Just like the immunoelectrode, the responses initially obtained by immunoFETs were too small to unequivocally declare success. One could arguably point to the work of Gotoh et al. in 1989 [GSK89] as the first immunoFET to get signals larger than 1mV (in terms of threshold voltage shifts) at the analyte concentration of interest to them.

The failure of the immunoelectrode and the immunoFET in detecting proteins was ascribed to Debye screening, the process by which counter-ions in an electrolyte surround a charged particle and screen its electric field. Proteins are large molecules, and when captured, they typically lie within a few nanometers of the FET's gate insulator. However, the Debye length (which is the characteristic length over which the electric field decays by a factor of $e$ in an electrolyte) is about 1nm in physiological solutions. As a result, the electric fields emanating from the proteins are severely screened, and the charge that is seen by the FET is drastically smaller than the actual charge carried by the protein [SBK90]. It

was argued that Debye screening was not such a big problem in ISFETs, because ions are captured much closer to the insulator surface, so their charge is not screened so drastically. In response to these assertions, most researchers attempted biomolecule detection in samples with low ionic strengths, i.e., with a lower concentration of salts, in which the Debye length is longer and screening is weaker [SWS07].

The next major breakthrough occured in 2001 when Cui et al. used a nanowire to make a bioFET [CWP01]. They demonstrated successful pH detection, but more importantly, they detected DNA at concentrations far below what had been previously demonstrated. Shortly thereafter, another research group demonstrated a bioFET whose channel was made out of a carbon nanotube, with similar results [BTZ03]. These works resulted in an explosion of interest into nanowire bioFETs for the detection of one analyte or another. In almost all such papers, the use of the nanowire is justified because its high "surface-area to volume ratio" causes it to be very sensitive. Nair and Alam provided a crude analytical justification to this claim. However, this author believes these arguments to be incorrect, as the reader shall see in chapter 3 of this document.

It is worth noting that nanowire bioFETs were the first bioFETs where a "back-gate" was used to bias the FET, while the "front-gate" was exposed to the sample-under-test. These gates are shown schematically in Fig. 1.1. The bias applied to the FET was no longer required to be applied via the sample-under-test. This is in contrast with regular immunoFETs and ISFETs, where the bias must be applied to the sample-under-test, because there is no other gate terminal present. The difference is significant, because freedom from having to bias the sample-under-test allows researchers to abandon the bulky reference electrode which hindered efforts to truly miniaturize bioFETs for 30 years. However, this author believes that reference electrodes are still necessary, and the consequences of not using one shall be discussed in chapter 4.

In parallel with these developments, some researchers realized that the salts present in physiological solutions, especially sodium, caused severe reliability problems for the silicon-based FET which made up most bioFETs. They decided to separate the sensing surface from the FET, in effect reverting back to the pre-Bergveld era. Sensors made this way, where the

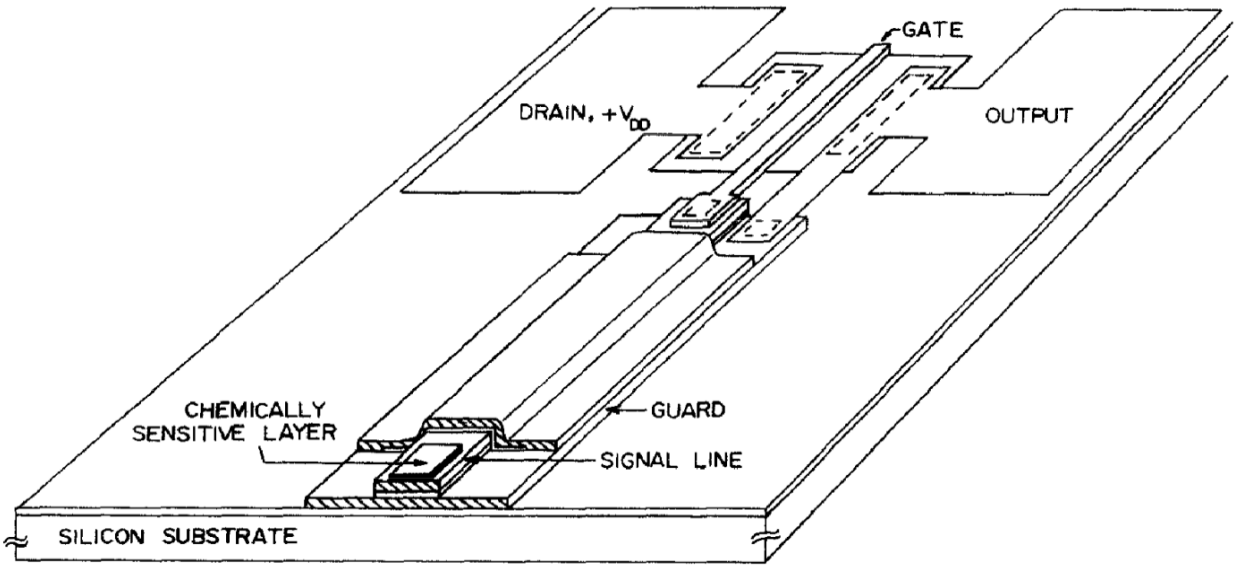


Figure 1.4: A schematic of the first EGFET (taken from [sLC83]). Contrary to the ISFET, the entire device is not submerged. Instead, the sample only comes in contact with the chemically sensitive layer, which is connected by a signal line to a separate MOSFET.

sensing surface is connected via some conductor to an FET that is some distance away, are called "extended-gate FETs" (EGFETs). The schematic of the first EGFET is shown in Fig. 1.4. The FET is frequently made on-chip, but can also be off-chip as well. EGFETs are identical in operation to coated wire electrodes, although this fact may be lost on many in our field.

Over the past 15 years, many exotic bioFET structures have been proposed or developed that are called by similar names, but have subtle differences that require them to be analyzed differently. For example, nanowire bioFETs made out of SOI substrates [SKR07] must be analyzed very differently from nanowire bioFETs made out of bulk silicon [AKC12], but both are called "nanowire bioFETs". As such, for the purposes of this thesis, this author finds it useful to divide all the aforementioned sensors into four groups based on two criteria: 1) whether they bias through the sample-under-test or not, and 2) whether the sensing surface is integrated with the FET or not.

Glass electrodes, ISEs, EGFETs, and coated wire electrodes, all belong to the first group,

where an electrode is connected to the sample-under-test (and may bias it), and there is a wire running from the sensing surface to the first FET in the amplification chain.

ImmunoFETs and ISFETs are in the second group, where the bias is applied through the sample-under-test, and the sensing surface is integrated with the FET.

Nanowire-based, graphene-based, nanotube-based, and other similar bioFETs where the active region of the FET is placed on an insulating substrate comprise the 3rd group, because the insulating substrate allows these devices to be biased from below, via a back-gate.

Devices similar to those in the third group that have an extended gate (i.e., whose sensing surface is far from the FET) belong to group 4. There are very few experimental results that use such structures, because it is not clear why one would incur the cost of fabricating nanowires if one does not take advantage of their sensing benefits. In fact, nanowires make for very poor FETs in this setting, because their rough surfaces result in $1/f$ noise that is higher than their non-nanowire counterparts.

For reasons not clearly known, no bioFET has been commercially successful to date, even though mind-boggling sensitivities have been reported under laboratory conditions.

## 1.3 Figure of Merit

The lowest analyte concentration at which the signal can be reliably (and reproducibly) distinguished from background noise is called the lower limit of detection (LLOD), and is closely related to the signal-to-noise ratio (SNR). Pushing the LLOD towards lower concentrations is a point of major effort in the research community, since it enables biomolecules to be detected at lower concentrations, and as a result, enables diseases to be detected earlier. There are many factors that affect the LLOD, including but not limited to the mass transfer rate to the sensor surface, reaction kinetics at the surface, and the response of the sensor to surface charge in the steady state. In this work, we only focus on the sensor itself: we assume that molecules carrying electric charges have already bound to the surface of the sensor. How do we get the largest signal from these molecules, assuming that their coverage

or charge state does not change?

In essence, we wish to maximize the sensitivity of the bioFET to changes in the charge density at its surface due to biomolecules, as opposed to the overall sensitivity of the bioFET to analytes. The latter would be represented by $\frac{\Delta I}{\Delta c}$, and is the official definition of "sensitivity" by IUPAC [NJK09]. The former, which is more closely related to the concepts in this thesis, is best represented by $\frac{\Delta I}{\Delta \sigma}$. In these expressions, $I$, $c$, and $\sigma$ represent the drain current of the FET, the concentration of the analyte, and the charge density at the surface of the bioFET due to the analytes, respectively. Neither of these metrics include any noise information, and are therefore only weakly related to LLOD.

SNR is much more closely related to LLOD than sensitivity is. If all measurements of the same sample produced the same results, then one could define LLOD as the concentration where the SNR is the lowest acceptable value, typically 3 or 4. However, in practice, unknown artifacts cause repeated measurements of the same sample to produce slightly varying results, and these variations are not accounted for in SNR, but do affect the LLOD. In the absence of a way to predict and quantify these variations, we must resort to SNR as the best indicator of LLOD.

There are many sources of noise in the operation of a bioFET. However, it has been shown (for ISFETs at least) that $1/f$ noise of the FET itself is dominant [JN99]. Importantly, lock-in techniques cannot be used to filter out the noise. The reason is due to the disparity in the time-scales of biological and electronic phenomena: the biological side responds to perturbations on a time scale on the order of seconds, whereas the electronic side is many orders of magnitude faster. To measure a biological disturbance, such as a change in analyte concentration (which we are ultimately interested in), the measurement of the drain current must *not* involve electronic filters that filter out the slow low-frequency components of the drain current signal. In essence, the measurement must be DC. In the DC limit, the current noise observed at the drain terminal of the FET is dominated by $1/f$ noise in the FET itself, as has been shown by Jakobson and Nemirovsky [JN99] in the case of pH measurement.

Analytically, it can be shown that the power spectral density (PSD) of the drain current

noise is proportional to the square of drain current itself. The power spectral density is given by [GRN91]:

$$S_I = \left(1 \pm \alpha\mu C_{\text{ox}} \frac{I}{g_{\text{m}}}\right)^2 g_{\text{m}}^2 S_{V_{\text{fb}}} \tag{1.1}$$

where $S_I$ represents the drain current noise PSD, $\alpha$ is Hooge's parameter, $\mu$ is the carrier mobility, $C_{\text{ox}}$ is the gate oxide capacitance, $g_{\text{m}}$ is the transconductance, $I$ is the drain current, and $S_{V_{\text{fb}}}$ is the power spectral density of fluctuations in the flatband voltage. Of all these quantities, $I$ and $g_{\text{m}}$ are the ones that change the most, and the rest can be considered constant for a particular device.

When the bioFET is operated in the subthreshold regime, the current is small, so the first term in the parentheses in equation 1.1 dominates. The $g_{\text{m}}$ in subthreshold is proportional to $I$ itself. The PSD can be rewritten as:

$$S_I = g_{\text{m}}^2 S_{V_{\text{fb}}} \propto I^2 \tag{1.2}$$

If the bioFET is not operated in the subthreshold regime, and the drain current is high enough so that the second term in the parentheses in equation 1.1 dominates, the drain current PSD will again become proportional to $I^2$:

$$S_I = (\alpha\mu C_{\text{ox}})^2 I^2 S_{V_{\text{fb}}} \propto I^2 \tag{1.3}$$

Either way, the drain current noise PSD becomes proportional to the square of the drain current itself. Note that in both equations above, we have assumed that $S_{V_{\text{fb}}}$ and $\mu$ are bias independent, which is reasonable to first order [GRN91].

Since we define changes in the drain current, $\Delta I$, as our "signal", the SNR can be written as:

$$\text{SNR} = \frac{\Delta I^2}{\int_{f_1}^{f_2} S_I(f)\,\mathrm{d}f} \propto \left(\frac{\Delta I}{I}\right)^2 \tag{1.4}$$

where $f_1$ and $f_2$ denote the frequency-domain limits of our measurement window. We include $f$ as an argument to $S_I$ as a reminder that the $1/f$ dependence of the noise is included within

$S_I$. We do not expand $S_I$ since we are not interested in the detailed form of the SNR. Instead, we only wish to highlight the fact that the SNR at each concentration is proportional to the square of $\frac{\Delta I}{I}$, with $\Delta I$ representing the change in drain current due to a change in analyte concentration $\Delta c$ relative to a blank sample. Maximizing $\frac{\Delta I}{I}$ will therefore result in maximum SNR. We shall use this sensitivity metric to discuss the optimum biasing point of bioFETs in Chapter 2.

Presently, bioFETs are still in their infancy. One of the main challenges facing them is to ensure that for a given analyte of interest, the LLOD of the sensor is below the lowest clinically relevant concentration of that analyte. In light of this, our goal is to simply maximize the $\frac{\Delta I}{I}$ for any given $\Delta c$, especially for small $\Delta c$. The quantity $\frac{\Delta I}{I}$, which in our field is confusingly known as "sensitivity" despite the official IUPAC definition, is therefore the metric we wish to maximize. Although "resolution" is a better term for this quantity, we shall continue to call it "sensitivity" in accordance with the literature.

For our purposes, assuming small $\Delta c$ is equivalent to assuming that the charge density change due to the capture of analytes on the sensor surface is small. We shall make use of this assumption in the following chapters.

## 1.4 Outline of Following Chapters

In the following chapters, we discuss three problems and their solutions.

First, in Chapter 2, we discuss the proper biasing of a bioFET in order to maximize sensitivity. Using electrostatic arguments and MATLAB simulations, we offer a recipe for biasing that applies to biomolecule detection using SOI-based FETs, including nanowire and nanoribbon bioFETs. We also discuss the opportunity to tune an extra degree-of-freedom: the electric charge on the surface of bioFETs that could be brought by other chemical species, such as linker molecules, probe molecules, or surface groups. We show that an optimum value exists for this surface charge.

Next, in Chapter 3, we proceed to study the electrostatics of a nanowire bioFET as we

change the geometry of the nanowire. We use analytical arguments to show that the commonly accepted explanation for the improvements brought on by small nanowire structures are incorrect. Using simulations, we highlight a simple electrostatic phenomenon that we believe is the cause for the improved sensitivity of nanowires bioFETs, and has not previously been discussed in this context.

In Chapter 4, we turn our sights onto the concept of solutions electrodes in bioFETs. We aim to explain how some groups are able to demonstrate biomolecule detection without a solution electrode. More generally, we also wish to find out whether a solution electrode is truly necessary for bioFET operation. We use simulations to show that without a solution electrode, an experiment would be sensitive to minor details of its setup that are not normally controlled very well. We use analytical arguments to show why this occurs, and recommend the use of a solution electrode to prevent it.

We conclude the dissertation in Chapter 5, where the contributions of this author in this dissertation are summarized. The vision of this author for future work in this area is also discussed.

# CHAPTER 2

# On the Biasing of SOI-based BioFETs



## 2.1 Introduction

Field-effect-transistor-based biological sensors (bioFETs) have become one of the major technologies for detection of ions [Ber70, CWP01], pH [CWP01, CWE06], DNA [BSY06], proteins [CWP01, SKR07], and other macromolecules in biologically relevant solutions. These sensors are very attractive because of their high sensitivity detection of charged analytes. There has been a drive to increase their sensitivity even further. One area of focus has been the biasing regime of sensors, since biasing greatly affects sensitivity.

There have been many works on the proper biasing of bioFETs, with more or less similar conclusions. References [CFS11, CXY08, EJB08, GZL10, LHL10, YAY10, VSI11] recommend subthreshold operation to maximize sensitivity, which is defined as $\Delta I/I$ , where $I$ is the steady-state drain current of the sensor when exposed to a reference sample, usually a blank sample; $\Delta I$ is the change in the drain current due to the capture or adsorption of analytes. However, given a solution electrode and a back-gate, there are many ways to bias an FET in the subthreshold regime, and most works do not address this issue, partly because they consider structures with one gate only. Chapman et al. consider the use of two gates, but not two independent gates [CFS11]. Elibol et al. study the effect of two independent gates, but do not offer enough details to allow their scheme to be extended to other structures [EJB08].

The improvement in sensitivity in every case is attributed to increased efficiency of the FET-action; the drain current responds exponentially to perturbations at the gate when biased in the subthreshold regime. It should be noted that sensitivity, as defined, does not directly capture the effects of noise. Indeed, it can be argued that signal-to-noise ratio (SNR) may be more important than sensitivity. However, if $\Delta I$ is considered as the signal of interest, it has been shown that subthreshold operation maximizes the SNR as well [GZL10][LAM05][DSR06].

Another serious issue that affects the sensitivity of sensors is electrostatic screening of the analyte charges, which is not addressed by any of the previously mentioned works [CFS11, CXY08, EJB08, GZL10, LHL10, YAY10, VSI11]. In the absence of ions in the buffer, a charge equal in magnitude and opposite in sign of the charges of the analytes appears on the sensor, i.e., the mobile carriers in the semiconductor channel screen the electric field emanating from the analytes. When a significant concentration of ions is present in the buffer, some of the analytes are screened by the ions in the buffer, and only a fraction of the analytes induce opposite charges in the sensor. The response of the sensor is thereby diminished. Screening by ions in the buffer is termed DebyeHückel (DH) screening, whereas both Debye and ThomasFermi (TF) screenings are used to refer to screening in the sensor; to avoid confusion, we will denote the screening in the semiconductor by TF screening only and reserve DH screening for the buffer solution. DH screening represents losses of usable analyte charge to buffer ions and is undesirable. TF screening represents the response of the sensor to analyte charge and is desirable.

DH and TF screenings have a profound effect on sensitivity. However, to our knowledge, none of the works that study the effect of biasing on sensitivity include DH screening alongside a full analysis of the phenomena in the semiconductor. Sørensen et al. consider the effect of TF and DH screenings, but only when the underlying FET is operating in the linear regime [SMB07]. They advocate having a very short TF screening length (i.e., very strong screening) so that the losses of usable analyte charge to DH screening are minimal. This recommendation goes against that of subthreshold operation advocated in references [CFS11, CXY08, EJB08, GZL10, LHL10, YAY10, VSI11]., and indeed, a tradeoff exists: if

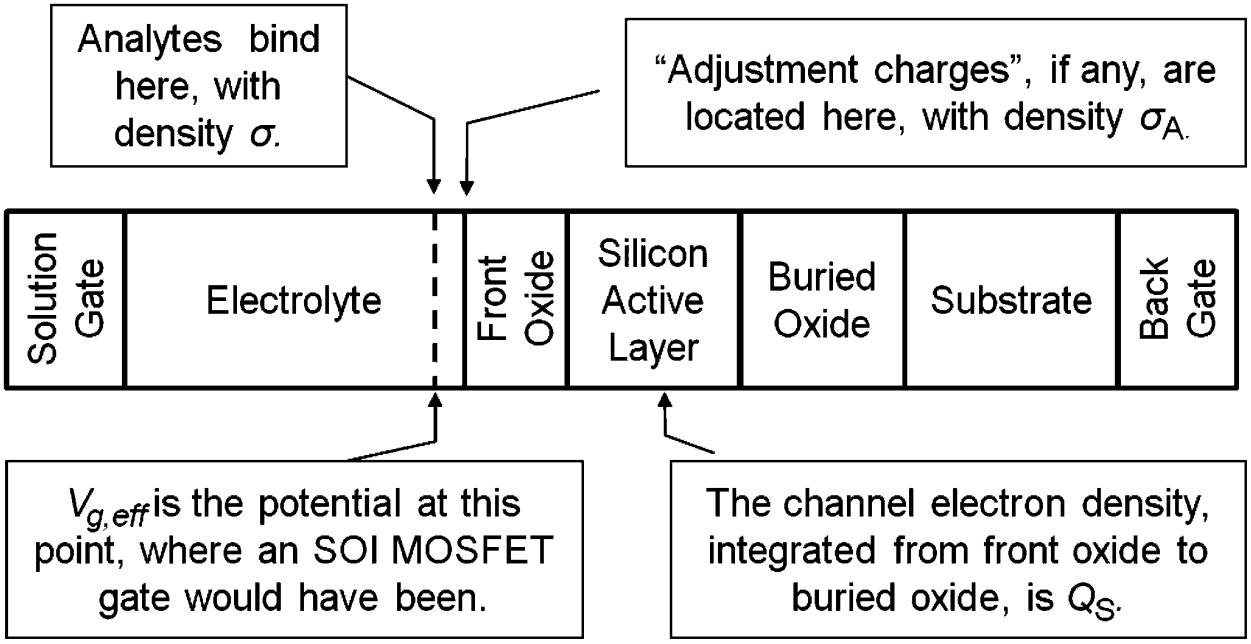


Figure 2.1: Schematic of the simulated 1-D structure

the sensor operates in the linear regime (with a short TF length), the sensor's capacitance becomes larger. As a result, the analytes produce a larger carrier concentration change in the semiconductor channel. On the other hand, if the sensor operates in the subthreshold regime, its capacitance is smaller; thus, the carrier concentration changes by a smaller amount. However, the drain current becomes more sensitive to changes in the carrier concentration, possibly producing a larger overall output current change. This tradeoff has been also alluded to by Lee et al., but a detailed analysis and recommendation is not presented [LNS09].

In this paper, we shall revisit the effect of biasing on sensitivity in an attempt to fill in the gaps left behind by previous works.

## 2.2 Simulation Structure and Method

We used MATLAB to simulate the electrostatics of a generic 1-D SOI $n$-channel accumulation-mode bioFET. The simulated structure is depicted in Fig. 2.1. This structure is essentially an SOI MOSFET with the following modification: the gate, which would have been to the left

of the front oxide, has been removed and replaced with a solution and a solution electrode. We believe the potential where the MOSFET gate would have been is a helpful quantity, and we shall call it the effective gate potential $V_{\mathrm{g,eff}}$. The response of the drain current to variations in $V_{\mathrm{g,eff}}$ will be identical to that of the SOI MOSFET.

The simulated structure was composed of a 1 µm-thick electrolyte, a 10 nm layer of $SiO_2$ (the front oxide), a 50 nm silicon active layer, 200 nm of buried oxide (BOX), and a 1 µm-thick silicon substrate handle. All silicon regions were doped $10^{16}\,\mathrm{cm}^{-3}$ $n$-type. We assumed no current could flow across such a stack; thus, carrier continuity equations were not solved. The silicon film thickness is small enough for this device to be considered fully depleted.

The electrolyte was assumed to be 1 mM NaCl with unity activity, resulting in a DH screening length of about 10 nm, far smaller than the thickness of our solution region. The $Na^+$ and $Cl^-$ ions were treated as holes and electrons, respectively, with a background concentration of $6.022 \times 10^{17}\,\mathrm{cm}^{-3}$ each, corresponding to a 1 mM NaCl solution. The ions were treated as point charges according to the Poisson Boltzmann (PB) model. The regular PB model is unable to capture the effects of the Stern layer directly; however, this does not pose a fundamental problem since the capacitance of the Stern layer is constant and can be considered to be lumped with that of the gate oxide. Modified Poisson Boltzmann (MPB) models provide a more accurate description of the double layer [WP11], however, we are only interested in qualitative behavior, which is adequately captured by the regular PB model. Moreover, as we shall see later, the operating point of interest will happen to be a bias at which the surface electric field is small, where the PB model is sufficiently accurate. The relative permittivity of the solution was set to 80. The work function of the solution was set to 4.61 eV, aligning it to the midgap of silicon. This value was chosen because it helps the observation of different phenomena that are present in a sensor without loss of generality.

Poisson's equation was solved in the entire device. The carrier concentrations in the oxide regions were assumed to be zero. Fermi statistics were applied to the carriers in silicon. The boundary conditions for Poisson's equation were imposed by the voltage of a solution gate in the electrolyte, i.e., $V_{\mathrm{SG}}$, and the voltage at a back gate under the substrate, i.e., $V_{\mathrm{BG}}$. We assumed that a low and constant drain voltage $V_{\mathrm{D}}$ (slightly above the thermal voltage) was

applied and that the source was grounded. We reflected these in our simulations by setting the Fermi level in the silicon active layer to zero. This implies that our 1-D cut was taken near the source. A layer of fixed charge with uniform density $\sigma$ was simulated inside the electrolyte, 2 nm away from the front oxide interface. This layer represents bound analytes in samples of interest. Our reference samples had $\sigma = 5 \times 10^{12}\, e\,\mathrm{cm}^{-2}$, where $e$ denotes elementary charge, and we studied the effect of a 0.1 % increase in analyte concentration. We did simulate scenarios in which a "blank" sample with $\sigma = 0$ was our reference, but since those results were qualitatively identical to those which we present, we will omit them in the interest of brevity.

In other cases, we included a layer of "adjustment charges" with density $\sigma_\mathrm{A}$ at the electrolyte/oxide interface (see Fig. 2.1), potentially representing the charge of the receptors or those of the protonated or deprotonated groups at the oxide interface. We neglected the intricate dynamics of analyte transport and binding. We modeled binding events by simply applying a change of $\Delta\sigma$ to the analyte charge, and we considered it to be a constant dependent only on analyte concentration and independent of biasing. Interface traps at the oxide/silicon interfaces were neglected in our simulations.

The simulated electrostatic data allowed us to extract the mobile electron density in the channel. We integrated this quantity from the front oxide to the back oxide. We did this twice for each scenario, once for a sample with analytes and once for a reference sample, denoting the results $Q_\mathrm{S}$ and $Q_\mathrm{S0}$, respectively. We then subtracted the two and denoted the difference by $\Delta Q_\mathrm{S}$. This difference represents the change in the total mobile carrier density at each horizontal position in the FET channel due to the binding of analytes. As we do not simulate a source or a drain, we cannot directly simulate the drain current. Instead, we use the quantity $\Delta Q_\mathrm{S}/Q_\mathrm{S0}$ as an approximation for the regular definition of sensitivity, i.e., $\Delta I/I$. We shall show that these two quantities are roughly equivalent if we consider the process of analyte binding to be a small-signal disturbance over the bias imposed by the external circuitry (i.e., that mobility, effective channel length, and other bias-dependent semiconductor parameters do not vary with analyte binding). This assumption will be valid when sensing samples with low analyte concentrations. Along similar lines, we will use $Q_\mathrm{S}$

as an indicator of the behavior of the drain current $I$.

The general results obtained from our simulations can be applied to sensors with other geometries (e.g., nanowires) or made of other materials (e.g., ZnO) as well. Since we consider electrons as the mobile carriers, we imply that the source and the drain of our sensor are doped $n$-type. Since the active silicon layer was doped $n$-type as well, our device is an $n$-channel accumulation-mode bioFET. By varying the simulated doping type or the extracted carrier type, $p$-type conduction and inversion-mode devices can be simulated using the same method.

### 2.2.1 Justification for Using $\Delta Q_{\mathrm{S}}/Q_{\mathrm{S0}}$ instead of $\Delta I/I$

We use $\Delta Q_{\mathrm{S}}/Q_{\mathrm{S0}}$ in place of $\Delta I/I$ as an approximation. Our justification is as follows.

When the device is biased in the subthreshold regime, the drain current can be approximated as

$$I_{\mathrm{D}} = A \times D \times \frac{Q_{\mathrm{S}}(L) - Q_{\mathrm{S}}(0)}{L} \tag{2.1}$$

where $Q_{\mathrm{S}}(0)$ is the total mobile electron density (integrated vertically across the channel) at the source end, $Q_{\mathrm{S}}(L)$ is the total mobile charge at the drain end, and $L$ is the effective channel length. $D$ and $A$ are the diffusion coefficient and device area, respectively. Note that the units of $Q_{\mathrm{S}}$ are $\mathrm{C\,cm^{-2}}$. Assuming low $V_{\mathrm{D}}$, one can write:

$$Q_{\mathrm{S}}(L) = Q_{\mathrm{S}}(0) \times \exp\left(\frac{eV_{\mathrm{D}}}{\mathrm{k_B}T}\right) \tag{2.2}$$

where $e$, $\mathrm{k_B}$, and $T$ have their usual meanings.

Combining Eq. 2.1 and Eq. 2.2, and canceling out $L$, $V_{\mathrm{D}}$ and the other constants yields:

$$\frac{\Delta I}{I} = \frac{Q_{\mathrm{S1}}(0) - Q_{\mathrm{S0}}(0)}{Q_{\mathrm{S0}}(0)} = \frac{\Delta Q_{\mathrm{S}}}{Q_{\mathrm{S0}}} \tag{2.3}$$

We are essentially assuming $Q_{\mathrm{S}}(0)$ and $Q_{\mathrm{S}}(L)$ will similarly respond to biasing changes; thus, we can analyze only one slice of the entire device (a 1-D simulation setting) and assume $I_{\mathrm{D}}$

is proportional to $Q_S$.

When the device is operating in the linear or saturation regimes, we can approximately write $I_D = Q_S \mu V_D / L$. If we assume that the effective channel length and mobility negligibly vary on binding events, we can consider them to be constants at each bias situation (they *will* vary significantly with bias). We can then write:

$$\frac{\Delta I}{I} = \frac{\Delta Q_S \times \mu \times \frac{V_D}{L}}{Q_{S0} \times \mu \times \frac{V_D}{L}} = \frac{\Delta Q_S}{Q_{S0}} \tag{2.4}$$

We can therefore assume that $\Delta Q_S / Q_{S0}$ and $\Delta I / I$ are roughly equivalent over all regions of operation.

## 2.3 Results and Discussion

### 2.3.1 Dissecting the Sensitivity

Since we are interested in studying the underlying physical effects that impact sensitivity, we will proceed to divide the operation of the sensor into three stages, each stage capturing a different physical effect. We will then determine the bias that optimizes each stage and that which optimizes the whole. Finally, we will show that by choosing the proper adjustment charge density, one can simultaneously optimize different stages at once.

A bioFET's operation can be viewed as having the following stages:

1. A change in analyte concentration causes a change in the density of bound charge at the sensor's surface, i.e., $\Delta\sigma$;
2. The resulting $\Delta\sigma$ is converted to a change in the effective gate voltage, i.e., $\Delta V_{g,eff}$;
3. $\Delta V_{g,eff}$ causes changes in the drain current, which is the output signal.

We have not modeled the intricacies of the first stage in this paper, such as mass transfer, adsorption, or desorption, and we have simply assumed that a fixed $\Delta\sigma$ is given. The second stage captures the effect of DH screening in the buffer; for example, if the linkers that capture

the analytes are rather long and the buffer ionic strength is high, then most of the captured analytes will be screened by the ions in the buffer, and $\Delta V_{\mathrm{g,eff}}$ will be small. The third term captures the FET action of the underlying transistor and is identical in operation to a regular SOI MOSFET. We can express the foregoing dissection mathematically:

$$\overbrace{\frac{\mathrm{d}I}{I}}^{\text{Overall sensitivity}} = \overbrace{\mathrm{d}c \cdot \frac{\mathrm{d}c}{\mathrm{d}\sigma}}^{\text{First stage}} \cdot \overbrace{\frac{\mathrm{d}V_{\mathrm{g,eff}}}{\mathrm{d}\sigma}}^{\text{Second stage}} \cdot \overbrace{\frac{\frac{\mathrm{d}I}{\mathrm{d}V_{\mathrm{g,eff}}}}{I}}^{\text{Third stage}} \tag{2.5}$$

Here, $\mathrm{d}c$ is an infinitesimal change in total analyte concentration in the sample, $\mathrm{d}\sigma$ is an infinitesimal change in the bound charge density at the sensor surface due to the analytes, and $\mathrm{d}V_{\mathrm{g,eff}}$ is an infinitesimal change in the potential at the electrolyte/oxide interface caused by $\mathrm{d}\sigma$. As a first-order approximation, we can replace the differential operators with differences, resulting in

$$\overbrace{\frac{\Delta I}{I}}^{\text{Overall sensitivity}} = \overbrace{\Delta c \cdot \frac{\Delta c}{\Delta \sigma}}^{\text{First stage}} \cdot \overbrace{\frac{\Delta V_{\mathrm{g,eff}}}{\Delta \sigma}}^{\text{Second stage}} \cdot \overbrace{\frac{\frac{\Delta I}{\Delta V_{\mathrm{g,eff}}}}{I}}^{\text{Third stage}} \tag{2.6}$$

$\Delta c$ and $\Delta \sigma$ now represent changes in analyte concentration and bound surface charge density, respectively, compared with some reference sample, and $I$ is the drain current measured under the reference sample. Substituting $\Delta Q_{\mathrm{S0}}/Q_{\mathrm{S0}}$ in place of $\Delta I/I$ in our case, we can write:

$$\overbrace{\frac{\Delta Q_{\mathrm{S}}}{Q_{\mathrm{S0}}}}^{\text{Overall sensitivity}} = \overbrace{\Delta c \cdot \frac{\Delta c}{\Delta \sigma}}^{\text{First stage}} \cdot \overbrace{\frac{\Delta V_{\mathrm{g,eff}}}{\Delta \sigma}}^{\text{Second stage}} \cdot \overbrace{\frac{\frac{\Delta Q_{\mathrm{S}}}{\Delta V_{\mathrm{g,eff}}}}{Q_{\mathrm{S0}}}}^{\text{Third stage}} \tag{2.7}$$

The first-stage term can be enhanced by techniques such as those presented by Gong [Gon10] and Vaknin et al. [VKM11]. For our purposes, the first stage is independent of biasing; therefore, we will not discuss it. We will therefore lump its influence into the second stage. Thus:

$$\overbrace{\frac{\Delta Q_{\mathrm{S}}}{Q_{\mathrm{S0}}}}^{\text{Overall sensitivity}} = \overbrace{\frac{\Delta V_{\mathrm{g,eff}}}{\Delta \sigma}}^{\text{Second stage}} \cdot \overbrace{\frac{\frac{\Delta Q_{\mathrm{S}}}{\Delta V_{\mathrm{g,eff}}}}{Q_{\mathrm{S0}}}}^{\text{Third stage}} \tag{2.8}$$

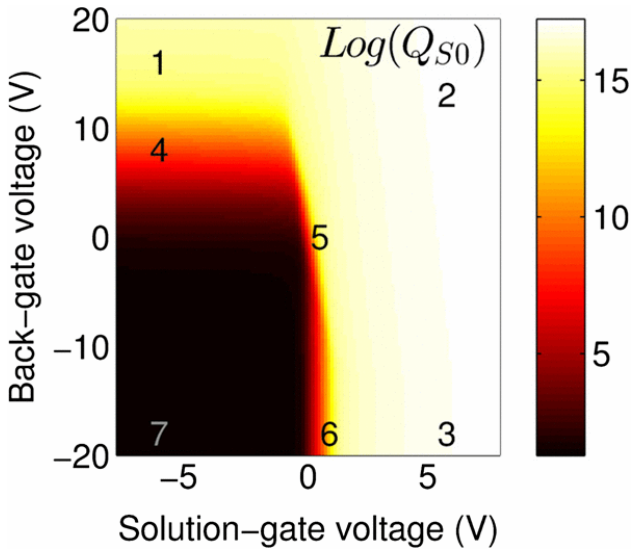


Figure 2.2: Plot of the logarithm of total electron density ($e\,\mathrm{cm}^{-2}$) integrated across the FET channel in the silicon active layer versus bias. The numbers mark different regimes of operation.

We can now proceed to analyze and optimize the impact of each term of Eq. 2.8 on the overall sensitivity and address the dilemma alluded to by Lee et al. [LNS09] and mentioned in the introduction of this paper.

To this end, we ran our first set of simulations: we considered our baseline to be a sample with $\sigma = -5 \times 10^{12}\, e\,\mathrm{cm}^{-2}$, whereas the sample of interest that was "being measured had $\sigma = -5.005 \times 10^{12}\, e\,\mathrm{cm}^{-2}$, a 0.1 % change. This quantity of charge is in the neighborhood of that seen in DNA sensing [PCI05]. Fig. 2.2 shows the baseline $Q_{\mathrm{S0}}$ versus $V_{\mathrm{BG}}$ and $V_{\mathrm{SG}}$ in log scale, which is an indicator of the drain current. The numbers on the image denote different regimes of operation of the underlying FET: (1) back-channel conduction; (2) volume conduction; (3) front-channel conduction; (4), (5), and (6) subthreshold conduction; and (7) off-state. Fig. 2.3a is a plot of $\Delta V_{\mathrm{g,eff}}$ versus bias, whereas Fig. 2.3b is a plot of $\left(\Delta Q_{\mathrm{S}}/\Delta V_{\mathrm{g,eff}}\right)/Q_{\mathrm{S0}}$ versus bias. These two figures show the bias dependence of the terms in the right-hand-side of Eq. 2.8. Fig. 2.3c is a plot of the overall sensitivity versus bias and is the result of multiplying Figs. 2.3a and 2.3b.

Although it may not be apparent from the plots presented here, the variation in the

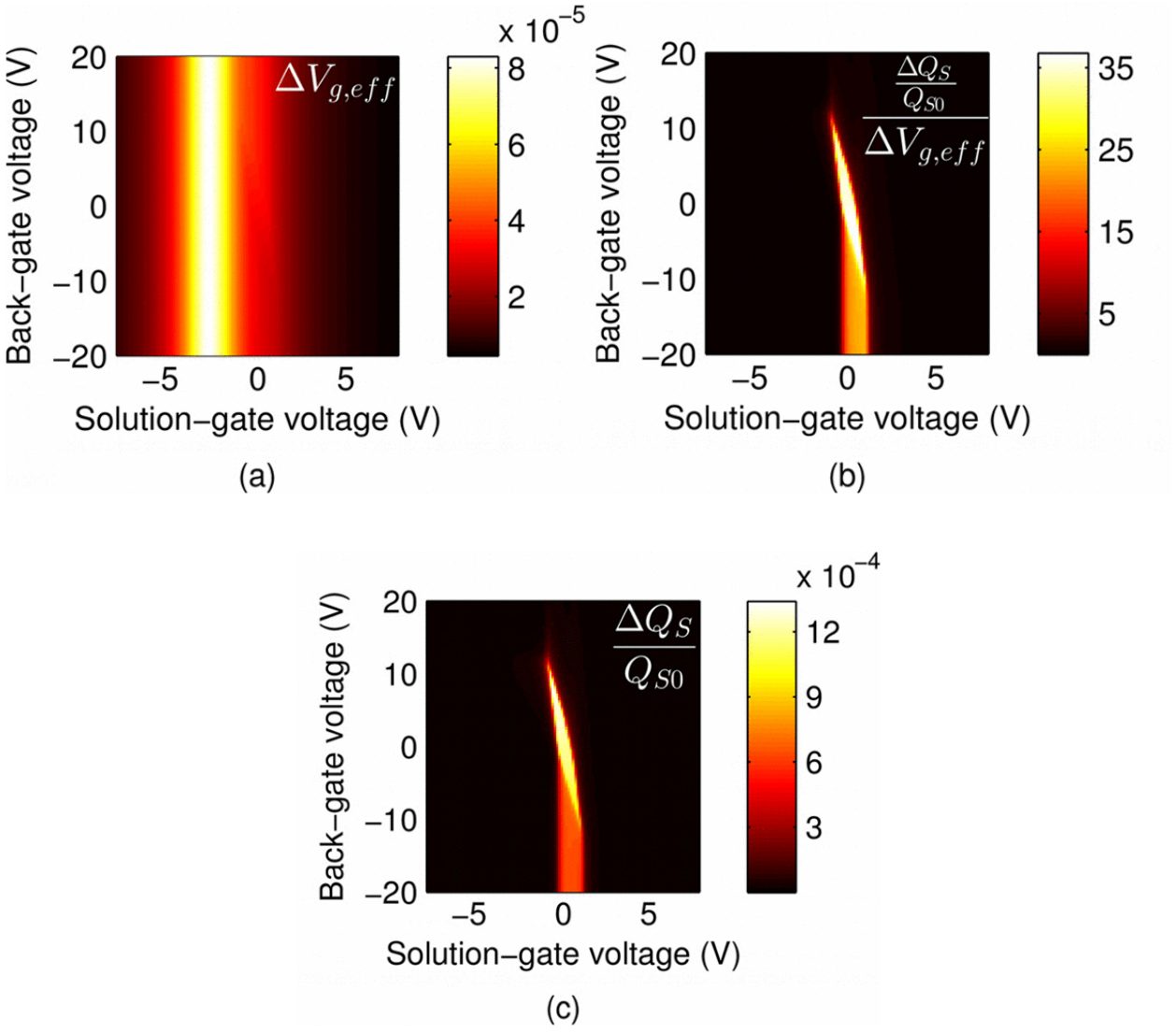


Figure 2.3: (a) Effective gate voltage change (V) versus biasing voltages. The brighter regions represent the voltages at which electrolyte screening is minimum; thus, the most amount of voltage change is produced due to a fixed amount of bound analyte charge. (b) Sensitivity per unit of effective gate voltage change ($V^{-1}$) versus biasing voltages. The optimum points on this plot represent the biases at which the $g_m/I_D$ of the FET is maximum. (c) Total sensitivity (dimensionless) versus biasing voltages.

$\Delta V_{\mathrm{g,eff}}$ term between its ideal bias and its worst bias is less than a factor of 10, whereas $\left(\Delta Q_{\mathrm{S}}/\Delta V_{\mathrm{g,eff}}\right)/Q_{\mathrm{S0}}$ varies over three orders of magnitude. The result is that Figs. 2.3b and 2.3c look almost identical. This means that proper or improper biasing of the sensor will affect the FET action far more dramatically than it will affect the screening of the charges by the buffer. The dilemma is therefore laid to rest: we should bias to optimize the FET, as mentioned in references [CFS11, CXY08, EJB08, GZL10, LHL10, YAY10, VSI11], and forgo the charges that are lost to DH screening in the buffer. We will however proceed to study the mechanism behind the peaks in Figs. 2.3a and 2.3b, and we will show that one can engineer the sensor in a way that causes the peaks to coincide, resulting in an increase in sensitivity beyond what biasing alone could offer.

We would like to point out that in real situations, the presence of interface states may severely degrade the subthreshold slope, softening the peak in Fig. 2.3b. However, we believe that the three-order-of-magnitude initial variation in Fig. 2.3b is so large that even with some degradation, it will still dominate over Fig. 2.3a, so that the bias that maximizes the third-stage term will still maximize the overall sensitivity. We therefore do not expect the optimum operation regime to change; we only expect changes in the magnitude of the highest attainable sensitivity.

### 2.3.2 Optimization of $\Delta V_{\mathrm{g,eff}}$

Given that we have fixed $\Delta\sigma$, a maximum in $\Delta V_{\mathrm{g,eff}}$ can only be caused by an increase in the sensor capacitance as seen from the position of the analytes, relative to the double-layer capacitance in the electrolyte. An increase in the sensor capacitance is caused by a reduction in the TF screening length in the semiconductor. A decrease in the double-layer capacitance is caused by an increase in the DH screening length in the buffer solution. We would like to point out that contrary to the conclusions in reference [SMB07], the bias that squeezes the most voltage change out of the analytes is *not* the bias that minimizes the TF screening length in, and maximizes the capacitance of, the FET. In our $n$-type FET, the TF length at the front interface is minimized at high values of $V_{\mathrm{SG}}$, whereas $\Delta V_{\mathrm{g,eff}}$ is maximized at

lower values of $V_{\mathrm{SG}}$ (we set the solution work function to 4.61 eV in order to dramatize and observe this difference). In fact, $\Delta V_{\mathrm{g,eff}}$ is maximized at a bias that shuts off the FET. We believe that a reduction of DH screening in the buffer is responsible for maximizing $\Delta V_{\mathrm{g,eff}}$.

The DH screening length depends on bias because of the proximity of the analytes to the sensor. The original DH formalism assumes that a uniform background of mobile carriers is present before a perturbation is applied in the form of a point charge. However, the proximity of the sensor causes changes in bias to disturb the uniformity of the local carrier concentrations in the electrolyte. One has to take into account the modified local ion concentrations, which will lead to stronger screening. Since the front- and back-gate voltages can affect the carrier concentrations near the analytes, they can also modify the DH screening length.

Here, we briefly reproduce the derivation that demonstrates the dependence of the DH screening length on the sum of the concentrations of co- and counter-ions. We begin by assuming that a point charge of $Q$ is present at the origin and that the PoissonBoltzmann equation applies to the surrounding medium, i.e.:

$$\nabla^2\phi(r) = \frac{e}{\epsilon}\left(c\exp(-\beta\phi) - c\exp(\beta\phi)\right) + \frac{Q\delta(r)}{\epsilon} \tag{2.9}$$

Here, $c$ is the bulk ionic concentration, $\epsilon$ is the permittivity of the medium, $\phi$ is the electrostatic potential, $e$ is elementary charge, $\beta = e/\mathrm{k_B}T$, $\mathrm{k_B}$ is Boltzmann's constant, $T$ is temperature, and $\delta(r)$ is the Dirac delta function. Now, let us consider a perturbation in the point charge $\Delta Q$ and its effect on the potential, $\Delta\phi$, i.e.,

$$\nabla^2\left(\Delta\phi(r)\right) = \frac{-e^2\Delta\phi}{\epsilon\mathrm{k_B}T}\left(c\exp(-\beta\phi) - c\exp(\beta\phi)\right) + \frac{\Delta Q\delta(r)}{\epsilon} \tag{2.10}$$

The solution to this equation is:

$$\Delta\phi(r) = \frac{\Delta Q}{4\pi\epsilon r}\exp\frac{-r}{\lambda} \tag{2.11}$$

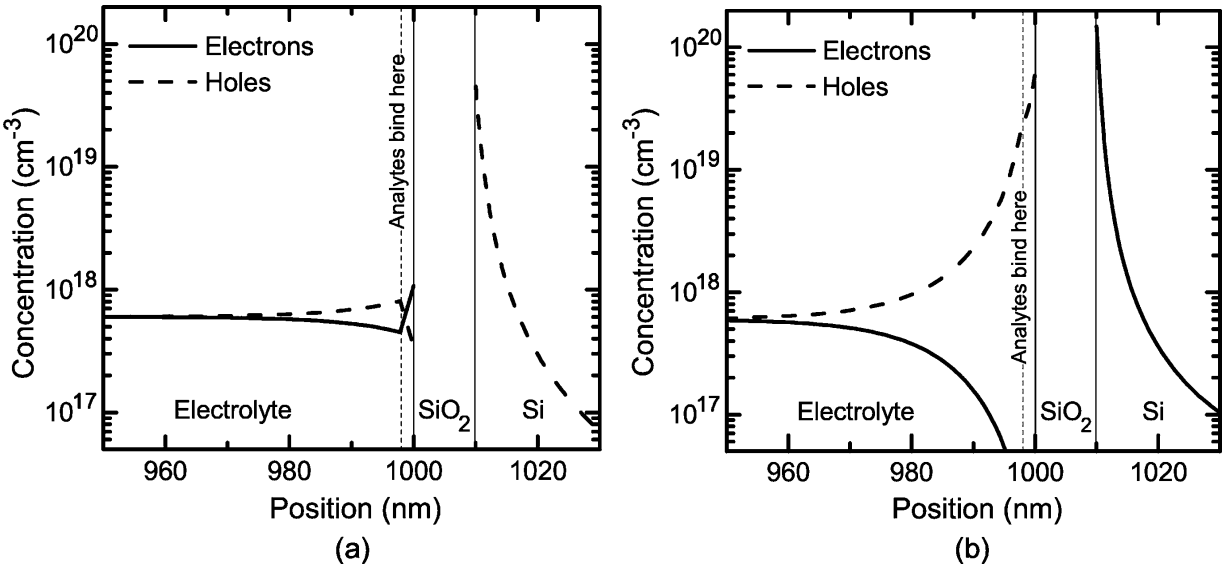


Figure 2.4: Ion concentration versus position in the vicinity of the bound analytes at (a) $V_{\mathrm{SG}} = -2.8\,\mathrm{V}$ and $V_{\mathrm{BG}} = 0$ and (b) $V_{\mathrm{SG}} = 5.2\,\mathrm{V}$ and $V_{\mathrm{BG}} = 0$. The vertical dashed line denotes the point where analytes bind. The effective gate voltage change in (a) is about $80\,\mu\mathrm{V}$, whereas it is only about $8\,\mu\mathrm{V}$ in (b). Note that the electrons and holes in the electrolyte regions represent anions and cations, respectively.

with

$$\lambda = \sqrt{\frac{\epsilon \mathrm{k_B} T}{e^2 c \left(\exp -\beta\phi + \exp \beta\phi\right)}} = \sqrt{\frac{\epsilon \mathrm{k_B} T}{e^2 \left(c_+ + c_-\right)}} \tag{2.12}$$

The foregoing derivation shows that the DH screening length has an inverse relationship with the sum of the co- and counter-ion concentrations, i.e., DH screening is weakest when the sum of the ion concentrations is minimum. Through these ion concentrations, the screening length becomes bias-dependent. Given that the product of co- and counter-ion concentrations is constant in equilibrium, one can conclude that DH screening will be weakest when the co- and counter-ion concentrations are equal, i.e., when there is no electric field in the vicinity of the bound analytes. It is noted that there are also techniques to reduce screening even further by disturbing the equilibrium [LSD08].

To confirm this hypothesis, we extracted the co- and counter-ion concentrations near the analytes at two different bias values, one that maximizes $\Delta V_{\mathrm{g,eff}}$ and one with the FET in

strong inversion. These are presented in Fig. 2.4a and Fig. 2.4b, respectively. In Fig. 2.4a, the ion concentrations are almost equal, so that their sum is smallest, resulting in the largest DH screening length and maximum $\Delta V_{\mathrm{g,eff}}$. The opposite is true in Fig. 2.4b: the large local anion concentration (represented by electrons) reduces the DH screening length, increasing DH screening and resulting in a smaller $\Delta V_{\mathrm{g,eff}}$.

Note that the Poisson-Boltzmann model that we have used here will overestimate the carrier concentration at high bias, so that the DH screening may not be as bad as this simulation shows. However, the conclusion regarding the qualitative behavior is valid nevertheless: DH screening is minimized when the co- and counter-ion concentrations are equal.

Fig. 2.3a shows that the back gate has almost no influence on $\Delta V_{\mathrm{g,eff}}$. The back gate is fully capable of modulating the carrier concentration and the TF screening length in the silicon film, but is incapable of affecting $\Delta V_{\mathrm{g,eff}}$ in Fig. 2.3a. This observation is consistent with our hypothesis that TF screening is not responsible for the behavior of $\Delta V_{\mathrm{g,eff}}$ and that the responsible phenomenon must be happening at or near the electrolyte/oxide interface. Only at one point does $\Delta V_{\mathrm{g,eff}}$ show any sensitivity to $V_{\mathrm{BG}}$. It is barely noticeable, and it happens only when $V_{\mathrm{BG}}$ is near point (5) of Fig. 2.2, when the silicon film is fully depleted, which is also the same point that maximizes the FET efficiency in Fig. 2.3b and the sensitivity in Fig. 2.3c. This is because the carriers in the silicon film screen the electric field from the back gate and prevent it from reaching the distant electrolyte/oxide interface; only when the silicon film is fully depleted can the field penetrate so far and affect the potential there.

Since any change in the concentration of charged analytes disturbs the electric field set by the bias, we decided to simulate a scenario where the analyte concentration $\sigma$ changes by only 0.1 %. The physics would have been the same for larger changes. However, confirming that maximum $\Delta V_{\mathrm{g,eff}}$ occurs because of minimal DH screening would have been much more difficult; the optimum bias would have been that which would cause the cancellation of the electric field at some $\sigma$ in between its initial or final values.

### 2.3.3 Optimization of the FET

The FET action of the bioFET is represented by the third-stage term of equation 2.5, i.e., $\left(\mathrm{d}I/\,\mathrm{d}V_{\mathrm{g,eff}}\right)/I$. This is the familiar $g_{\mathrm{m}}/I_{\mathrm{D}}$ ratio metric of MOSFETs. It is well known that $g_{\mathrm{m}}/I_{\mathrm{D}}$ is maximized by biasing the FET in the subthreshold regime and that maximizing $g_{\mathrm{m}}/I_{\mathrm{D}}$ is the same as minimizing the subthreshold slope (SS). Therefore, any bias that minimizes SS in a MOSFET would also minimize it in a bioFET.

The presence of the back insulator in fully depleted (FD) SOI and nanowire structures enables FDSOI-based FETs and sensors to achieve near-ideal SS [Col86]. Tokunaga and Sturm clearly describes how to bias such a FET to minimize SS when a back gate is present and why such a bias produces a minimum [TS91]. We will omit the details and simply report the results: the silicon film has to be fully depleted, putting the device in the subthreshold regime, as reported in references [CFS11, CXY08, EJB08, GZL10, LHL10, YAY10, VSI11]. A key point not mentioned in these works is that an accumulation or inversion layer at either interface is detrimental to the SS. Moreover, the channel should form near the front interface. This means that the back gate should "deplete more than the front gate. Elfström et al. also demonstrate the benefits of having the channel near the front interface [EKL08]; however, they do not use two gates, and therefore, they cannot achieve a near-ideal SS.

By comparing Figs. 2.2 and 2.3b, it becomes apparent that our simulations are consistent with the foregoing instructions. The maximum of Fig. 2.3b occurs in the subthreshold region. Moreover, the subthreshold regime in Fig. 2.2 is wide and encompasses three general regions: front accumulation with back depletion near point (6), front depletion with back accumulation near point (4), and depletion at both interfaces near point (5). Only depletion at both interfaces produces the maximum in Fig. 2.3b.

It is noteworthy that once the instructions of Tokunaga and Sturm [TS91] have been followed, the SS of both a nanowire FET sensor and an SOI-based FET sensor will be near ideal; therefore, the nanowire will have no advantage in this regard. If a sensitivity advantage exists, it must come from the second-stage term of equation 2.8.

The third-stage term of equation 2.8 suggests that novel devices with SS steeper than

60 mV per decade could provide a sensitivity advantage over regular FETs, which are fundamentally limited to 60 mV per decade. Tunneling FETs (TFETs), in particular, seem like prime candidates for use as bioFETs. Their low current drive is a major obstacle for their use in microelectronics but is a not a problem for biosensing, since biosensors do not require high-speed operation. Once they can be cheaply and reliably manufactured with consistent subthermal subthreshold swings, we can expect them to be adapted for use as bioFETs.

### 2.3.4 Concurrent Optimization of Both Stages

Since the maxima in Figs. 2.3a and 2.3b do not coincide normally, one has to cause a shift in these curves along the $V_{\mathrm{SG}}$ axis to create overlap. A change in the front-gate threshold voltage of the sensor would shift Fig. 2.3b nicely in any direction we desire. Unfortunately, the front threshold voltage strongly affects $\Delta V_{\mathrm{g,eff}}$ as well; thus, Fig. 2.3a will shift in the same direction as Fig. 2.3b, eliminating any gained benefits. Instead, one has to locally change the electric field near the analytes, shifting *only* Fig. 2.3a, and affecting *only* $\Delta V_{\mathrm{g,eff}}$.

This can be done by engineering the amount of surface charge present near the electrolyte/oxide interface. Such "adjustment" charges will not shift the threshold voltage of the FET but will adjust the electric field near the analytes to zero. These charges, ideally, would only shift the position of the maxima in Fig. 2.3a and Fig. 2.3b, without altering the magnitude of the maximum. Their polarity and density can be determined from simulations and will be dependent on the details of the sensor. Linker molecules, receptor molecules, or charged groups at the insulator surface can be possible sources of these charges.

We added varying densities of adjustment charge $\sigma_{\mathrm{A}}$ to the electrolyte/oxide interface of our sensor, as depicted in Fig. 2.1, and re-simulated the structure. As expected, the only change we observed was that the peak in Fig. 2.3a shifted; the peak in Fig. 2.3b did not move, nor did the magnitudes of the maxima change significantly. As a function of $\sigma_{\mathrm{A}}$, the values of the maxima are plotted in Fig. 2.5a; the $V_{\mathrm{SG}}$ values that produce the maxima are plotted in Fig. 2.5b; and the overall sensitivity along with the $V_{\mathrm{SG}}$ that produces it are plotted in Fig. 2.5c. The maximum overall sensitivity was observed at an adjustment charge

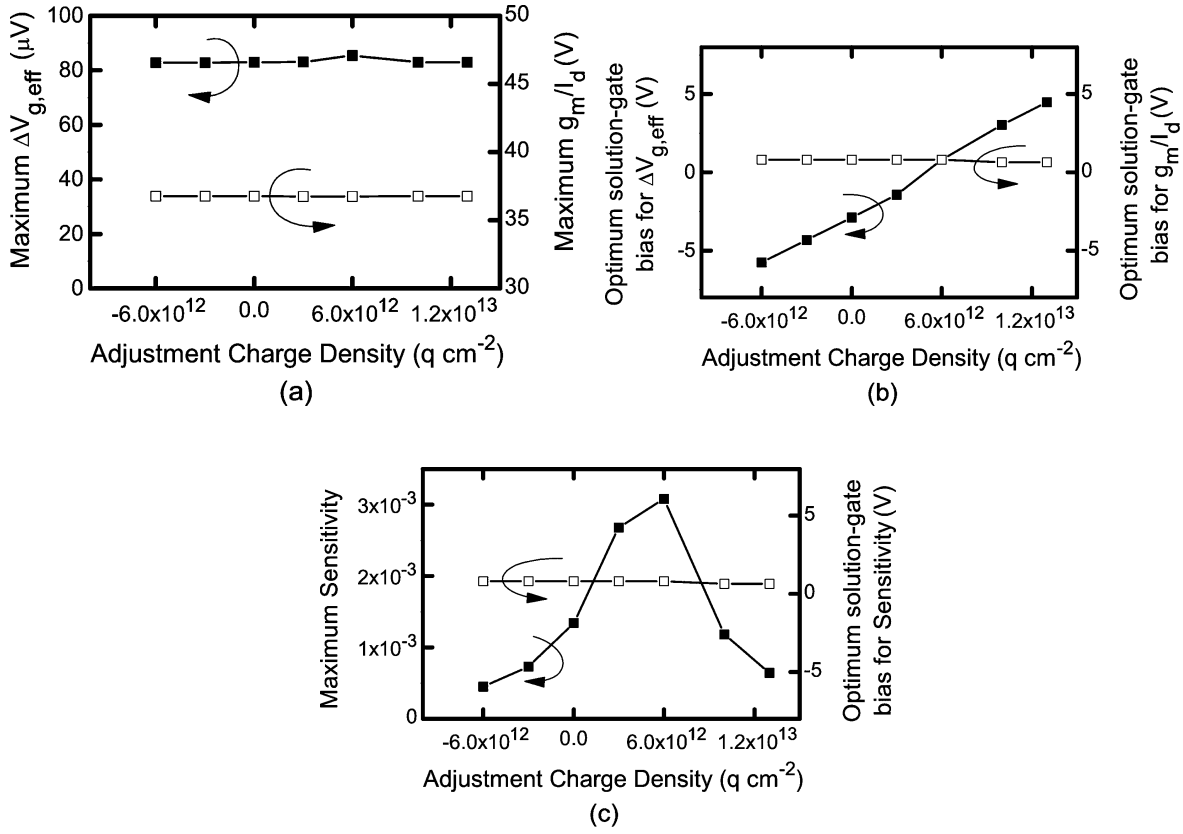


Figure 2.5: Plots of (a) the maximum possible $\Delta V_{\mathrm{g,eff}}$ (left $y$-axis) and maximum possible $g_{\mathrm{m}}/I_{\mathrm{D}}$ (right $y$-axis), (b) the $V_{\mathrm{SG}}$ that maximize $\Delta V_{\mathrm{g,eff}}$ (left $y$-axis) and $g_{\mathrm{m}}/I_{\mathrm{D}}$ (right $y$-axis), and (c) the maximum possible sensitivity (left $y$-axis) and the $V_{\mathrm{SG}}$ that maximizes it (right $y$-axis), all plotted versus the adjustment charge density $\sigma_{\mathrm{A}}$ present at the electrolyte/oxide interface. The maximum achievable values for the $\Delta V_{\mathrm{g,eff}}$ and $g_{\mathrm{m}}/I_{\mathrm{D}}$ do not vary as the adjustment charge density is varied, but the $V_{\mathrm{SG}}$ that maximizes them does vary. When the plots in (b) coincide, the $\Delta V_{\mathrm{g,eff}}$ and the $g_{\mathrm{m}}/I_{\mathrm{D}}$ are maximized at the same $V_{\mathrm{SG}}$, and the sensitivity in (c) becomes maximum.

density of $\sigma_A = 6 \times 10^{12}\, e\,\mathrm{cm}^{-2}$. Not surprisingly, at this same $\sigma_A$, both terms in Eq. 2.8 reach their peak at the same $V_{SG}$, as shown in Fig. 2.5b. In Fig. 2.5a, we can see that the increase in sensitivity does not come from an increase in the magnitude of the maximum of either of the terms in Eq. 2.8.

It may seem that given the fact that our analytes are negatively charged, it is not surprising that a positively charged $\sigma_A$ would increase sensitivity, due to its ability to attract and bind more analytes. In our setting, this would be an incorrect conclusion since we have not considered the dynamics of analyte binding at all. Moreover, excessive amounts of $\sigma_A$ happen to reduce the sensitivity, as shown in Fig. 2.5c. Although oppositely charged $\sigma_A$ will help to attract analytes, it should not be engineered for that purpose. Techniques such as those of Gong [Gon10] and Vaknin et al. [VKM11] should be used to attract analytes, and $\sigma_A$ should be used to maximize sensitivity. Accurate simulations will be required to determine the correct density of $\sigma_A$.

We have shown that for fully depleted FET-based biosensors with a BOX and a back gate, there is an optimum biasing point that maximizes sensitivity, and it is the same bias that optimizes the subthreshold slope of the underlying FET. Moreover, we have identified DH screening near the electrolyte/oxide interface as the leading bias-dependent phenomenon that affects the amount of charge that is induced in the sensor; the bias dependence of TF screening in the semiconductor seems to be unimportant. We have also shown that other charges that may be present near the analytes will affect the sensitivity. In addition to explaining why this happens, we have shown that it can be used to our advantage.

## 2.4 Conclusions

We have shown that for fully depleted FET-based biosensors with a BOX and a back gate, there is an optimum biasing point that maximizes sensitivity, and it is the same bias that optimizes the subthreshold slope of the underlying FET. Moreover, we have identified DH screening near the electrolyte/oxide interface as the leading bias-dependent phenomenon that affects the amount of charge that is induced in the sensor; the bias dependence of TF

screening in the semiconductor seems to be unimportant. We have also shown that other charges that may be present near the analytes will affect the sensitivity. In addition to explaining why this happens, we have shown that it can be used to our advantage.

# CHAPTER 3

# On the Origin of Enhanced Sensitivity in Nanowire BioFETs

The contents of this chapter have been previously published by PNAS [SC14].

## 3.1 Introduction

It is widely believed that surface-area-to-volume ratio is directly related to the sensitivity of field-effect-transistor-based bioFETs. This has led to a massive drive to use nanowires, which are costly and difficult to make, for use in such sensors. Although nanowires do exhibit superior performance in certain situations, we believe increased surface-area-to-volume ratio is not the cause. We find that in general, smaller wires do worse, unless they are placed on an insulating substrate. In the corners between the nanowire and the substrate, the electrolyte exhibits weaker Debye screening and smaller capacitance density, causing the sensor to have larger charge sensitivity. Our understanding enables researchers to design better biosensors, possibly using large-scale structures that are cheaper to make.

In fabricating bioFETs, the transistor is frequently based on a quasi-1D nanostructure such as a nanowire (NW) or nanotube, and the biomolecules bind directly to the surface of the nanoscale structure [Wan06, JPV10]. The use of such nanostructures is justified by the belief that nanoscale biosensors are more sensitive, with sensitivity defined as the relative change in drain current or a shift in threshold voltage in response to a change in bound biomolecule density. A few experiments specifically studied the effect of shrinking nanowire radii on sensitivity, albeit with varying structures, analytes, and sensing circumstances, and found that shrinking a sensor's dimensions indeed improves its sensitivity [EJS07, LZT11, SKR07].

The enhanced sensitivity has been loosely attributed to the increase in the sensor's surface-area-to-volume ratio, which is a direct result of shrinking its dimensions. This argument has been analytically justified in the context of gas sensors [FL06]. However, there is a fundamental difference between gas and biomolecule sensing: biomolecule sensing is performed in an electrolyte, and the ions therein will screen the charge of bound biomolecules in a phenomenon known as Debye Screening [BF01, McL77]. The direct application of the gas sensing result to the biosensing environment implicitly assumes that the screening effect does not change with shrinking dimensions, an assumption we believe to be false. There have been studies that included a rigorous treatment of screening in biosensors, but they studied neither the specific cause of increased sensitivity at the nanoscale, nor the effect of varying size on screening behavior [SMB07]. We believe the phenomenon responsible for the increased sensitivity of nanowires in particular, and nanostructured biosensors in general, has not yet been uncovered by the research community.

In the previous chapter, we have dissected the operation of bioFETs into two independent parts in order to better understand the underlying physics [SC12]: first, biomolecule charges cause a change in the local electrostatic potential at the outer surface of the gate dielectric. This potential change in turn causes a change in the drain current of the underlying semiconductor channel. The latter part is simply the transconductance effect of an FET-based transistor; nanoscale bioFETs have no advantage in this respect over planar sensors. The nanoscale advantage should therefore lie in the first part of the sensor operation, which is a capacitive transduction effect, dominated by the capacitance of the Debye screening layer. We therefore believe understanding screening behavior at the nanoscale is key to understanding the behavior of nanoscale bioFETs.

In this paper, we revisit screening near curved nanostructure surfaces by solving the Poisson-Boltzmann equation that led to the original Debye-Hückel formalism. Our simple analytical arguments will show that screening is stronger near surfaces with convex curvature, and weaker near surfaces with concave curvature. We only consider simple convex and concave surfaces because almost all non-planar surfaces can be decomposed into local areas with either convex or concave curvature.

Next, we apply the basic insight we gain from the previous step to understand and analyze the specific case of nanowire bioFETs. Increasing the surface-area-to-volume ratio of nanowire sensors actually means increasing their convexity, which should result in increased Debye screening and reduced sensitivity. However, nanowires placed on insulating substrates create concave corners between the nanowire and the substrate. We believe biomolecules bound in such concave corners are responsible for the increased sensitivity experimentally observed in nanowires.

## 3.2 Methods

### 3.2.1 Analytical Calculations

We begin by noting that biosensor sensitivity has been shown to be maximum when the biosensor is operated in the subthreshold regime [SC12, GZL10]. In this regime, sensitivity can be defined as either a change in effective gate potential (or threshold voltage), or a relative change in drain current. These definitions are proportional to one another, as shown below. We will therefore treat them as equivalent for the purposes of assessing the effects of nanowire radius on sensitivity.

$$
\begin{aligned}
I_{\mathrm{D,baseline}} &= I_{\mathrm{D,off}} \times \exp\left(\frac{qV_{\mathrm{E,baseline}}}{nk_{\mathrm{B}}T}\right) \\
I_{\mathrm{D,analyte}} &= I_{\mathrm{D,off}} \times \exp\left(\frac{qV_{\mathrm{E,analyte}}}{nk_{\mathrm{B}}T}\right) \\
\frac{I_{\mathrm{D,analyte}}}{I_{\mathrm{D,baseline}}} &= \exp\left(\frac{q\Delta V_{\mathrm{E}}}{nk_{\mathrm{B}}T}\right) \approxeq 1 + \frac{q\Delta V_{\mathrm{E}}}{nk_{\mathrm{B}}T} \\
\frac{\Delta I_{\mathrm{D}}}{I_{\mathrm{D,baseline}}} &= \frac{q\Delta V_{\mathrm{E}}}{nk_{\mathrm{B}}T}
\end{aligned}
\tag{3.1}
$$

In the above expressions, $I_{\mathrm{D,off}}$, $I_{\mathrm{D,baseline}}$, and $I_{\mathrm{D,analyte}}$ represent the drain current in the off-state, the baseline drain current in the absence of target analytes, and the drain current in the presence of target analytes, respectively. $n$, $q$, $k_{\mathrm{B}}$, and $T$ represent the subthreshold ideality factor, elementary charge, Boltzmann's constant, and temperature, respectively. $V_{\mathrm{E}}$ denotes

the electrode potential in "extended-gate" bioFETs, which corresponds to the potential at the electrolyte/oxide interface for nanowire bioFETs; this potential acts upon a biosensor's channel as the gate voltage would in a regular FET. $\Delta I_{\mathrm{D}}$ and $\Delta V_{\mathrm{E}}$ represent the change in drain current and electrode potential due to target biomolecule binding. We have assumed that the target analyte concentration is small, resulting in $q\Delta V_{\mathrm{E}} \ll nk_{\mathrm{B}}T$.

In a previous paper [SC12], we dissected a generic FET-based biosensor's response into four parts, as follows:

$$\frac{\Delta I_{\mathrm{D}}}{I_{\mathrm{D,baseline}}} = \Delta c \times \frac{\Delta \sigma}{\Delta c} \times \frac{\Delta V_{\mathrm{E}}}{\Delta \sigma} \times \frac{\frac{\Delta I_{\mathrm{D}}}{\Delta V_{\mathrm{E}}}}{I_{\mathrm{D,baseline}}} \tag{3.2}$$

Here, $\Delta c$ is the change in target analyte concentration and $\Delta \sigma$ is the change in surface charge density due to the target analytes. These are unaffected by geometry. The third term in the equation above represents capacitive transduction, whose geometry dependence is dealt with later in this paper. The final term captures the transistor action of a biosensor. This term is none other than the familiar $\frac{g_{\mathrm{m}}}{I_{\mathrm{D}}}$ of a transistor, which is largest when the FET is operated in the subthreshold regime, and is the main reason why sensitivity is maximum under subthreshold operation. However, it should be noted that in subthreshold, $\frac{g_{\mathrm{m}}}{I_{\mathrm{D}}}$ has a theoretical maximum:

$$I_{\mathrm{D,baseline}} = I_{\mathrm{D,off}} \times \exp\left(\frac{qV_{\mathrm{E,analyte}}}{nk_{\mathrm{B}}T}\right)$$

$$g_{\mathrm{m}} = I_{\mathrm{D,off}} \times \frac{q}{nk_{\mathrm{B}}T} \times \exp\left(\frac{qV_{\mathrm{E,analyte}}}{nk_{\mathrm{B}}T}\right)$$

$$\frac{g_{\mathrm{m}}}{I_{\mathrm{D,baseline}}} = \frac{q}{nk_{\mathrm{B}}T} \leq \frac{q}{k_{\mathrm{B}}T} \qquad \text{since } n \geq 1 \tag{3.3}$$

The above maximum for $\frac{g_{\mathrm{m}}}{I_{\mathrm{D}}}$ is simply the familiar 60mV/decade limitation for the subthreshold swing of thermionic FETs. Reducing nanowire diameter will improve sensitivity by improving $\frac{g_{\mathrm{m}}}{I_{\mathrm{D}}}$. However, once the fundamental maximum has been reached, further reduction in size does not provide any improvement. Biosensing nanowires are typically doped at around $10^{16}\mathrm{cm}^{-3}$, for which the maximum depletion width is about 300nm at room temperature. This is far larger than the typical dimensions of the nanowires; most nanowires are

thinner than 100nm. This means that nanowires used in most biosensing experiments are already fully-depleted, and further reduction in size will not noticeably change or improve subthreshold swing. Once a nanowire is fully depleted, changing its radius will only change the third term in Equation 3.2, which represents the capacitive transduction of biomolecule charge into surface potential at the electrolyte/oxide interface. We can therefore safely ignore the FET-action of the nanowire, and focus our analysis on the capacitive term and its variations due to surface curvature. It should be noted that most nanowires do not exhibit the 60mV/decade ideal swing, even though they are fully depleted; this is due to the large number of interface trap states created during processing.

To describe sensing near generic curved surfaces, it is sufficient to solve the Poisson-Boltzmann equation, subject to the proper boundary conditions; this method is known as the Gouy-Chapman model [BF01]. This model neglects the finite size of the ions in the electrolyte. It is adequate for gaining insight into the qualitative behavior of electric double layers; for low surface potentials and dilute electrolytes, it is also quantitatively acceptable [TV80]. Calculations using more sophisticated Modified Poisson-Boltzmann formalisms have arrived at potential distributions similar to ours [WP11].

To make the problem analytically tractable, we solve the equation in 1D, and extend it to 3D using cylindrical and spherical symmetries. We consider five different types of structures: a) flat, b) convex spherical, similar to a nanoparticle, c) convex cylindrical, similar to a nanowire, d) concave spherical, similar to a cavity in an otherwise solid electrode, and e) concave cylindrical, similar to a cylindrical pore through an electrode, such as those used in nanopore translocation sensing. We vary the radii of curvature in the curved structures, and extract sensitivity as a function of radius. Cross sections of concave, flat, and convex structures are shown in Figs. 3.1 (a), (b), and (c), respectively; the cross sections of concave cylindrical and spherical structures look identical, as do their convex counterparts.

All structures are composed of a 1:1 electrolyte in contact with a polarizable sensing electrode. A grounded reference electrode immersed in the electrolyte is modeled by fixing the electrolyte Fermi level at 0 V. For the convex and flat cases, the electrostatic potential from the sensing electrode is required to vanish far away from the electrode surface. For the

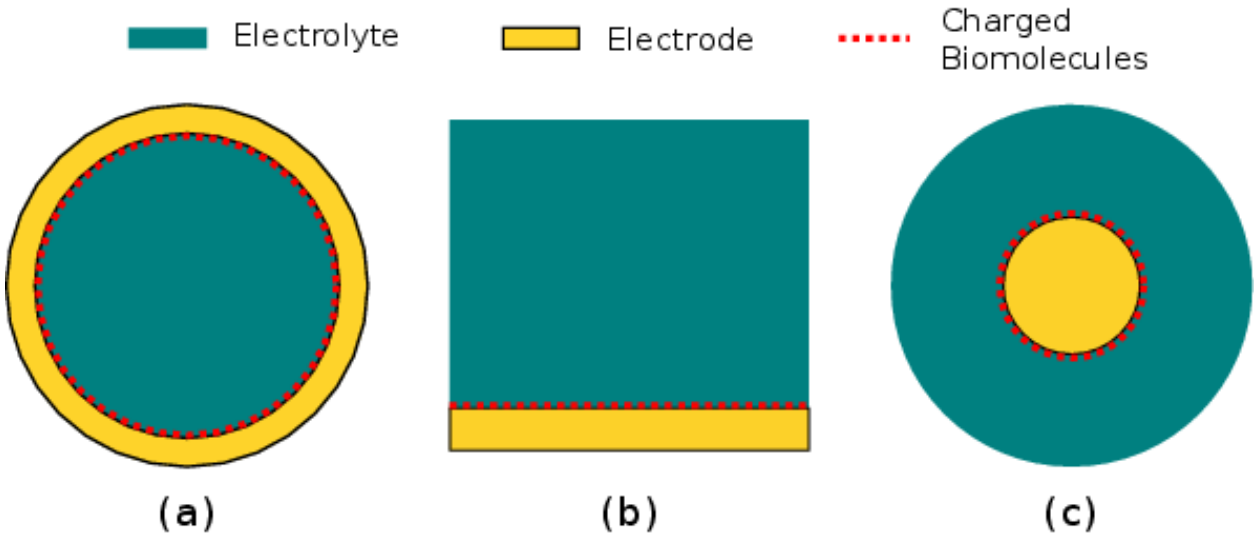


Figure 3.1: Cross sectional schematics of the structures that were analytically studied. The concave, flat, and convex structures are shown in (a), (b), and (c), respectively; the cross sections of concave cylindrical and spherical structures look identical, as do their convex counterparts. The gold areas represent the sensing electrode, the teal areas represent the electrolyte, and the dotted red lines represent the charged target biomolecules.

concave cases, the electric field is required to vanish at the center of the structure, due to symmetry.

For the next steps, we refer the reader to Fig. 3.2. We solve Poisson's equation, find the electrostatic potential in the electrolyte in terms of the electrode potential $V_{\mathrm{E}}$, and find the total ionic charge in the electrolyte as a function of the $V_{\mathrm{E}}$. The derivative of this charge with respect to $V_{\mathrm{E}}$ gives the capacitance density of the diffuse ionic layer, denoted by $C_{\mathrm{DL}}$. The calculation is straightforward, and the details are given in the accompanying Supporting Information.

The charges brought by biomolecules to the electrode surface are modeled as a uniform layer of sheet charge of density $\Delta\sigma_{\mathrm{Bio}}$. These can be viewed as a small-signal disturbance, with the sensing and reference electrodes representing small-signal ground. The capacitance between the biomolecule charges and ground is therefore the parallel combination of the diffuse layer capacitance, $C_{\mathrm{DL}}$, and the capacitance to the sensing electrode, $C_{\mathrm{E}}$. The justification for such an equivalent circuit model is given in the Supporting Information section.

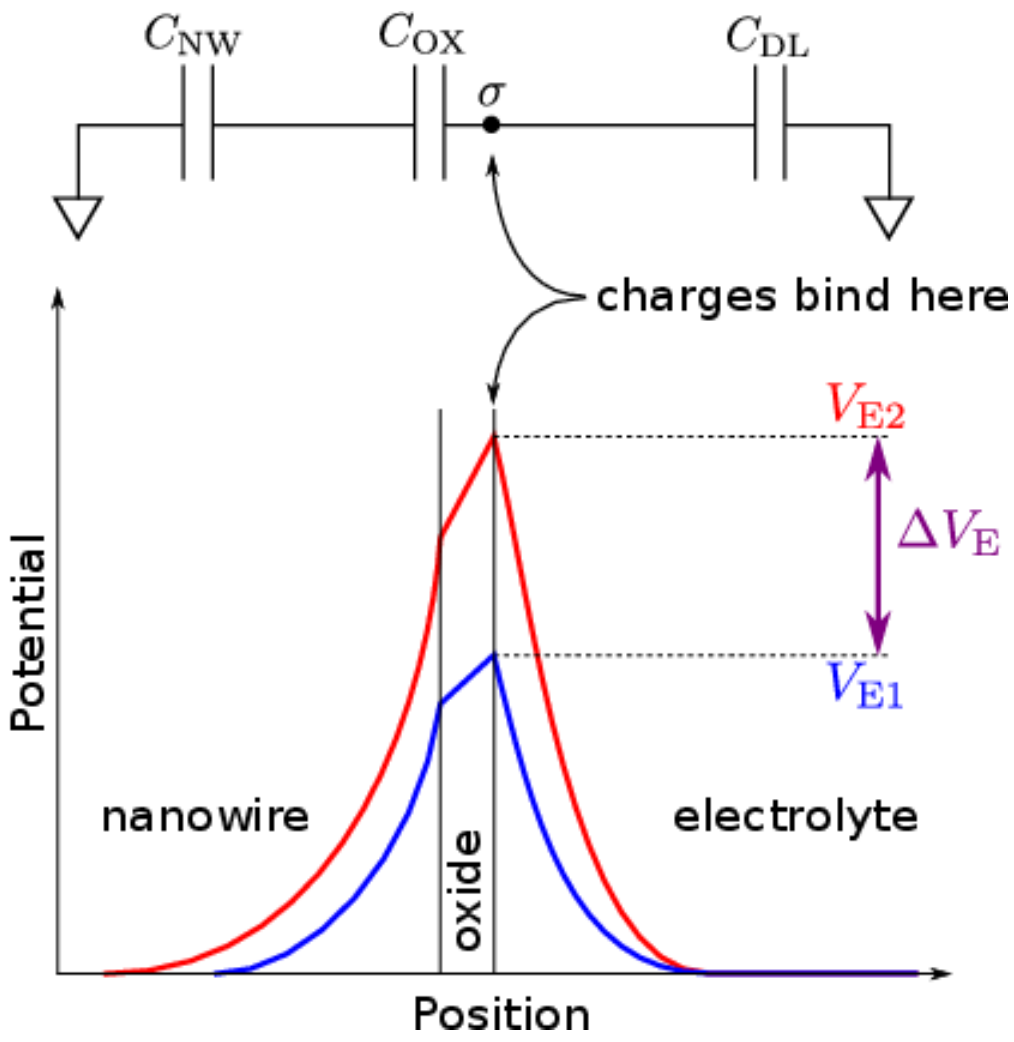


Figure 3.2: Schematic depiction of the potential diagram across a generic nanowire biosensor, as well as the capacitance divider that is seen by the biomolecules. This generic diagram applies to all structures of interest. $C_{DL}$, $C_{OX}$, and $C_{NW}$ represent the capacitances due to the diffuse layer in the electrolyte, the gate dielectric, and the mobile carriers in the nanowire, respectively. The blue and red potential diagrams correspond to the pre-binding and post-binding states of the sensor; *i.e.*, the blue diagram has only charged receptors at the oxide surface, whereas the red curve has both charged receptors and charged analytes. The analytes cause a potential change $\Delta V_E$ at the outer surface of the gate dielectric, which we consider to be the sensor's sensitivity. The potential change is screened, and decays with distance in the nanowire and electrolyte regions.

The local potential change near the biomolecules is determined by the following equation:

$$\Delta V = \frac{\Delta\sigma_{\mathrm{Bio}}}{C_{\mathrm{DL}} + C_{\mathrm{E}}} \tag{3.4}$$

In a real system such as a nanowire FET-based biosensor, $C_{\mathrm{E}}$ includes the "gate" dielectric capacitance between the FET and the electrolyte, $C_{\mathrm{OX}}$, in series with the semiconductor capacitance of the underlying FET, $C_{\mathrm{NW}}$. If the FET-part of the sensor is made of silicon, and is operated in the subthreshold regime as recommended [SC12, GZL10], the Debye length in the FET channel will be on the order of 40 $\mu$m, and the relative permittivity will be 11.7. The gate dielectric capacitance can be neglected when in series with the much smaller semiconductor capacitance. In stark contrast, the Debye length in the electrolyte, assuming physiological ionic strength, will be on the order of 1 nm, with a relative permittivity of 80. The electrolyte capacitance $C_{\mathrm{DL}}$ is therefore almost always dominant, allowing us to forego calculating the potential and capacitance of the sensor itself. At this point, the only meaningful dependence of a nanowire biosensor's sensitivity on its radius is through changes in electrolyte screening, i.e., the capacitance of the diffuse ionic layer, $C_{\mathrm{DL}}$.

### 3.2.2 Numerical Calculations

Taking advantage of symmetry allows simple structures to be reduced to 1D and solved analytically. However, for more complex geometries, the analytical calculation becomes intractable. We therefore used a numerical simulator [se] to solve Poisson's equation. The use of this simulator has the added benefit of solving drift-diffusion equations in the semiconductor regions, allowing us to directly extract drain currents, threshold voltages, and sensitivities.

We simulate two types of 3D nanowires, a) suspended in solution (suspended nanowire, SNW), and b) placed on an insulating substrate (nanowire-on-insulator, NWoI). The former is not commonly encountered in real biosensor systems, while the latter is very common. We also consider two cases of biomolecule binding: uniform functionalization (UF) where biomolecules bind to all dielectric surfaces, and selective functionalization (SF) where biomolecules bind only to the outer surfaces of the nanowires' gate dielectrics [PLP07]. Over-

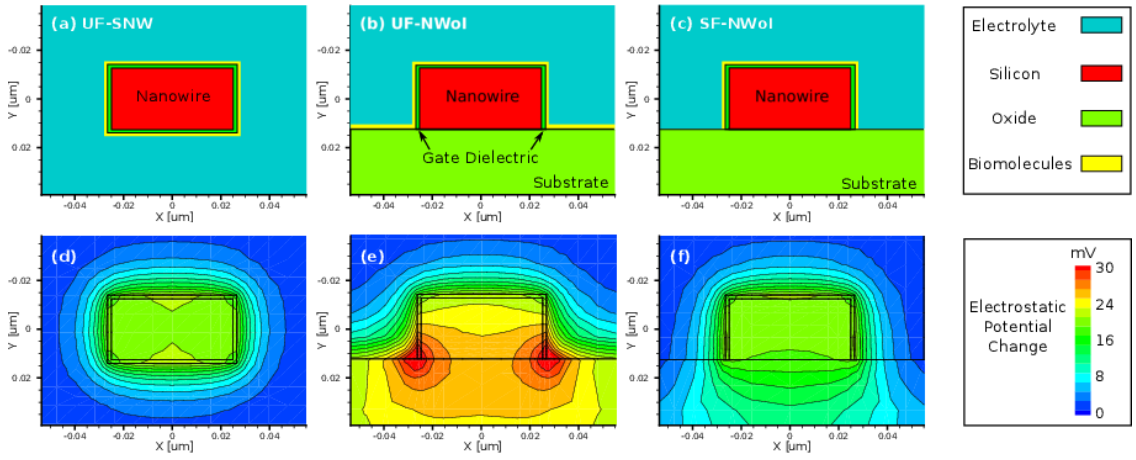


Figure 3.3: 2D cross-sectional plots of the simulation structure (a)-(c) and the *change* in electrostatic potential due to the charge of the biomolecules, taken across the center of the channel (d)-(f). Structures (a) and (d) depict the suspended nanowire case (UF-SNW), surrounded by electrolyte; (b) and (e) depict the nanowire-on-insulator case with biomolecules at all dielectric/electrolyte interfaces (UF-NWoI); (c) and (f) depict the selectively-functionalized nanowire-on-insulator case with biomolecules on the gate dielectric/electrolyte interface only (SF-NWoI). Note how the potential change is larger near the concave corners, and smaller near convex corners. The lower (concave) corners in (f) behave like a flat surface (for screening purposes), because there are charges only on the nanowire side of the corner. The yellow "Biomolecule" layers in (a)-(c) are artificially added for clarity to denote the locations where biomolecules are present; the simulated biomolecules have no thickness.

all the three structures depicted in Figs. 3.3(a-c) are considered: (a) UF-SNW, (b) UF-NWoI, and (c) SF-NWoI. The lack of a dielectric substrate makes selective functionalization meaningless for suspended nanowires. We vary the nanowire width in these structures and study the sensitivity behavior.

The nanowires are presumed to be silicon, covered by a thin dielectric; the outer surface of the gate dielectric is exposed to the electrolyte. The biomolecules were modeled as a sheet charge of uniform density of $10^{12}$ q.cm$^{-2}$ at the electrolyte/dielectric interface. Although in reality the molecules are discrete, the random nature of their binding will, on average, resemble a uniform layer of charge. The justification for our choice of biomolecule model is given in the Supporting Information section. The biomolecule density and electrode potentials were chosen to ensure that the sensor surface potential remained low enough to justify neglecting the finite size of the ions [TV80], and high enough to ensure accuracy in the presence of quantization errors. Further details of the simulation structure are given in the accompanying Supporting Information. The sensitivity, in the form of threshold voltage change $\Delta V_{\text{th}}$, which is proportional to $\Delta I/I$, is extracted and plotted as a function of nanowire radius for our different structure types.

## 3.3 Results

### 3.3.1 Analytical Results

First, we look at the electrostatic potential in the electrolyte as a function of distance from various simple surfaces, shown in Fig. 3.4. The electrostatic potential is normalized to the electrode potential $V_{\text{E}}$. The distances are normalized to the Debye length $\lambda$. All the curved surfaces in this figure have the same radius, equal to five Debye lengths. Note that this figure serves merely to compare the strength of screening near various surface geometries for a given electrode potential; in real bioFETs, the electrode potential is measured, not fixed.

The diffuse layer capacitances for the various geometries that were analyzed are given in Table 3.1 as a function of the radius of curvature. Here, I and K denote the modified

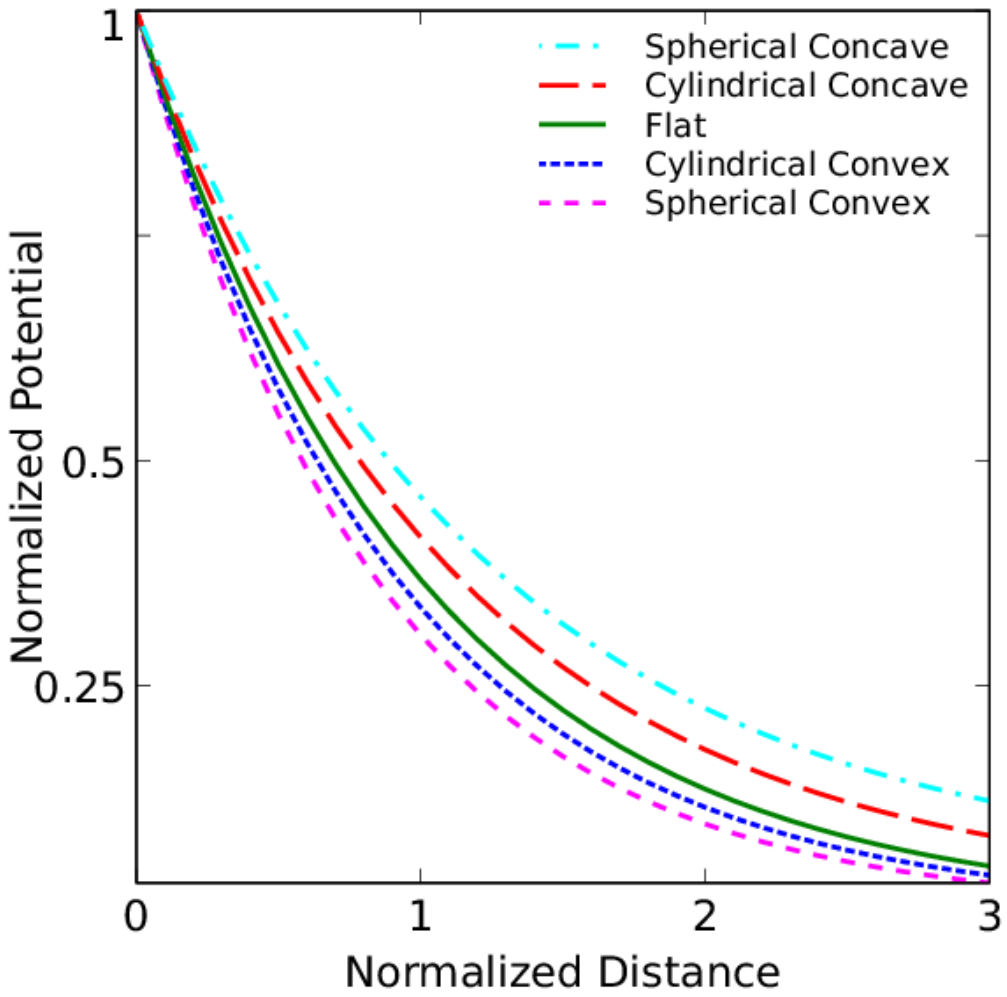


Figure 3.4: Plot of electrostatic potential in the electrolyte vs. distance from the surface of the electrodes. The distance is normalized to the Debye length $\lambda$, and the potential is normalized to the electrode potential $V_{\mathrm{E}}$ The radius of curvature of the curved surfaces is $5\lambda$.

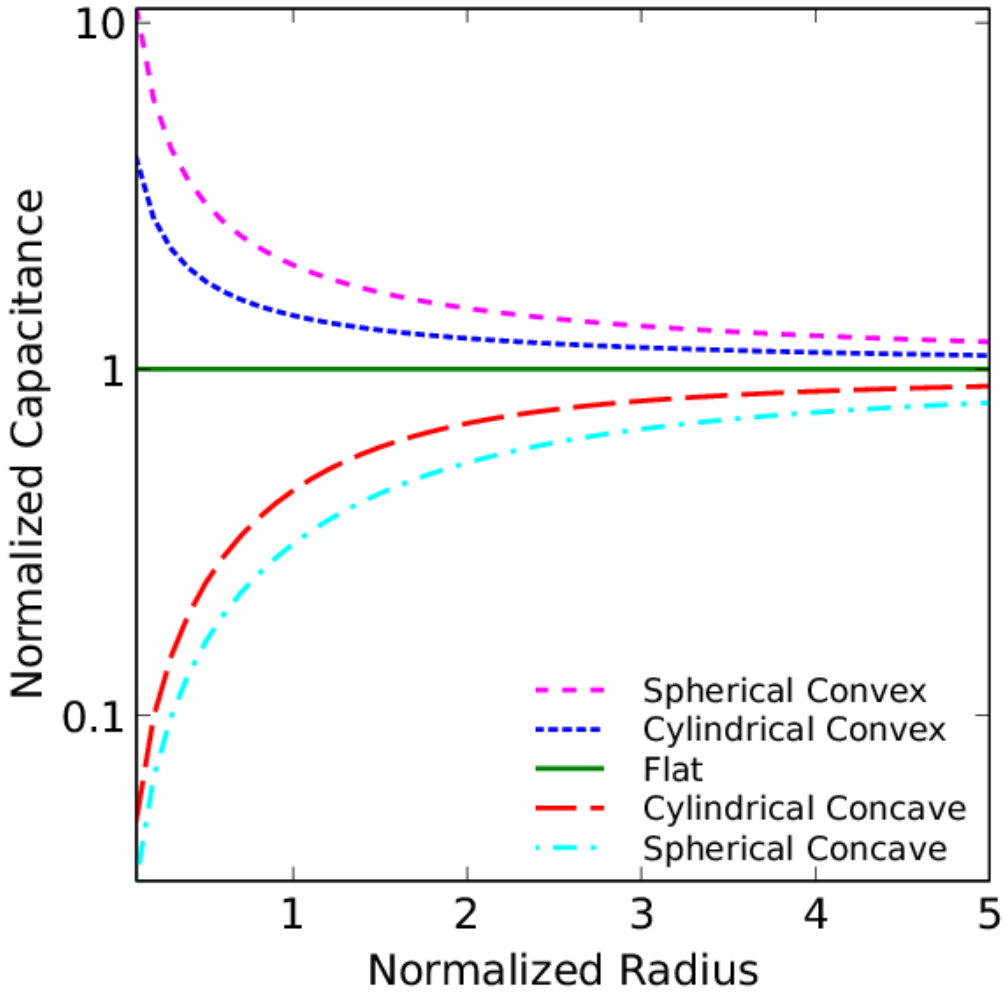


Figure 3.5: Plot of electrolyte capacitance density vs. radius of curvature of electrode. The radius is normalized to the Debye length $\lambda$, and the capacitances are normalized to that of the flat electrode. Note that the vertical axis is on a logarithmic scale.

Table 3.1: Capacitance of the diffuse layer near electrode with various geometries

| Structure | Screening Capacitance |
|---|---|
| Convex Spherical | $\frac{\epsilon}{\lambda}\left(\frac{x+1}{x}\right)$ |
| Convex Cylindrical | $\frac{\epsilon}{\lambda}\frac{\mathrm{K}_1(x)}{\mathrm{K}_0(x)}$ |
| Flat | $\frac{\epsilon}{\lambda}$ |
| Concave Cylindrical | $\frac{\epsilon}{\lambda}\frac{\mathrm{I}_1(x)}{\mathrm{I}_0(x)}$ |
| Concave Spherical | $\frac{\epsilon}{\lambda}\left(\coth(x)-\frac{1}{x}\right)$ |

Bessel functions of the first and second kinds, respectively; $\lambda$ denotes the Debye length in the electrolyte, $\epsilon$ denotes the permittivity of the electrolyte, $R$ is the radius of curvature, and $x \equiv \frac{R}{\lambda}$ is a dimensionless radius variable. The capacitance densities, normalized to that of the flat case, are plotted in Fig. 3.5 as a function of the dimensionless radius variable $x$.

### 3.3.2 Simulation Results

The simulations offer two sets of results. The first is a set of 2D cross-sectional plots of the *change* in electrostatic potential due to the charge of the biomolecules, taken across the center of the channel. These are shown in Fig. 3.3 (a), (b), and (c), for the three structure types, UF-SNW, UF-NWoI, and SF-NWoI, respectively. Contour lines are provided as a visual guide. Note how the potential change is smaller near convex corners, e.g. all the corners in Fig. 3.3(a), and the top corners in Fig. 3.3(b) and Fig. 3.3(c). Conversely, the potential change is larger near the concave corners, i.e. the bottom corners in Fig. 3.3(b). It is important to note that the bottom corners in Fig. 3.3(c) do not behave like a corner at all, because there are no biomolecules on the substrate, so there is no screening contribution

from that facet of the corner.

The second set of results is shown in Fig. 3.6 as a plot of the sensitivity vs. nanowire width for all three structure types.

## 3.4 Discussion

We begin our analysis with the analytical results in Fig. 3.4. This plot shows that the electrostatic potential drops more quickly to its bulk value when the surfaces are convex, and more gradually when the surfaces are concave. Both effects are more drastic for the spherical curvatures. A similar result was obtained by Dickinson and Compton [DC09] for hemispherical electrodes in the context of electrochemistry. This trend is a direct indicator of screening strength: concave surfaces experience less screening than a flat surface, whereas convex surfaces see more screening. It seems that the more the electrolyte surrounds the surface, the stronger the screening will be. Conversely, the more the surface surrounds the electrolyte, the weaker the screening will be.

Next, we calculated the capacitance due to the electrolyte, and from that, the sensitivity of the electrolyte to biomolecule charges. The results are plotted in Fig. 3.5 as a function of the radius of curvature of the surface. The increased screening near the convex structures is seen once again, this time in the form of increased capacitance, and over *all* radii. Similarly, concave structures always exhibit lower screening. Unsurprisingly, the effect is once again more drastic for the spherical surfaces. The potential change is intimately and inversely related to the capacitance, so concave surfaces exhibit higher sensitivity than convex surfaces over all radii.

Intuitively, this trend can be explained as follows: a convex curvature will allow a larger volume of solution to approach the surface, carrying with it more ions, leading to more screening. The opposite happens for the concave curvature. Moreover, a convex spherical surface allows more solution ions to approach a unit of surface area than a convex cylindrical surface, explaining the increased screening for the spherical convex case. A similar argument can be made for the spherical concave case.

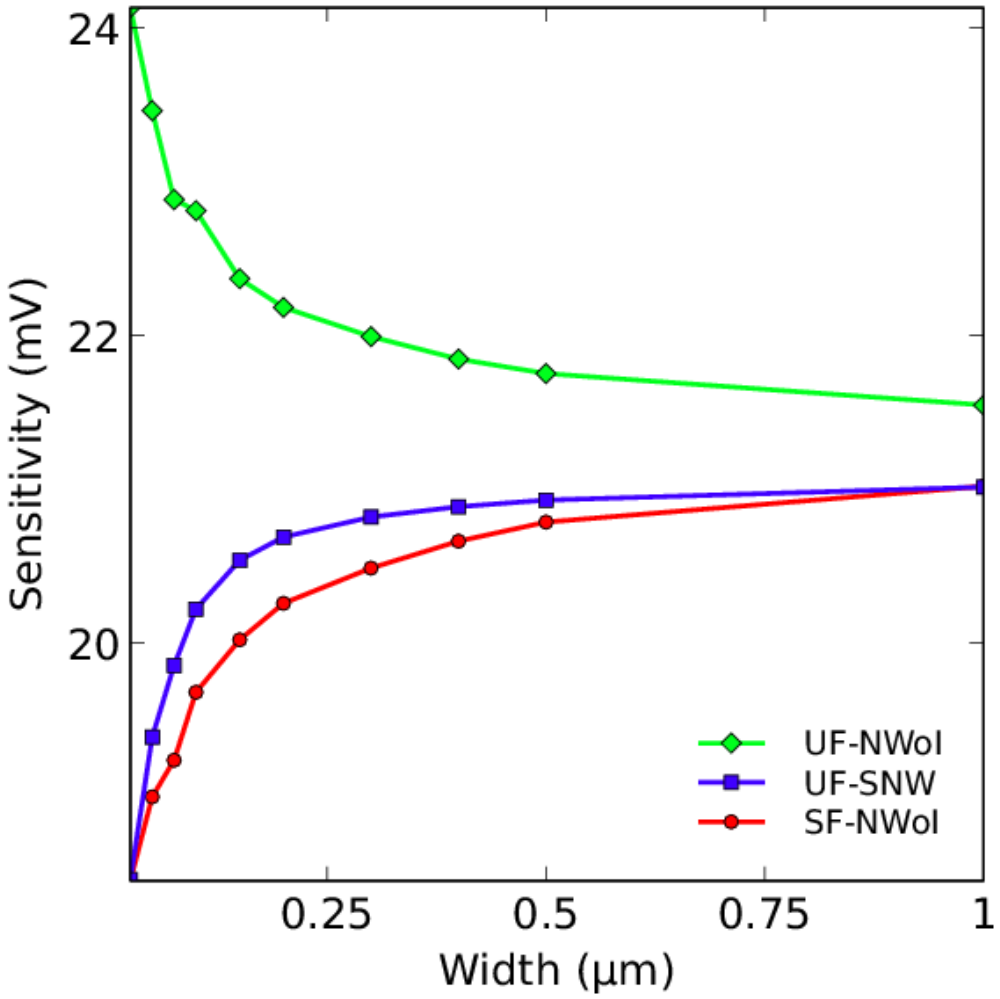


Figure 3.6: Plot of the simulated sensitivity vs. nanowire width for the UF-SNW (blue line with square markers), UF-NWoI (green line with diamond markers), and SF-NWoI (red line with circular markers). The sensitivity of the UF-NWoI improves with shrinking width, but those of the UF-SNW and SF-NWoI degrade. The sensitivities of all structures converge to the same value at large widths.

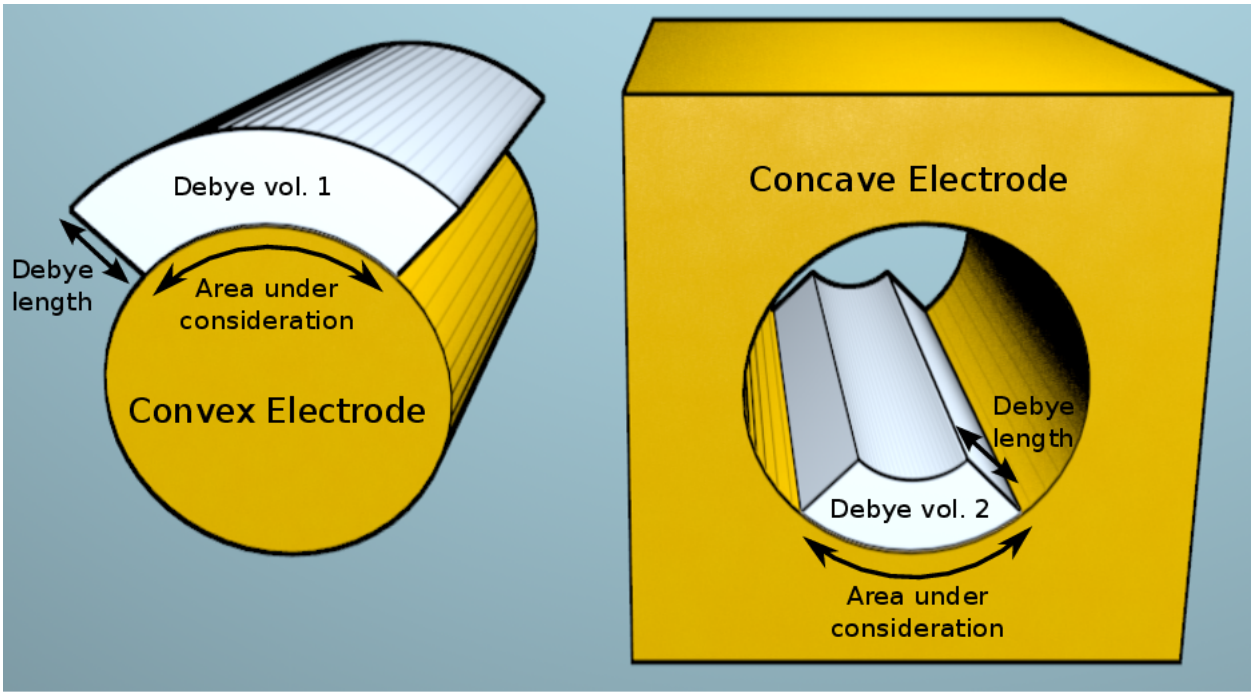


Figure 3.7: A sketch of the imaginary Debye volume of two electrodes. The structure on the left is a convex electrode, whereas (the pore of) the structure on the right is a concave electrode. The electrolyte environment has been omitted for clarity. The Debye volumes are part of the electrolyte environment, and are sketched here for one quarter of the electrode surfaces. The radii of curvature are equal, and so the surface areas under consideration are equal as well (marked with black curved double-sided arrows). The Debye length is marked with a straight double-sided arrow. Although the Debye lengths and surface areas under consideration are equal, the Debye volume belonging to the convex surface ("Debye vol. 1") is larger than that of the concave surface ("Debye vol. 2"). The variation in Debye volume depends on the relative size of the radius of curvature compared to the Debye length. The Debye volume is correlated with the screening strength, which is stronger near the convex surface relative to the concave surface. By qualitatively evaluating the Debye volume of arbitrary surfaces, one can get a rough idea of the relative screening strength near those surfaces.

We can extend our intuition further by loosely defining a "Debye volume" as the volume of electrolyte within one Debye length of a surface, similar to a Debye sphere in Plasma physics [Jac75]. This concept is depicted in Fig. 3.7. In this figure, we have two electrodes with cylindrical surfaces, one convex (similar to a nanowire) and one concave (similar to a pore). For clarity, we omit the bulk of the electrolyte environment from the drawing, and consider the Debye volume for only a fraction of the electrode surfaces. Due to the direction of the curvature, a patch of the surface of the concave electrode has a larger Debye volume than an equally-sized patch on the convex electrode, even though the Debye lengths are the same. Since this Debye volume is filled with counter-ions, it makes intuitive sense that the convex surface will have more counter-ions near it than the concave surface, and consequently will have stronger screening as well. To roughly compare the screening strength near surfaces with arbitrary geometry, we can compare the "surface-area-to-Debye-volume ratio": the smaller it is, the stronger the screening will be. Of course, there is no rigorous quantitative use for such a quantity; it is only an intuitive guide to help us design electrode structures with appropriate screening. For biosensing purposes, we should seek to increase the surface-area-to-Debye-volume ratio of electrodes. In nanoscale sensors where the semiconductor region shares a surface with the electrolyte, down-scaling dimensions and increasing the surface-area-to-volume ratio are inevitably accompanied by reduced surface-area-to-Debye-volume ratio, and hence, with increased screening and reduced sensitivity.

The simulation results convey the same idea. In all cases, the charge density is constant, so the potential change is a direct indicator of screening strength. In Fig. 3.3(a), the corners can be viewed as extremely small areas of extreme convexity; this results in increased screening and smaller potential change, which is directly apparent in the figure. Conversely, in Fig. 3.3(b), the corner between the NW and substrate is concave, giving rise to reduced screening and increased potential change. In Fig. 3.3(c), there are no charges on the substrate, so the lower corners have charges only on one of their sides. The contour lines are nearly parallel to the vertical side of the NW, indicating that the screening is similar to screening near a flat vertical surface; this indicates that the substrate side merely serves as an end to what otherwise behaves like a flat vertical surface.

In all structures, as the NW width is varied, the "size" of the corner regions remain unchanged. As the nanowires become wider, these corners constitute a smaller fraction of the total sensor surface, and their effect diminishes; eventually, all three structures begin to resemble a flat electrode. This is seen in the plots of sensitivity vs. width in Fig. 3.6, where all three curves converge to the same value for large widths. Conversely, as the width shrinks, the relative importance of the corner effect increases. The sensitivity of the UF-SNW structure decreases, since this structure has four convex corners. The SF-NWoI structure of Fig. 6 has two convex corners, and two neutral, so the sensitivity fares better than the UF-SNW structure. The UF-NWoI structure has two concave corners whose effect apparently dominates the convex corners, resulting in increased sensitivity with reduced width.

It is worth noting that the sensitivity of the suspended NW structure in Fig.3.3(a) decreases with shrinking width, even though its conventional surface-area-to-volume ratio increases. This indicates that contrary to conventional wisdom, increased surface-area-to-volume ratio does not cause enhanced sensitivity in nanowires.

Although we have only varied width in this study, similar results are expected for varying thickness: for a structure with more overall convexity, reducing surface area harms sensitivity, and should be avoided; conversely, if the structure has more overall concavity, reducing the total surface area will increase sensitivity. The latter case applies to nanowires, so long as biomolecules can bind to the substrate as well.

There is an alternative way to analyze the results above, as follows: of all the biomolecules that bind to the substrate, the few who are within a certain distance of the nanowire are capable of influencing it. The quantity of these biomolecules is independent of the nanowire size. They provide an extra boost to the sensitivity in addition to the biomolecules that bind directly to the nanowire. As the nanowire shrinks, the relative importance of the substrate-bound biomolecules increases, increasing the overall sensitivity.

## 3.5 Conclusions

Although the Gouy-Chapman model is over a century old, the results of it's application to non-planar structures is not well known in the biosensor community. The conclusion is rather simple: screening is weaker near concave surfaces, and stronger near convex surfaces. We believe understanding the effects of curvature on Debye screening enables us to design better electrode surfaces. Although such optimizations have not been discussed here, the surface-area-to-Debye-volume ratio is a concept that could be of use in such optimization efforts. We hope the insight gained here will be useful for other sensor systems in which electrostatics are important, such as FET-based sequencing technologies [RHR11] or nanopore sensors [RBR12].

Our analysis has also enabled us to determine that increased surface-area-to-volume ratio is not responsible for the sensitivity enhancement that accompanies quasi-1D nanoscale biosensor structures. Instead, it is the overall concavity of the structure, and the binding of biomolecules in concave areas, that results in higher sensitivity. This finding has important implications for the future of bioFETs: efforts are underway to increase the limit of detection (LOD) of bioFETs by ensuring that biomolecules bind only to the NW directly [PLP07, KCM13]. However, the conventional wisdom – that nanoscale structures are more sensitive – fails in this regime. It should be noted, however, that our crude modeling of the biomolecules as a uniform sheet of charge neglects many factors that become important when one seeks to detect samples with very low concentrations of analytes. Further studies should include the intricacies of ion and biomolecule size, and the finite supply of biomolecules when analyte concentrations are near the LOD.

# CHAPTER 4

# On the Necessity of a Solution Electrode for BioFET Operation

## 4.1 Overview

It is the opinion of this author that the true mechanism of bioFET operation is frequently misunderstood. While the physics behind the device's operation is quite basic, the apparent complexity and the multidisciplinary nature of the bioFET itself makes it difficult to apply basic physical concepts to the system in order to derive useful insights. We will therefore dedicate this chapter to using basic physical intuition to shine light on an aspect of bioFET operation that is commonly overlooked.

The usefulness of these insights will become apparent when one tries to actually design and operate a bioFET. There are many decisions that must be made regarding the details of a bioFETs structure and operation. The analysis presented here were actually born out of a desire to answer one such question.

In this chapter, we wish to determine whether it is truly necessary, for the correct operation of a bioFET, to include a reference electrode in measurements. A reference electrode, if used, would be contacting the sample solution. Reference electrodes are bulky items, and they negate the promise of miniaturization afforded by bioFETs. Due to the high impedance nature of the interface between the solution and the FET, without a reference electrode, the solution can pick up the spurious electromagnetic signals from the surrounding environment. This phenomenon is not what we intend to study; we assume the measurements are done in a Faraday cage with no ambient light present. Instead, we wish to know if the presence of

an electrode by which we can set the electric potential of the sample-under-test is necessary for bioFET operation. As such, by "reference electrode", we mean any such electrode that can set the potential, so from here on, we shall refer to it as "solution electrode" or simply "electrode". We ignore all non-ideal chemical processes at the surface of the electrode.

This debate was settled for the case of ISFETs long ago, and it was decided early on that solution electrodes were indeed necessary in order to bias the FET, [BR79, Ber03]. However, with the advent of nanowire bioFETs, many experiments were reported in the literature in which no solution electrode was used, yet surprisingly, positive results were obtained. Some researchers have expressed surprise at the success of these experiments, because based on established ISFET theory, they expect that a bioFET requires a solution electrode as well [PCI05]. The reason for the satisfactory operation of these bioFETs has not been uncovered to date, nor has it been conclusively established that their results are incorrect.

To understand if a solution electrode is necessary, we use analytical calculations and TCAD simulations to see what happens if a solution electrode is not used. We first consider the large-signal response of the bioFET (i.e, its bias point) when a solution electrode is not provided. Subsequently, we will discuss the small-signal response of the bioFET to biomolecule charge in the absence of a solution electrode. When discussing biasing, we limit our discussion to bioFETs that can be biased means other than the front gate, such as nanowire bioFETs that have a back gate. BioFETs with only one gate, such as ISFETs and ImmunoFETs made out of bulk silicon [GSK89], must include a solution electrode to bias the FET and turn it on. In rare cases, the threshold voltage can be adjusted so that at zero bias the FET is at its desired operating point; such cases are rare. The only such example that comes to mind is the work of Casal et al. [CWG12].

As such, we shall assume that proper biasing is attempted by some means other than the solution electrode, so that without the electrode, the FET is assumed to operate properly.

## 4.2 Analytical Theory

### 4.2.1 Drift and Irreproducibility in the BioFET Bias Point

Without a solution electrode, the sample solution is effectively floating. The only electrical connection to the sample will be via parasitic leakage paths, and leakage through the gate oxide of the bioFET itself. For now, we assume all these to be negligible.

For simplicity, we assume the sample solution is initially uncharged. We note that it is unclear whether the sample solution will pick up static charge during handling. If any static charge is present in the sample solution, it will either discharge itself via the solution electrode in cases where an electrode is included, or will eventually discharge via parasitic leakage paths that are to be discussed later. Therefore such static charge will only serve to shift the initial bias point of the bioFET, and it will not affect the analyis presented here; we are therefore justified in assuming the sample solution has zero net charge. Note that the charge on biomolecules is due to dissociation of hydrogen from oxygen on the hydroxyl groups, or addition of hydrogen to nitrogen on amine groups on these molecules. These and other chemical processes do not alter the net charge of the solution.

Without a solution electrode, the potential of the sample will be determined by capacitive couplings to various bioFET terminals. A nanowire bioFET typically has a source, a drain, and a back-gate. The connection to these terminals is schematically shown by the circuit diagram of Fig. 4.1.

Care should be taken in using the term "potential". In the context described above, the sample solution is "connected", albeit capacitively, to the bioFET's terminals. These terminals are "reservoirs" from a statistical mechanical point of view, and therefore have a fixed *electrochemical* potential. The connection of the sample solution to these reservoirs in turn sets the electrochemical potential of the sample solution, since these reservoirs have the *potential* to drive *steady* current through the sample solution. In contrast, the biomolecules that are captured at the sensor surface cannot cause steady current to flow; these biomolecules therefore only change the local *electrostatic* potential. The only current

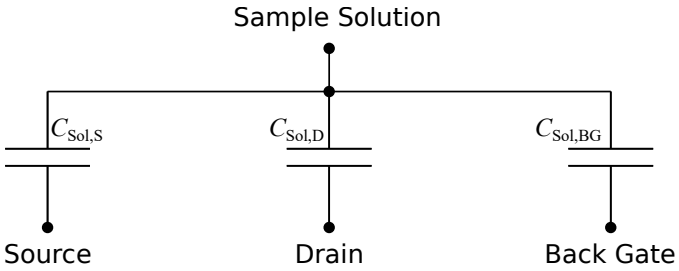


Figure 4.1: Capacitive connection of solution to various FET terminals. If the underlying FET is a specific structure with more terminals, capacitive connections to those terminals would be included accordingly.

flow directly caused by the biomolecules is a transient rearrangement of charge in the vicinity of where they bind. Of course, the biomolecules also cause the bioFET current to change, although this is an indirect effect, caused by a change in the carrier concentration in the bioFET channel, which is in turn a result of the electric field that begins at the biomolecules and terminates in the bioFET channel. The electric field itself does not directly cause steady current to flow.

Having cleared up the meaning of "potential", we calculate the (electrochemical) potential in the bulk of the sample solution as follows:

$$V_{\mathrm{Sol}} = \sum_i \frac{C_{\mathrm{Sol},i} \times V_i}{C_{\mathrm{Sol},i}} \tag{4.1}$$

where $i$ runs over all the terminals of the bioFET, $V_i$ denotes the potentials at these terminals, $V_{\mathrm{Sol}}$ denotes the potential in the bulk of the solution, and $C_{\mathrm{Sol},i}$ denotes the capacitance between the solution and the $i$th terminal of the bioFET.

Since the potential of the solution is $V_{\mathrm{Sol}}$, the bioFET's front-gate (which is its biologically sensitive gate) will be biased as if a solution electrode was present and its (inner) voltage set to $V_{\mathrm{Sol}}$, neglecting interfacial potential differences. Obviously, any charge leakage anywhere would disturb $V_{\mathrm{Sol}}$, so for now, we assume the front-gate oxide of the FET is perfectly insulating. With this assumption, $V_{\mathrm{Sol}}$ will remain unchanged in perpetuity.

Nevertheless, we must at least consider the qualitative effects of leakage currents to or from the sample solution to various bioFET terminals and the system ground. Sources of

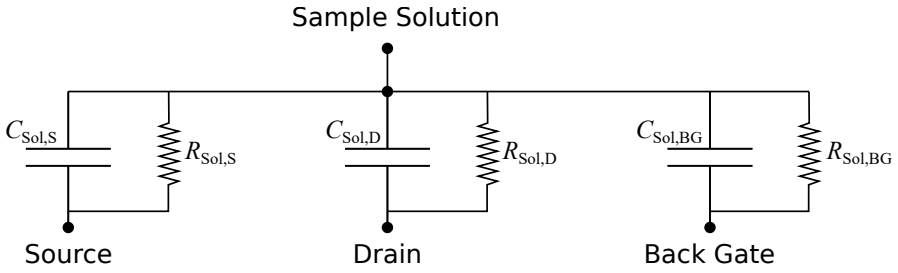


Figure 4.2: Capacitive connection of solution to various FET terminals. If the underlying FET is a specific structure with more terminals, capacitive connections to those terminals would be included accordingly.

leakage may range from pinholes in the encapsulation, to tunneling across the front oxide, to leakage through moisture adsorbed on the chip. These sources of leakage are typically parasitic and uncontrolled, so their precise value is not known. We shall represent them as resistors in the equivalent circuit model, shown in Fig. 4.2, having in mind that their "resistance" is effectively voltage dependent.

With this equivalent circuit, the value of $V_{\mathrm{Sol}}$ will drift over time. The initial value will be given by equation 4.1, but its final value will not depend on the capacitances at all; instead, it will depend on the leakage rates, which are typically uncontrolled and unknown. If the resistors were truly linear, the steady-state value of the electrochemical potential in the bulk of the sample could be calculated as follows:

$$V_{\mathrm{Sol}} = \frac{\sum_i \frac{V_i}{R_{\mathrm{Sol},i}}}{\sum_i \frac{1}{R_{\mathrm{Sol},i}}} \tag{4.2}$$

where as before, $i$ runs over all the terminals of the bioFET, $V_i$ denotes the potentials at these terminals, $V_{\mathrm{Sol}}$ denotes the potential in the bulk of the solution, and $R_{\mathrm{Sol},i}$ denotes the "resistance" between the solution and the $i$th terminal of the bioFET.

The results of these simple equations are can be summarized in two points:

1. The bias point set for the bioFET via its front oxide will begin from a value determined by the capacitive divider of equation 4.1.

2. There will be an initial transient, after which the bioFET current will reach a steady-state value set by leakage current rates to and from the liquid sample, which are usually undetermined, as expressed in equation 4.2.

The second point is particularly problematic. Successful measurement of analyte concentrations during the initial bioFET transient requires a precise knowledge of the time dependence of the drain current during the transient period. This knowledge is usually hard to come by, because the transient current depends heavily on the bioFET bias, which in turn depends on unknown leakage rates and capacitance values. This fact holds despite the initial assumption that the bioFET is biased via other means. For example, the back-gate can be used to the bias the nanowire in a desirable regime of operation, but the nanowire is still far more sensitive to potential changes at its front gate, because the front gate oxide is typically much thinner.

One could wait until the transient period has run its course and steady-state is reached. However, the leakage current rates can be affected by environmental conditions (e.g. ambient moisture) or inadvertent variations in the setup (e.g. changes in size of the liquid sample), so the steady-state value of the bioFET's front-gate bias, and in turn, the bioFET's drain current, will be affected by these factors as well. Repeated measurements of the same sample could yield different results. This lack of reproducibility is effectively a source of random error in the measurement in addition to the usual sources of bioFET drain current noise, and will reduce the measurement resolution and raise the lower limit of detection.

Practically speaking, this source of error could either pose a huge problem, or no problem at all, depending on the relative magnitude of the leakage currents. If the current leakage to one terminal is always significantly larger than other leakage paths, the potential of the liquid sample will always settle to the voltage of that terminal, and variations will be minimized.

It should be noted that in cases where the leakage is mostly to the bioFET channel, there may be a feedback effect where the bioFET's bias point will affect the leakage rate, and the leakage rate will in turn affect the bioFET bias point. In such a scenario, more than one stable operating point may exist. Further studies are necessary to determine the actual

outcome in such cases, and the degree to which any of the practical bioFET designs would suffer from such a problem.

The analysis so far does not assume anything particular to the structure of the device, number of terminals, mechanism of leakages, sources of capacitances, or the values of these quantities. The results are therefore very general.

There are two general ways to mitigate this problem. First is to identify all the significant leakage paths, measure the leakage rates, and design the measurement setup so as to minimize variations. Second is to deliberately include a leakage path that dominates all others; in effect, including a solution electrode.

### 4.2.2 Signal Return Path

Gauss' law dictates that the electric flux exiting a region is proportional to the charge enclosed within it. Since the sample solution is neutral, the net electric flux leaving the sample solution must be zero. The detection of charged biomolecules requires an electric flux to leave the sample solution and enter the bioFET, so an equal amount of electric flux must enter the sample via some other path. Since we assume no solution electrode is present, the flux is therefore entering via an uncontrolled path(s). This uncontrolled path(s) represent a parasitic capacitance(s) $C_{\text{par}}$ to the outside world. There may be many parasitic capacitances to various different places, but these will be lumped together, as we shall see shortly. For the sake of simplicity, we assume these capacitances connect the sample solution to the terminals of the bioFET. These capacitances can be considered as return paths for the electric flux, which is the signal that we detect.

As mentioned in previous chapters, the charge of the biomolecules is a small-signal disturbance over the bias point of the bioFET. As such, we can describe the system with a small signal equivalent circuit model, where the bioFET channel and all its terminals are considered small signal ground. However, contrary to the models in the previous chapters, the sample solution is not connected to small-signal ground directly; we must therefore include a parasitic capacitive connection $C_{\text{par}}$ which couples the droplet to small-signal ground.

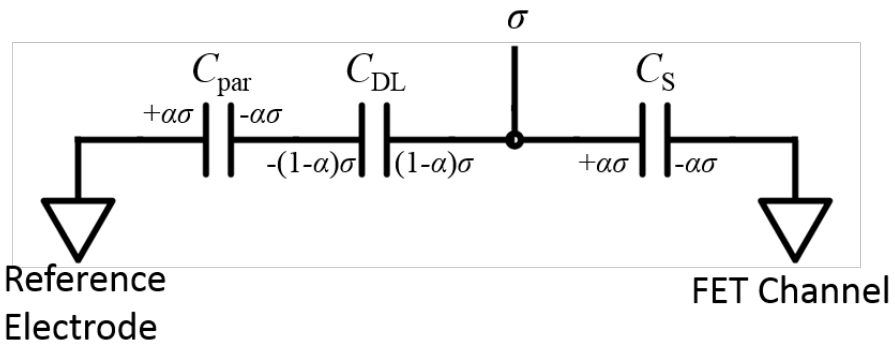


Figure 4.3: Equivalent circuit model of bioFET detection without a reference electrode. A capacitance $C_{\text{par}}$ serves as a return path for the signal emanating from the biomolecules. A fraction $\alpha$ of the total charge $\sigma$ is detected by the bioFET.

Although there may be more than one capacitance connecting the sample to more than one terminal, since all the terminals are considered as small signal grounds, these capacitances are all effectively connected in parallel and their values can be added together to obtain an equivalent capacitance. So $C_{\text{par}}$ can be interpreted as the total capacitance between the sample solution and small-signal ground. The equivalent circuit model is shown in Fig. 4.3. In this model, $C_{\text{S}}$ represents the capacitance to the small-signal ground via the bioFET channel, and $C_{\text{DL}}$ represents the double-layer capacitance in the sample solution. The equivalent circuit model when a reference electrode is included is shown again as Fig. 4.4, in which $C_{\text{par}}$ no longer appears, and the sample solution is connected to small signal ground directly.

We note that if the capacitive connection to the bioFET channel is accurate when the bioFET is "turned on", and so the channel is quite conductive. However, if the bioFET is operated in the subthreshold regime, then one would need to consider the effects of the finite resistance between the channel and the bioFET terminals. The effect of this resistance would simply be to limit bandwidth, and since we are not concerned with transient effects in this chapter, we can ignore the effects of such resistances, and treat the bioFET channel as small-signal ground for DC or slowly varying perturbations.

Now, we consider the effect of biomolecules being captured at the bioFET surface. These bring a surface charge density $\sigma$ to the bioFET surface. We assume only a fraction $\alpha\sigma$ is

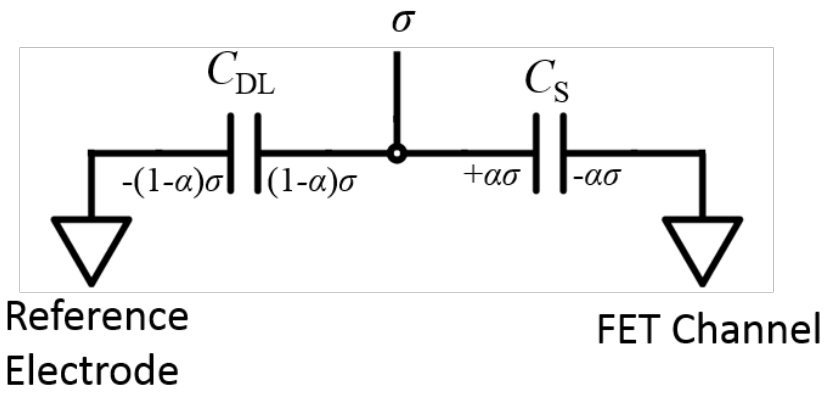


Figure 4.4: Equivalent circuit model of bioFET detection with a reference electrode. A fraction $\alpha$ of the total charge $\sigma$ is detected by the bioFET.

detected by the bioFET, so $-\alpha\sigma$ is induced in the bioFET, with $0 \leq \alpha \leq 1$. A fraction $(1-\alpha)\,\sigma$ is lost to Debye screening by counter-ions in the sample solution.

Since the sample solution is floating, its total charge can be considered constant; so if $(1-\alpha)\,\sigma$ is induced in the double layer at the surface of the bioFET, $-\alpha\sigma$ must appear across $C_{\text{par}}$. Note that the sample solution is taken as the "positive" polarity side of $C_{\text{Sol}}$, whereas the oxide/solution interface is taken as the positive polarity of capacitors $C_{\text{DL}}$ and $C_{\text{S}}$.

We continue in order to calculate $\alpha$. When a solution electrode is present, the model depicted in Fig. 4.4 is solved trivially:

$$\alpha = \left(1 + \frac{C_{\text{DL}}}{C_{\text{S}}}\right)^{-1} \tag{4.3}$$

When a solution electrode is not present, we continue by invoking Kirchoff's voltage law:

$$\Delta V_{\text{Sol}} - \Delta V_{\text{DL}} - \Delta V_{\text{G}} = 0 \tag{4.4}$$

where each term represents the potential change across its respective capacitor due to the capture of biomolecules. The potential change across the bioFET's gate oxide is denoted by $\Delta V_{\text{G}}$.

We rewrite each term in the above equation using the fraction of charge induced across

each capacitor:

$$\frac{-\alpha\sigma}{C_{\mathrm{Par}}} + \frac{(1-\alpha)\,\sigma}{C_{\mathrm{DL}}} - \frac{\alpha\sigma}{C_{\mathrm{S}}} = 0 \tag{4.5}$$

and then rearrange to solve for $\alpha$:

$$\alpha = \frac{1}{1 + C_{\mathrm{DL}}\left(\frac{1}{C_{\mathrm{S}}} + \frac{1}{C_{\mathrm{par}}}\right)} \tag{4.6}$$

Equation 4.6 highlights an interesting phenomenon: previously, in the case with a solution electrode, $\alpha$ was smaller than one, which meant that we are not able to detect all of the biomolecules' charge. The responsible mechanism was Debye screening, and the relative magnitude of Debye screening compared to the capacitive coupling of the biomolecule charge to the bioFET channel determined $\alpha$; hence the appearance of $C_{\mathrm{DL}}$ and $C_{\mathrm{S}}$ in equation 4.3. However, when a solution electrode is omitted, $\alpha$ depends on $C_{\mathrm{par}}$ as well.

The mechanism for this dependence is no longer Debye screening; instead, it can be traced back to $\Delta V_{\mathrm{par}}$ which can be written in terms of the charge across $C_{\mathrm{par}}$:

$$\Delta V_{\mathrm{Sol}} = \frac{-\alpha\sigma}{C_{\mathrm{Par}}} \tag{4.7}$$

Combining equations 4.6 and 4.7, we can isolate $\Delta V_{\mathrm{Sol}}$:

$$\Delta V_{\mathrm{Sol}} = \frac{-\sigma}{\left(C_{\mathrm{Par}} + \frac{C_{\mathrm{DL}}C_{\mathrm{par}}}{C_{\mathrm{S}}} + C_{\mathrm{DL}}\right)} \tag{4.8}$$

Given that we have assumed $\sigma$ to be positive, the result above means that the detection of positively charged particles causes $\Delta V_{\mathrm{Sol}}$ to become negative; i.e., the potential of the sample solution actually drops. When $C_{\mathrm{par}}$ is large, the drop in $V_{\mathrm{Sol}}$ is negligible. However, when $C_{\mathrm{par}}$ vanishes, we have:

$$\Delta V_{\mathrm{Sol}} = \frac{-\sigma}{C_{\mathrm{DL}}} \tag{4.9}$$

This is an intriguing result, which is not seen when a solution electrode is included, because a solution electrode does not allow the potential of the sample solution to change. This shift in the negative direction works against the intended effect of the biomolecules' (positive) charge, which is to *increase* the potential at the oxide/solution interface.

We can take also $C_{\text{par}}$ to its limits to gain some further insight regarding $\alpha$. If $C_{\text{par}}$ approaches infinity, equation 4.6 reduces to 4.3:

$$\lim_{C_{\text{par}} \to \infty} \alpha = \frac{1}{1 + \frac{C_{\text{DL}}}{C_{\text{S}}}} \tag{4.10}$$

This is no surprise, since having a solution electrode prevents the potential of the bulk of the sample solution from changing, and in this regard is akin to having a very large capacitance to ground. This setup maximizes the achievable value of $\alpha$.

When $C_{\text{par}}$ is zero, which means there is no capacitive coupling to anywhere, $\alpha$ vanishes:

$$\lim_{C_{\text{par}} \to 0} \alpha = 0 \tag{4.11}$$

This result is forced by Gauss' law. A nonexistent $C_{\text{par}}$ means there is no other source of electric flux for the sample solution, so no electric flux can exit the sample towards the bioFET, regardless of how much surface charge there is, or what the magnitude of $C_{\text{DL}}$ and $C_{\text{S}}$ may be.

Thus, not having a solution electrode can cause two problems:

1. The fraction of the biomolecule charge that is detectable by the bioFET drops.
2. If $C_{\text{par}}$ is not well-controlled, then it could vary between repeated measurements of the same sample, resulting in another source of random error.

Both of these effects can be countered by either including a solution electrode, or ensuring that a $C_{\text{par}} \gg C_{\text{S}}$ exists so that $\alpha$ can approach its maximum value, and variations in $C_{\text{par}}$ do not cause the value of $\alpha$ to change appreciably.

## 4.3 Simulations

Using TCAD to simulate the aforementioned scenario helps to convey the ideas discussed above. We note that Gauss' law, which was used to arrive at the conclusions above, is one of the basic equations solved by TCAD, so TCAD simulations should not be viewed as

validation of the aforementioned concepts. In fact, the TCAD simulations were actually run first, and the peculiar results obtained prompted the author to study the problem further in order to elucidate the mechanism responsible for these results, which was presented above in a very basic and general way.

Up until now, all the simulations shown in previous chapters have had an electrode contacting the solution, thereby precisely setting its potential. This is in line with all modeling papers on bioFETs. Modeling papers either explicitly include a solution electrode (typically a reference electrode) [LAM05], or implicitly do so by fixing the Fermi level in the solution [SC12], assuming that the electric field decays to zero at infinity [NA07], or assuming that the solution can become charged in order to screen the charge of the bound analytes [SMB07].

We therefore begin with simulations that correctly mimic the floating nature of the sample solution, and then use analytical arguments to analyze the simulation results.

As in previous chapters, we used Sentaurus TCAD to simulate a structure that included a solution and an FET. However, we used a "charge" type electrode specification to tell Sentaurus that the solution is effectively a floating region, with a net charge of zero.

Nanowire bioFETs are the most common type of bioFET, and they are most affected by the lack of a solution electrode. As such, we simulated and studied a nanowire bioFET, although the conclusions we arrived at are general enough that they can be applied to almost all bioFETs.

For the sake of simplicity, we assumed that all the insulators in the simulation were perfect insulators. The TCAD we used, Sentaurus Device, cannot handle floating regions and leaky insulators at the same time very well.

We simulated both a 3D model and a 2D cross section (lengthwise) of a nanowire bioFET. In the 3D case, the nanowire was rectangular, with a height and width of 25 nm each. It had a source and drain region, each 100 nm long, and doped $1 \times 10^{20}\,\mathrm{cm}^{-3}$ $n$-type. The channel itself was 100 nm. The source was "grounded" and the drain voltage was set to 100 mV, so short channel effects are not a concern here. The solution region, as before, was modeled as a semiconductor with a wide bandgap, and an effective density of states chosen such that

the carrier concentration in the solution would be $6.022 \times 10^{17}\,\mathrm{cm}^{-3}$, corresponding to an ionic strength of 1 mM. A height of 100 nm of solution region was included in the simulation, which is equivalent to about 10 Debye lengths at the ionic concentration simulated. This was far enough to ensure that the size of the simulation domain did not affect the simulation results. The solution "length" was 100 nm, so 50 nm from each side of the channel was not exposed to it, effectively modeling "underlap". The areas above the source and drain, and above the "underlap" region of the channel, were covered with oxide to mimic encapsulation. The nanowire was covered with a 1.5 nm layer of oxide, which is about the same thickness as the native oxide on silicon. Although we should note that Sentaurus assumes this insulator to be leak-free, whereas native oxide is actually very leaky. The buried oxide was assumed to be 145 nm thick. Biomolecules were modeled as a sheet charge with uniform density $\sigma = 1 \times 10^{13}\,e\,\mathrm{cm}^{-2}$; this sheet has no thickness. The amount of biomolecule charge is larger than what we had simulated in previous chapters, in order to dramatize the response for the sake of clarity. In some cases, the biomolecules were only on the gate oxide of the nanowire, but in other cases, the biomolecules covered the buried oxide as well, the latter being a more realistic situation. We note that many of these numbers are not realistic at all; their purpose is to help elucidate the qualitative behavior of the system. In all simulation "experiments", the simulations were run twice: once with no biomolecules, and once with them, and the difference was taken and plotted. Due to the superposition principle in electrostatics, this difference completely cancels out the effects of biasing, and only shows the electric fields and potentials that result from the presence of biomolecular charges. The simulated 3D structure is shown in Fig. 4.5.

The first simulation experiment we ran was to simply vary the $C_{\mathrm{par}}$ that is intrinsic to the structure, and measure the change in sensitivity (defined as $\Delta I/I$). In the case of 3D simulations, much of $C_{\mathrm{par}}$ comes from the coupling between the sample solution and the back-gate, via the buried oxide. We simply increased the simulation domain in order to change the contact area between the solution and the buried oxide. No other parameter was changed. The simulated structures are shown in Fig. 4.6. For these simulations only, the bioFET was biased in the linear regime, so as to increase semiconductor capacitance $C_{\mathrm{S}}$, and

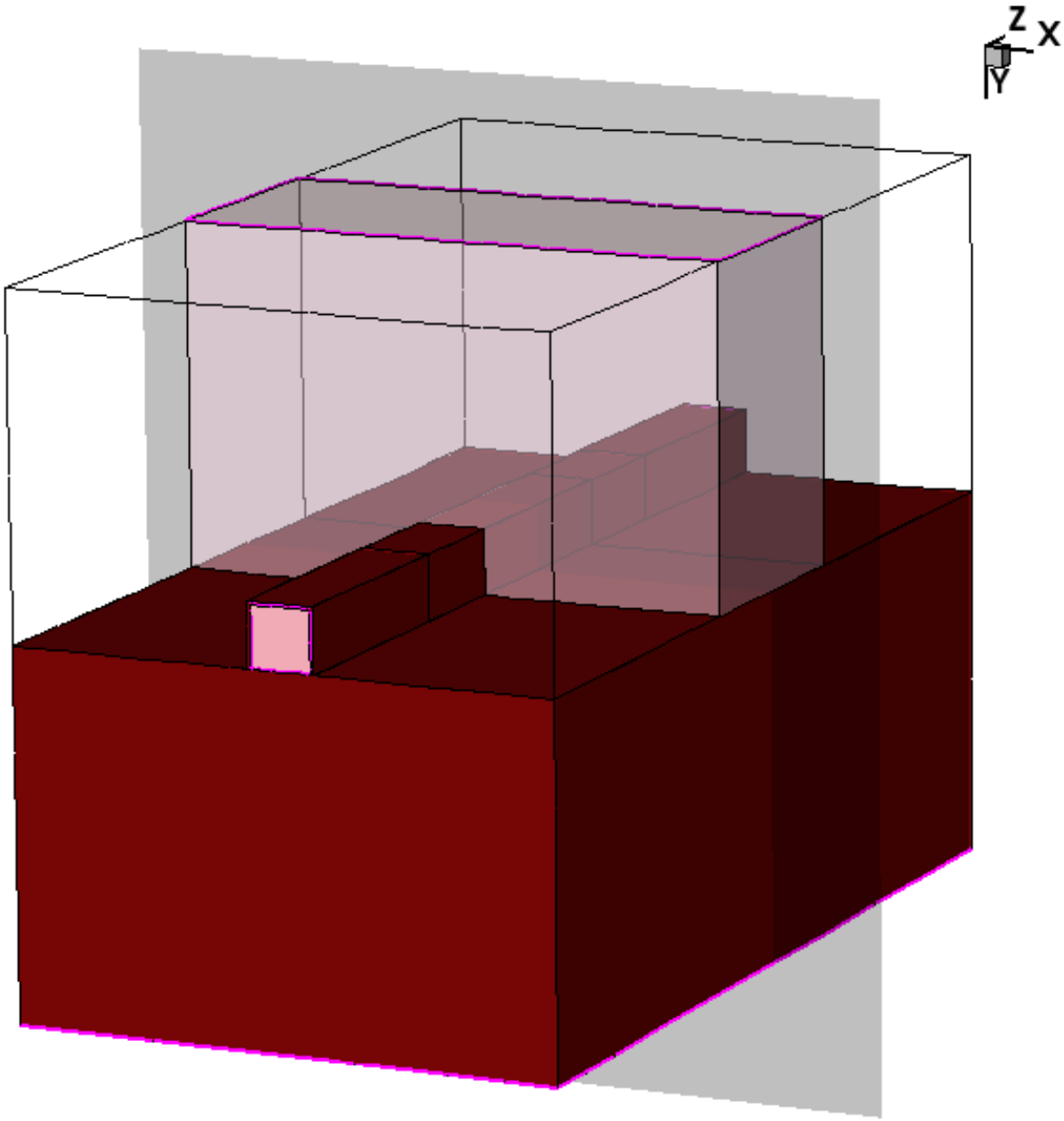


Figure 4.5: The 3D simulation structure. The translucent pink region is the solution, and the maroon-colored regions are oxide. The nanowire itself is seen in opaque pink. An electrical contact is defined at the very bottom of the structure, under the buried oxide. The encapsulation regions are omitted in the image for clarity, although their outline is visible. The gray plane that cuts through the structure denotes the location of the 2D cut that is shown in Figs. 4.7a and 4.7b.

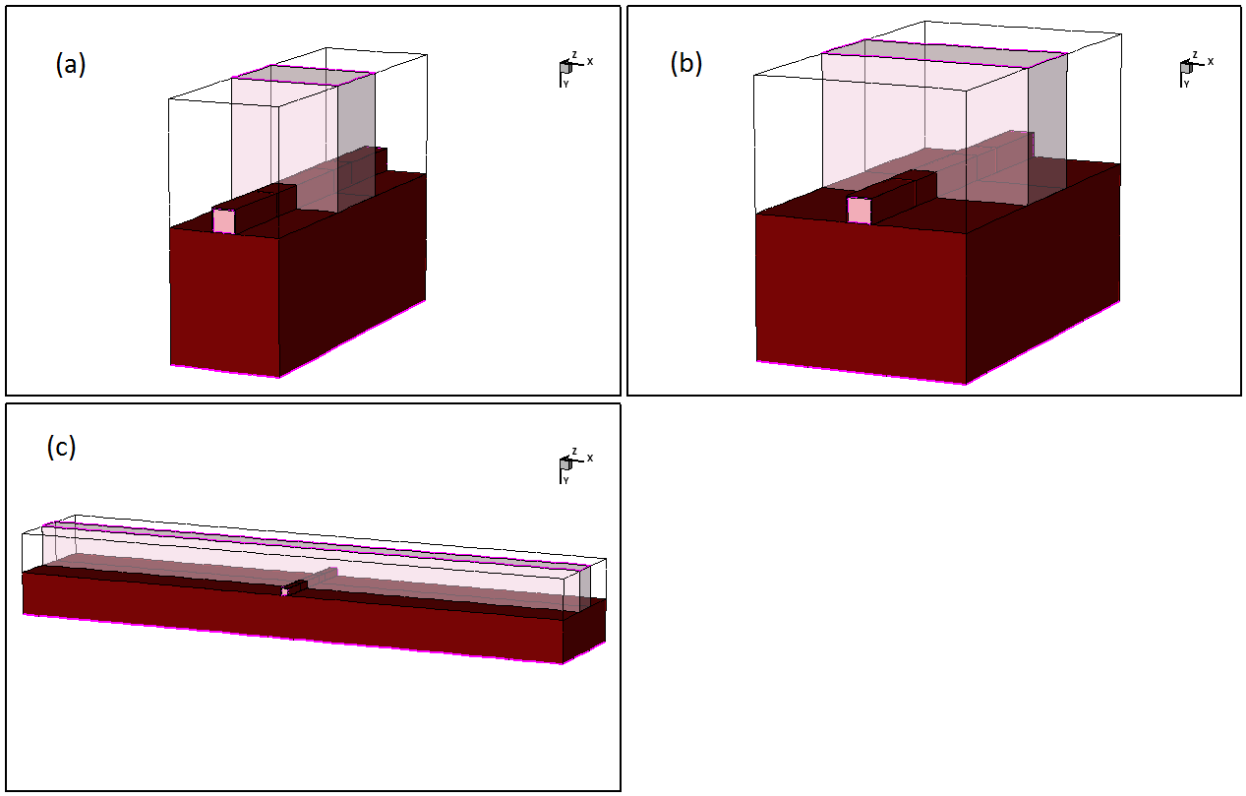


Figure 4.6: The 3D simulation structure, with varying simulation domain. The distance from the nanowire to the edge of the domain is 50 nm, 100 nm, and 1000 nm, for structures (a), (b), and (c), respectively. No other parameter is changed.

increase the value of $C_{\text{par}}$ required to achieve full sensitivity, as predicted by equation 4.6. This choice was made only in order to increase the effect of $C_{\text{par}}$ in the plots that are to be presented for easier viewing.

The results from these simulations are shown in Table 4.1. These results are surprising considering that the nanowires are the same in all cases, but unsurprising considering the analysis given in the previous sections. An argument can be made that when biomolecules are on all oxide surfaces, changing the simulation domain will increase the total amount of biomolecule charge present, and that could cause a change in the sensitivity. We therefore consider the case where the biomolecules are included *only* on the surface of the nanowire itself. Even in that case, increasing the simulation domain increases the sensitivity, which can be explained as an increase in $C_{\text{par}}$, in agreement with the qualitative behavior described in

Table 4.1: Sensitivity as a function of size of simulation domain, for two cases: with biomolecular charges at all oxide/solution interfaces, or only on the gate-oxide/solution interface. The "Structure Size" column refers to the distance between the nanowire and the edge of the simulation domain.

| | Sensitivity to biomolecules | |
|---|---|---|
| Structure Size (nm) | Everywhere | on NW only |
| 50 | $2.29 \times 10^{-2}$ | $7.11 \times 10^{-2}$ |
| 100 | $3.76 \times 10^{-2}$ | $8.35 \times 10^{-2}$ |
| 1000 | $9.78 \times 10^{-2}$ | $3.72 \times 10^{-1}$ |

the previous sections. We do not presently understand why the sensitivity is lower when the biomolecular charges are included at all oxide/solution interfaces. We hypothesize that these extra charges are located along the path of the "return" electric fields, and thus interfere with it. In other words, they require their own return path, which is not provided here. However, this hypothesis requires further study.

These results seem to suggest that $C_{\text{par}}$ is indeed changing by changing the simulation domain. If this is true, one expects that field lines must enter the solution from the buried oxide. The first evidence of this is presented in the form of a 2D plot of the potential change due to the biomolecular charges. This are shown in Fig. 4.7a for the case of biomolecules everywhere, and Fig. 4.7b for the case of biomolecules on the nanowire only. In both figures, it is clearly apparent from the contour lines that the presence of biomolecular charges forces electric fields to enter the solution in areas far from the nanowire itself, albeit the field is stronger in Fig. 4.7a, because there are biomolecules everywhere.

Interestingly, another consequence of the concave corner effect described in the previous

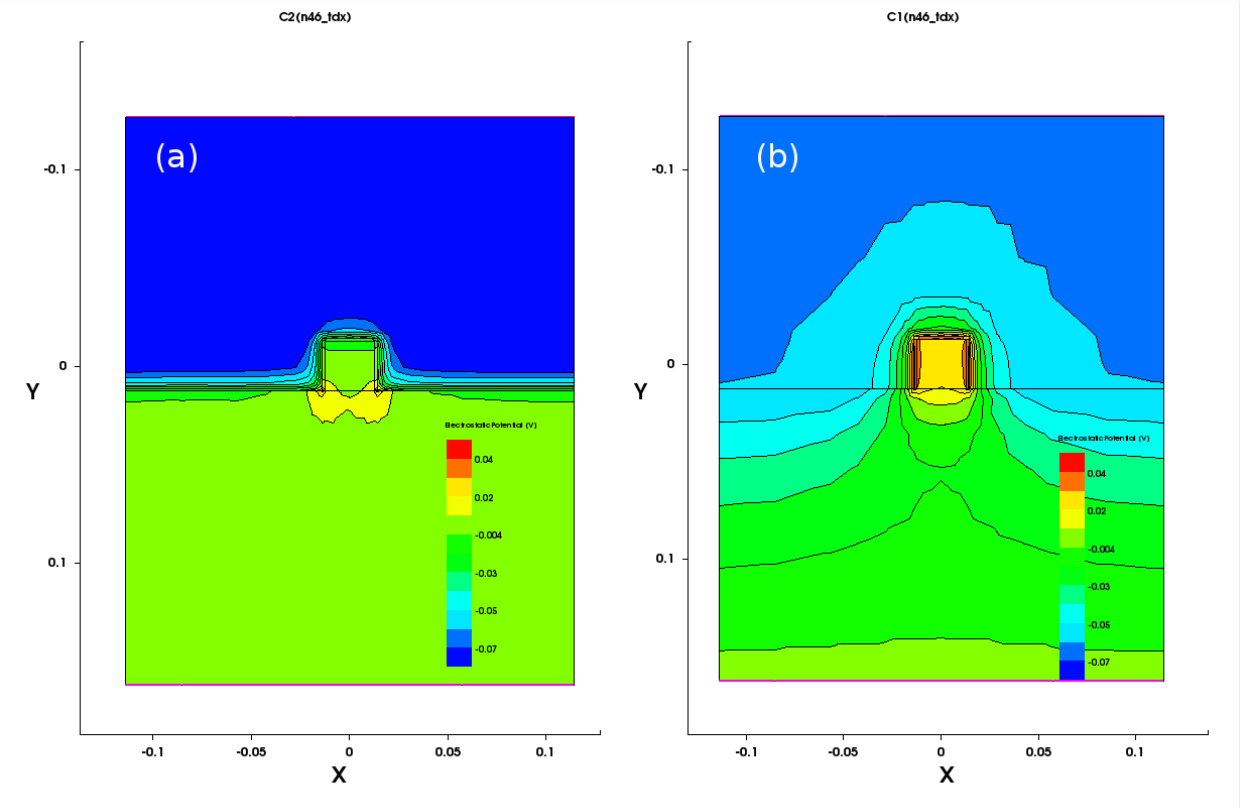


Figure 4.7: 2D plots of potential change due to the presence of biomolecule charge, when (a) biomolecules are captured at all oxide/solution interfacs, and (b) when biomolecules are only captured on the nanowire gate oxide. The 2D cuts are taken at the location of the gray plane in Fig. 4.5. The contour lines show that electric fields enter the solution from the buried oxide for both structures. The interface between the buried oxide and the solution thus provides the return path for the signal, and constitutes part of $C_{\mathrm{par}}$.

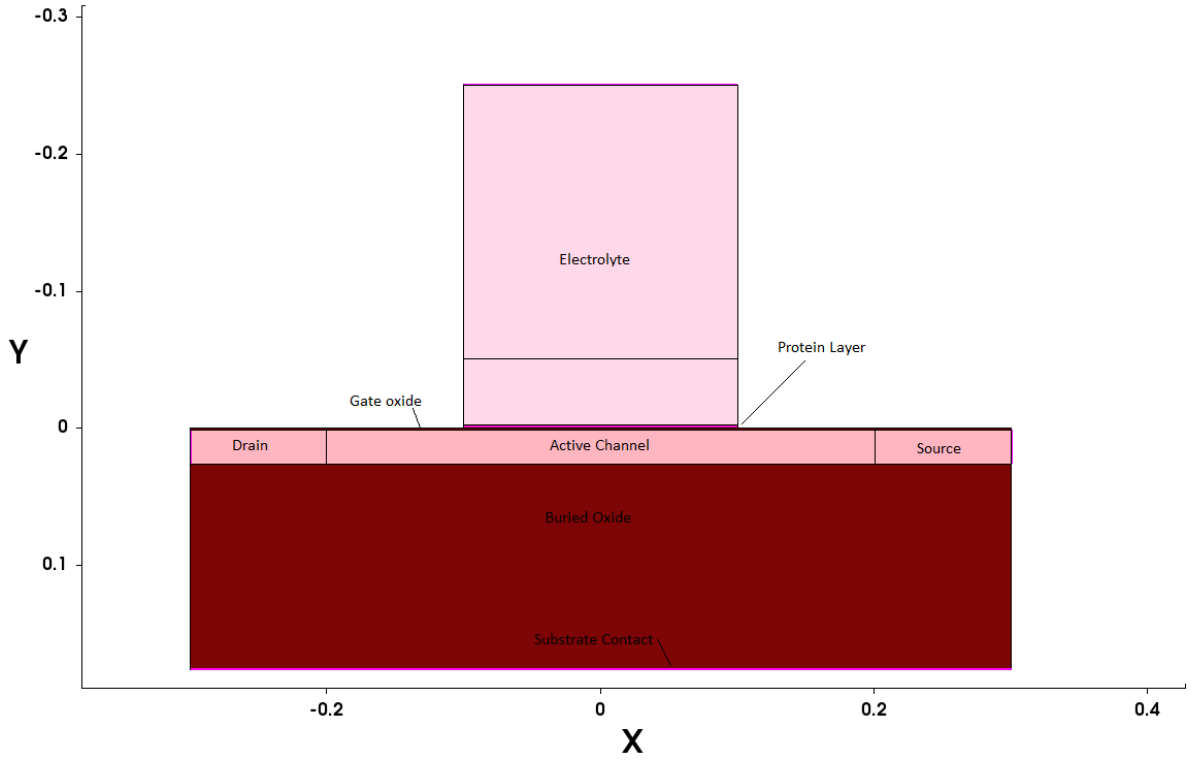


Figure 4.8: The 2D simulation structure. An electrical contact is defined at the very bottom of the structure, under the buried oxide. The encapsulation regions are omitted, which results in the odd shape of the structure.

chapter is visible in Fig. 4.7a: when the biomolecules are everywhere, the potential change at the concave corners become larger than everywhere else, so much so that the fields that enter the nanowire do so only at the corners; at all other locations on the nanowire surface, fields *leave* the nanowire and enter the solution, even though biomolecules are present. This effect is not seen in Fig. 4.7b where the biomolecular charge is only on the sides of the nanowire. Here, electric fields enter the nanowire wherever biomolecules are present, with the exception of the convex corners, where the potential change is weakest.

The results above show that even in the absence of a solution electrode, parasitic capacitive couplings still allow biomolecule detection to take place, which explains the success of experimental works that report biomolecule detection without the use of a solution electrode [CWP01, CWG12].

Due to computational limitations, the structures simulated above had to be kept small. Small structures result in small $C_{\text{par}}$, much smaller than what is encountered in experimental settings.

In order to cover a wider range of $C_{\text{par}}$, we simulated a 2D structure as well. The simulated structure, shown in Fig. 4.8, was effectively a length-wise cross section of the previous 3D simulations, with all the dimensions remaining the same. However, we removed all encapsulation regions from the simulation structure so as to minimize the intrinsic capacitive couplings that contributed to $C_{\text{par}}$ in the previous simulations. In Sentaurus, Neumann (reflective) boundary conditions are assumed for all outer boundaries that are not contacts [se]. This means that no electric field lines can exit the structure, except at the user-defined "contacts" removing the encapsulation regions from the simulation structure ensures that no electric flux exits the structure except at the contacts.

We then took advantage of a capability in Sentaurus to simulate a floating region as if it was coupled to one of the terminals via a capacitance of our choosing, specified in the Sentaurus command file. We used this capability to connect the sample solution to the back-gate with a variable capacitance. Since we minimized other source of intrinsic capacitance, the variable capacitance set by us constituted almost the entirety of $C_{\text{par}}$. We then artificially varied this capacitance (and hence, $C_{\text{par}}$) from 1 aF to 1 nF and extracted sensitivity. Note that since all terminals would be equivalent from a small-signal point of view, it does not matter to which terminal $C_{\text{par}}$ actually connects. These simulations were run with $\sigma = 1 \times 10^{12}\, e\,\text{cm}^{-2}$, in order for the biomolecule's signal to be more like a small-signal disturbance. Due to the varying coupling between the back-gate and the solution, the same back-gate voltage does not produce equivalent electrostatic biasing for all the simulated points. Because of this, the sensitivities were extracted at the bias point that resulted in a bioFET current of 1 nA, putting the bioFETs in the subthreshold regime, and ensuring that the various simulated situations were on equal footing.

For comparison, a 3D nanowire bioFET with dimensions similar to the previous 3D structures was also simulated with its encapsulation regions removed; this structure is shown in Fig. 4.9. Due to the nature of the 3D structure, contact between the solution and the

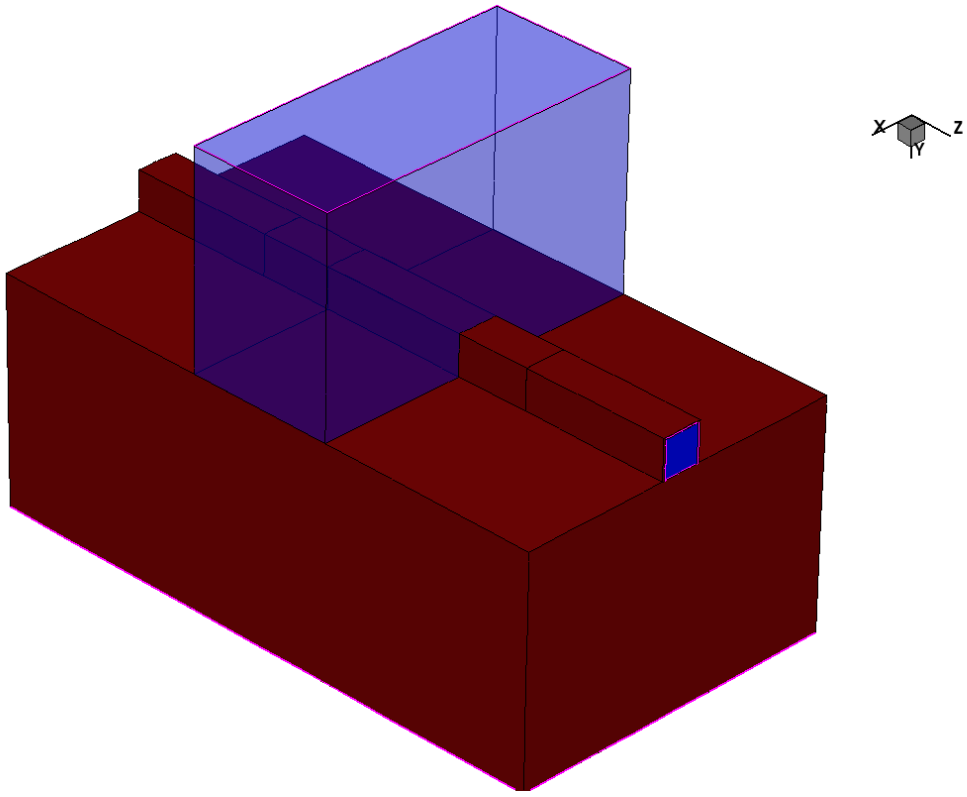


Figure 4.9: The 3D simulation structure without encapsulation regions. The translucent blue regions are the solution, and the maroon regions are oxide. The nanowire itself is seen in opaque blue. An electrical contact is defined at the very bottom of the structure, under the buried oxide. Even though the encapsulation regions are omitted, the solution region is in contact with the buried oxide due to the 3D nature of the simulation, which results in unavoidable coupling.

buried oxide was unavoidable, so despite our efforts, some intrinsic $C_{\text{par}}$ remained, in addition to the explicitly specified capacitance in the simulator's command file. Because of this, the total parasitic capacitance $C_{\text{par}}$ is a bit larger in the 3D cases than in the 2D cases that we have simulated. One can estimate this coupling using the thickness of the buried oxide (145 nm) and the contact area in contact between the solution and the buried oxide (about $9.2 \times 10^4\,\text{nm}^2$); so the extra capacitance is about 20 aF in this simulation, and is therefore negligible for most of the simulated range of $C_{\text{par}}$, which runs from 1 aF to 1 nF.

The simulation results are extracted in the form of a plot of sensitivity vs. the explicitly-

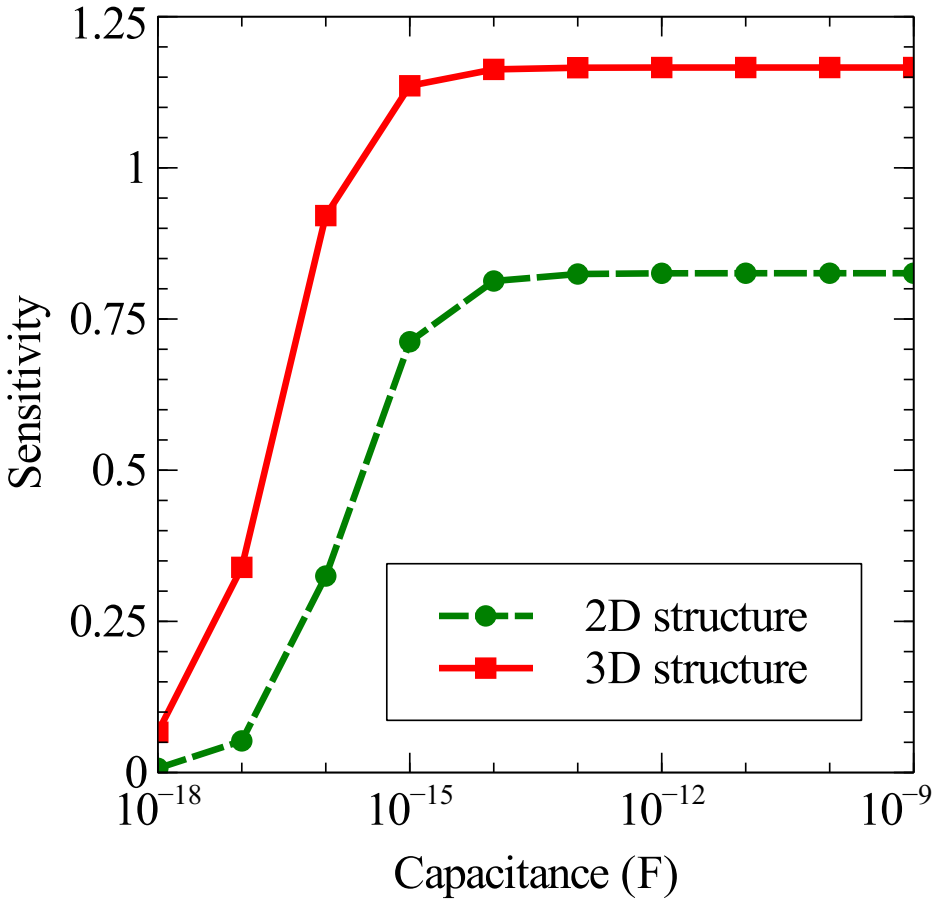


Figure 4.10: Sensitivity, extracted from 2D and 3D simulations, as a function of the capacitive coupling $C_{\text{par}}$ between the solution and the back-gate. Note how sensitivity drops at low $C_{\text{par}}$, and saturates at high $C_{\text{par}}$.

specified capacitive coupling $C_{\text{par}}$, which is shown in Fig. 4.10. The sensitivity is defined as $\Delta I/I$, as usual.

As predicted by equation 4.11, when $C_{\text{par}}$ approaches zero, the sensitivity also approaches zero. As $C_{\text{par}}$ increases, the sensitivity reaches a maximum value, as predicted by equation 4.10.

Another interesting effect can be seen here: the 3D bioFET is more sensitive than the 2D bioFET for all $C_{\text{par}}$. This has nothing to do with $C_{\text{par}}$; it is the result of the corner effect discussed in the previous chapter.

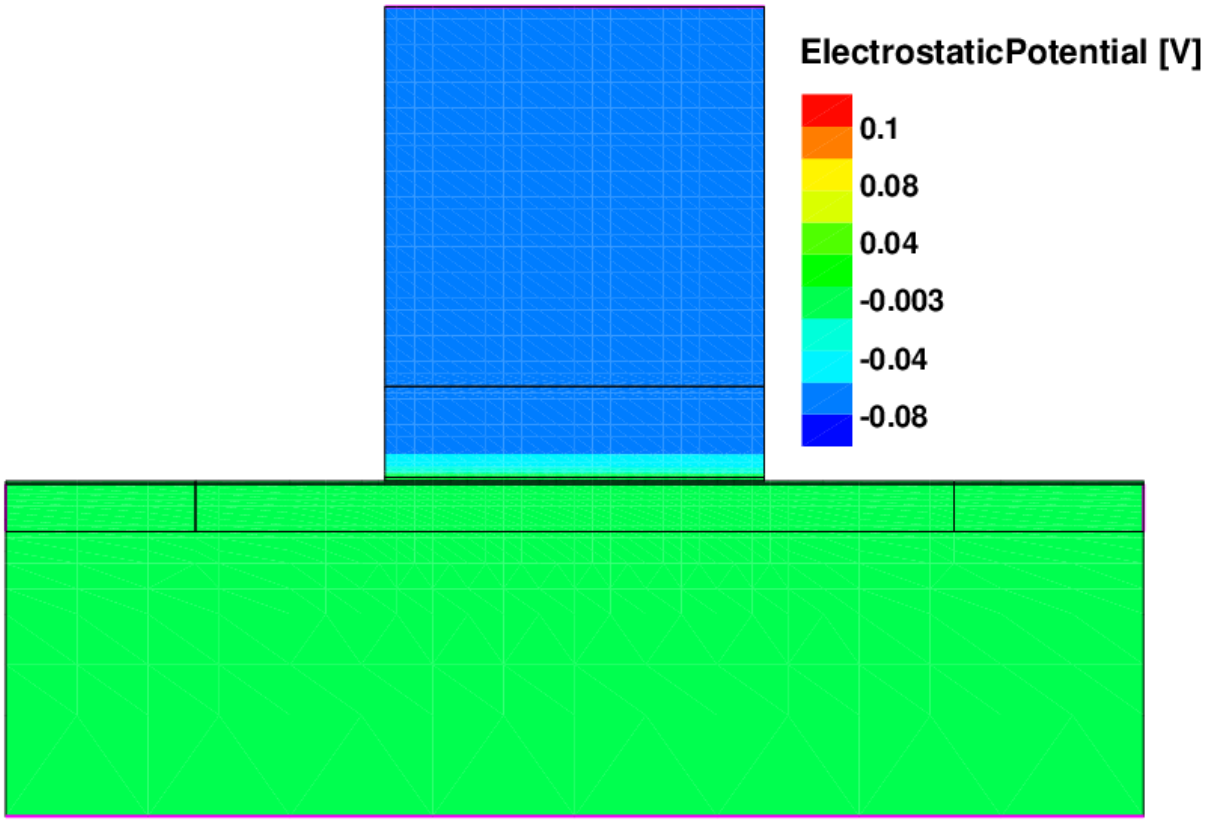


Figure 4.11: 2D color plot of *change* in electrostatic potential as a function of position for when $C_{\text{par}} = 0$. Note how the potential in the solution bulk reduces in response to biomolecular charges that are positive, as well as how the potential in the channel barely changes. The scale bar is the same as in Fig. 4.12.

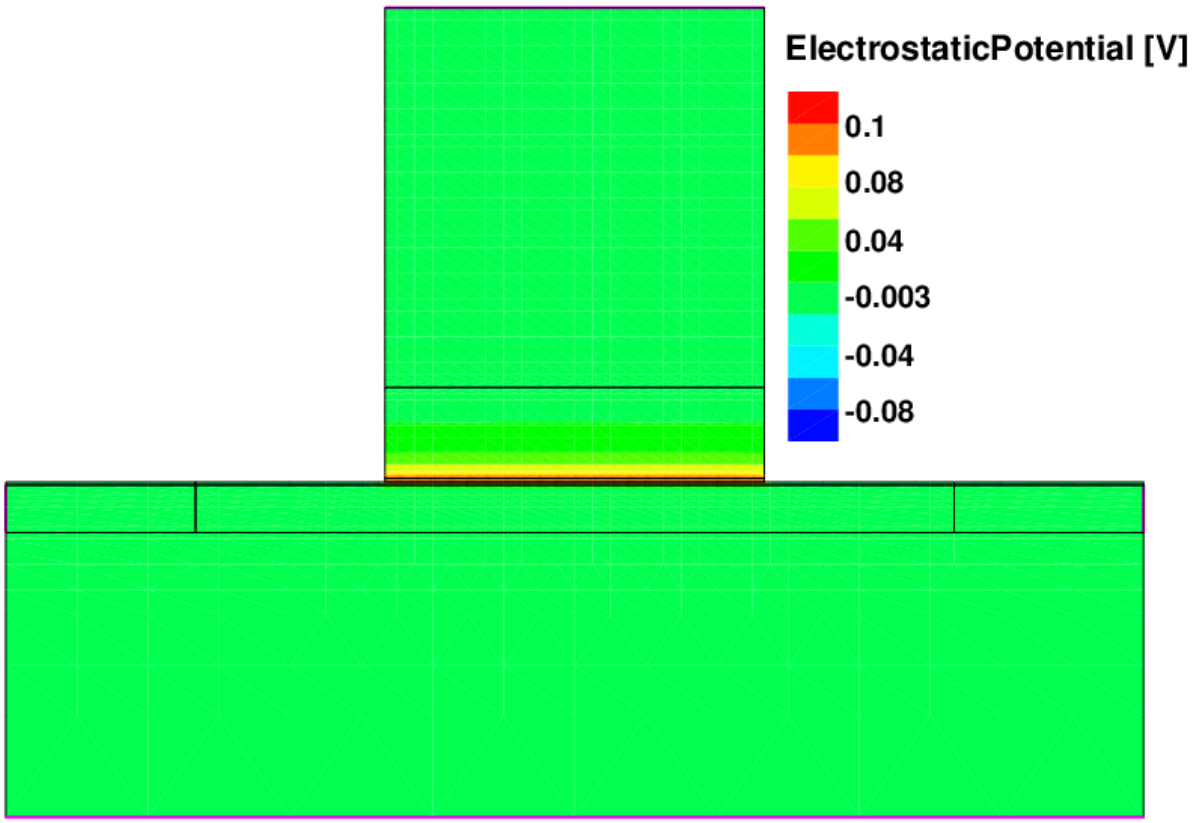


Figure 4.12: 2D color plot of *change* in electrostatic potential as a function of position for when $C_{\text{par}} = 1\text{nF}$. The potential in the bulk of the solution still reduces as a result of the positive biomolecular charges, but negligibly so. The potential change at the position of the biomolecules is a much more pronounced positive value compared to Fig. 4.11. The scale bar is the same between the two figures.

To test the predictions of equation 4.7, we simulated an extra case of $C_{\text{par}} = 0$ using the 2D structure depicted in Fig. 4.8, and extracted the change in electrostatic potential, as a function of position, due to the capture of biomolecules onto the 2D structure. The resulting plot is shown in Fig. 4.11. We repeated the same exercise for $C_{\text{par}} = 1\,\text{nF}$, with results shown in Fig. 4.12. These values were chosen because they result in the maximum and minimum attainable values of $\alpha$ and sensitivity, as is evident from Fig. 4.10.

According to equation 4.8, we expect the potential of the sample solution to always be negative when biomolecular charges are positive. However, the negative change is a finite value described by equation 4.9 negligible when $C_{\text{par}} = 0$, yet is negligible when $C_{\text{par}}$ is large.

The simulations confirm this behavior. In Fig. 4.12, where $C_{\text{par}} = 1\,\text{nF}$, the potential change in the solution bulk is nearly zero, and there is a pronounced peak in the potential change at the location where the biomolecules bind. Conversely, in Fig. 4.11 where $C_{\text{par}}$ is set to zero, the potential change in the solution bulk is a considerable negative value, and no peak is seen at the location of the biomolecules.

The simplest way to interpret this result is to view $\alpha$ as the degree of charge separation in the solution due to the biomolecules. When $\alpha$ is near zero, there is very little charge separation, and the potentials in the system barely change at all.

## 4.4 Conclusion

Based on the reasoning presented herein, we conclude that not including a solution electrode has consequences that are not obvious. The best recommendation is to include a reference electrode, so that the potential of the solution is at equilibrium with that of the electrode, and excess noise from the electrode/electrolyte interface is avoided. However, a reference electrode is prohibitively large for some applications. In those applications, a psuedo-reference electrode can be fabricated on-chip, and can be considered the next best alternative [SZD10]. In the absence of both of these options, a platinum electrode can be used [MJH07], perhaps deposited on-chip in the form of an exposed strip that makes contact with the solution.

It is best if the reference electrode is connected to a voltage source. That way, electromagnetic interferences can be shunted to ground, the bias point of the bioFET will not drift (due to the mechanisms mentioned in this chapter), and the steady-state value of the bias point is well known. Such a setup also provides an ideal return path for the electric flux emanating from the biomolecules. This setup has one drawback: DC current flow through the electrode could cause irreversible surface reactions to occur at the oxide/solution interface of the bioFET, contributing to drift. If this current is kept low, either by careful choice of biasing or by ensuring that the bioFET has a good quality gate insulator, then the reaction rate will also be low, so its effects will not disturb the measurement if its performed quickly.

If one does not wish to directly connect the solution electrode to a voltage source, capacitive coupling can be used. The value of the capacitance should be chosen to ensure that it is significantly larger than the capacitive coupling between the sample solution and the bioFET channel. This coupling can readily be measured in any real-world situation.

The capacitive coupling can also be achieved using a structure similar to a MOSCAP, where one of the capacitor's "plates" is the sample solution.

Finally, one could get away with characterizing the parasitic capacitances and taking steps to ensure that they do not change from one measurement to the next, but this approach does not guarantee that the bioFET will operate at peak sensitivity.

# CHAPTER 5

# Conclusions

## 5.1 New Results of this Work

In this dissertation, we have answered three very important questions regarding bioFET operation.

1. In Chapter 2, we have offered a recipe for biasing of bioFETs that are based on an SOI-structure, i.e., have an active layer that is placed on an insulating substrate. Previous works had studied the biasing of such structures using only a back-gate. However, these structures also have a solution-gate, and the proper biasing using both gates was studied here for the first time. We have included the effect of surface charges in our discussion of biasing.

2. In Chapter 3, we disprove the incorrectly-held idea that surface-area-to-volume ratio is responsible for the enhanced sensitivity seen in nanowire bioFETs. Instead, we show that an alternative explanation exists that is due to the electrostatics of Debye screening in concave and convex regions.

3. In Chapter 4, we discuss the necessity of a solution electrode in bioFET measurements. We show that without such an electrode, parasitic capacitances in the system will affect the response in a way that could cause unpredictable measurement results.

## 5.2 A Few Notes on the Importance of these Results

In Chapter 2, we discussed biasing. It had previously been known that when using a single gate, the bioFET must be biased in the subthreshold regime to maximize its sensitivity. However, in a practical setting with nanowire bioFETs, one has two gates (one is the back-gate, and one is the very necessary solution-gate, as discussed in Chapter 4). With a single gate, an operator could simply sweep the gate voltage and record the current, identify the region of exponential current growth (subthreshold), and bias the bioFET at the highest point in the subthreshold region. But when two gates are present, the defintion of subthreshold is not clear. For example, in an accumulation-mode nanowire bioFET, an operator could mistakenly bias the solution such that the front surface of the bioFET channel is strongly inverted (i.e., turned off), and then sweep the back-gate and bias in the region of exponential current growth. The bioFET will then be depleted at its back interface, and inverted at its front interface. In such a scenario, the sensitivity will actually be minimum (as shown in Chapter 2), because the carriers at the front interface of the channel will screen the rest of the channel from the fields of the biomolecules. The contributions of this author in the first chapter help to avoid such mistakes by clearly stating that the entire channel must be in depletion to optain maximum sensitivity.

With such a recipe, the bias point is clear. However, the biasing affects the Debye screening in the solution, so one must choose whether to bias the FET itself at its optimum point, or bias the system such that Debye screening is minimum. We have discussed and settled this issue: biasing the FET itself is far more important.

However, we showed that one does not necessarily have to forego minimizing the Debye screening as well. We showed that when the right amount of charge is present at the surface of the bioFET, the bias point that optimizes the FET and minimizes Debye screening can be made to coincide.

We have therefore given would-be bioFET designers an extra consideration during design: the amount of surface charge present at the bioFET surface prior to biomolecule capture. This charge could be affected by numerous factors, such as choice of insulator (e.g. $SiO_2$

vs. $Al_2O_3$), or choice of capture probe molecules. There are many molecules that can be used as capture probes. For example, DNA can be captured by both negatively charged DNA molecules, or neutral peptide nuclear acid (PNA) molecules. Of course, surface charge is only one of the many considerations for the choice of capture probe; all others, such as binding kinetics, must be taken into account as well.

There is a subtle piece of insight offered by the results of Chapter 2 that could be quite useful for future researchers. A careful reader would note that the term $k_B T/e$ appears quite a few times in the expressions of sensitivity in Chapter 2. This is a result of the bioFET being a thermionically activated device, and limited to 60mV/decade subthreshold slope. A device that could beat this limit could provide the basis for a more sensitive bioFET. Concurrently with the publication of this author's first paper (which makes up Chapter 2 of this thesis), Sarkar and Banerjee proposed to use a tunneling-field-effect transistor (TFET) for use as a bioFET [SB12]. TFETs are capable of beating the 60mV/decade limit. As such, the results of Chapter 2 support the proposal of Sarkar and Banerjee to make a bioFET using a TFET. It should be noted that the microelectronics industry has been working on TFETs for a long time, with the same goal of beating the 60mV/decade limit. However, TFETs only beat this limit at low drain currents [PCC13], which is a problem for microelectronics, because low drain currents translate to unacceptably slow circuits. In contrast, the response time of bioFETs is limited by biological and chemical aspects of the sensor, and not by the FET itself, so bioFETs could get by with low drain current without problems. TFETs are therefore ideal candidates for use as bioFETs.

In the opinion of this author, Chapter 3 constitutes his most important contribution from an academic point of view. When looking at the entire body of literature, one cannot conclusively accept that nanowire bioFETs are truly orders of magnitude more sensitive than planar bioFETs. Usually, the more experimental data there is in the literature, the more insights can be drawn regarding the topic, but that does not hold true for this question. Many considerations affect the sensitivity of bioFETs, including bias point, choice of capture probes, geometry, inclusion of solution electrode, and more. There are many experimental results reported in the literature, but they vary widely from one another in these respects,

so clear-cut conclusions cannot be drawn. In the absence of clear-cut experimental proof, researchers resort to theoretical results to guide themselves. Unfortunately, the sole theoretical argument on this topic is the surface-area-to-volume ratio argument, which is incorrect, as shown in Chapter 3. By challenging this argument, we hope to prevent future researchers from investing in costly nanowire bioFET structures solely on the basis of this argument.

Additionally, we have shown that an alternative mechanism exists that causes nanowires to become more sensitive than their planar counterparts. This mechanism is the "corner effect", where Debye screening is weaker in concave corners and stronger in convex cornes, so that sensitivity in nanowire bioFETs is dominated by the response of concave corners. We emphasize that this is only one of the many possible mechanisms that make nanowire bioFETs more sensitive; there may be other effects, potentially of more importance, that remain undiscovered. However, understanding this mechanism is still important, because it helps to analyze future simulations results that one could encounter, as did this author in the analysis of Fig. 4.10.

More importantly, however, this author hopes that the knowledge presented in Chapter 3 – that concave regions are good for sensing charge – would be used by future researchers to come up with bioFETs that are more sensitive than nanowires, or at least cheaper to fabricate. For example, a metallic electrode could be used as an extended gate and connected to wide-area FET; the electrode itself could be large, yet contain many nanoscale concave depressions. Debye screening in these depressions would be weaker, so these structures could make superior bioFETs. One could imagine these depressions being fabricated by using anodic aluminum oxide or diblock copolymers as etch masks for photolithography. The fabrication would therefore be easier than that of nanowires, which are typically made using expensive and time-consuming e-beam lithography (in top-down methods).

In Chapter 4, the requirement for a solution electrode is analyzed. We divide the bioFET response into two parts: a large-signal bias, and a small-signal perturbation caused by the biomolecules. We show that in the absence of electrodes, the bias would be unpredictable and could drift. This result isn't very surprising. However, the surprising result is the small-signal response in the absence of a solution electrode. We show that a return path *must*

exist for the fields emanating from the biomolecules, and without such a path, the potential of the solution will go in the opposite direction as what we expect, negating any potential change caused by the biomolecules, and severely reducing sensitivity. Moreover, we show that in the absence of an explicit return path provided by-design, a parasitic return path will have to dominate the response. Due to the unpredictable nature of parasitics, the response of the bioFET could also become unpredictable.

This chapter contains perhaps the most important contribution from a practical standpoint. This author has personally seen many of his colleagues' experiments fail due to lack of reproducibility in repeated measurements of the same sample. These failures cost a lot of time and money, yet the reason behind the failures could not be found. Frustratingly, the failures were intermittent, so the simplest solution was to simply throw away the irreproducible data and try again until the results became reproducible. While this approach does yield correct results, it is far from satisfactory. Moreover, in a commercial setting, one cannot simply throw away bad data, which may (or may not) be the reason why nanowire bioFETs have not been successfully commercialized, despite their 15 year history in research labs worldwide. The insights gained from Chapter 4 show that lack of a solution electrode could very well be one of the results for these failures. Since failures are rarely reported in the literature, this author was not able to use existing data to prove that lack of a solution electrode will result in failure, and had to resort to simulations instead. We hope that future researchers will continue this work experimentally, proving that a solution electrode is necessary for correct bioFET operation, and paving the way for the commercial success of bioFETs.

## 5.3 Future Works

It is the opinion of this author that experimental results in this field have gone beyond firm theoretical foundations, to the point that new experiments are rarely able to answer a question unequivocally, and many experiments produce results that are at odds with one another. For that reason, this thesis has been focused on clearing up some theoretical

concepts, so that experimental works can be more focused and better able to answer long-standing questions. The experiments that this author would like to see performed include the following:

1. An experiment that uses *LLOD* instead of sensitivity to compare the performance of nanowire bioFETs (of various sizes) and bulk bioFETs, *taking care to include a reference electrode.*

2. An experiment to use concave depressions in a sensing surface and see if the LLOD can be improved in accordance with the predictions of Chapter 3 regarding sensing in concave corners.

3. An experiment to displace the solution volume in the vicinity of the bioFET surface, in hopes of limiting the access of ions to the biomolecules, and reducing Debye screening. Such an experiment has recently been performed: by attaching long-chain PEG molecules to the sensor surface, researchers were able to lower the LLOD of their bioFETs, although the mechanism is not clear [GZJ15]. An experiment to determine whether the mechanism is related to displacing the solution volume would be very enlightening indeed.

4. An experiment to see if it is possible to reduce Debye screening by operating the bioFET during a transient following a voltage pulse. After such a pulse, the bioFET will return to equilibrium far faster than the solution environment, meaning that the bioFET can perform the measurement while the solution environment is still in transient. The Poisson Boltzmann equations that govern Debye screening assume equilibrium conditions, and simulations performed by Liu et al. [LSD08] reduce screening by causing current flow in the solution. These suggest that by disturbing the equilibrium in solution, one should be able to reduce Debye screening.

5. A bioFET experiment in which a solution electrode is not used, and the parasitic capacitances are minimized as much as possible. Instead, the sample solution would

be capacitively coupled to a voltage source using increasing values of capacitance in an attempt to experimentally validate the predictions of Chapter 4.

Additionally, a theoretical study is needed to see if bioFETs have any intrinsic limitations, similar to the limitations of ISFETs; ISFETs have a fundamental limitation, called the Nernst limit, that limits their response to 60mV of threshold voltage shift per unit of pH change. It is not clear whether such a limit exists for bioFETs. Most experiments first incubate the sample solution over the bioFET, and then wash it away with a low-ionic-strength buffer solution to make a measurement. In the buffer environment, the biomolecules begin to separate from their capture probes, but this takes a long time due to the high binding affinity of the biomolecules to their capture probes. this means that bioFETs effectively operate in a transient from a chemical point of view. In contrast, ISFETs respond to pH instantly, and the sample solution is not removed, meaning that ISFETs operate in chemical equilibrium. As such, the bioFET may not be subject to a limitation similar to the Nernst limit if the measurement is performed quickly; the meaning of "quickly" should be experimentally determined for each biomolecule capture probe pair.

# References


[AKC12] J.-H. Ahn, J.-Y. Kim, K. Choi, D.-I. Moon, C.-H. Kim, M.-L. Seol, T. J. Park, S. Y. Lee, and Y.-K. Choi. "Nanowire FET Biosensors on a Bulk Silicon Substrate." *IEEE Transactions on Electron Devices*, **59**(8):2243–2249, August 2012.

[Bau85] F. G. K. Baucke. "Glass Science and Technology Problems and Prospects for 2004 The glass electrode applied electrochemistry of glass surfaces." *Journal of Non-Crystalline Solids*, **73**(1):215–231, August 1985.

[Ber70] P. Bergveld. "Development of an Ion-Sensitive Solid-State Device for Neurophysiological Measurements." *IEEE Transactions on Biomedical Engineering*, **BME-17**(1):70–71, January 1970.

[Ber72] Piet Bergveld. "Development, Operation, and Application of the Ion-Sensitive Field-Effect Transistor as a Tool for Electrophysiology." *Biomedical Engineering, IEEE Transactions on*, **BME-19**(5):342–351, 1972.

[Ber03] P. Bergveld. "Thirty years of ISFETOLOGY: What happened in the past 30 years and what may happen in the next 30 years." *Sensors and Actuators B: Chemical*, **88**(1):1–20, January 2003.

[BF01] Allen J. Bard and Larry R. Faulkner. *Electrochemical Methods: Fundamentals and Applications*. Wiley, 2001.

[BR79] P. Bergveld and N. F. de Rooij. "From conventional membrane electrodes to ion-sensitive field-effect transistors." *Medical and Biological Engineering and Computing*, **17**(5):647–654, September 1979.

[BSY06] Yuri L. Bunimovich, Young Shik Shin, Woon-Seok Yeo, Michael Amori, Gabriel Kwong, and James R. Heath. "Quantitative Real-Time Measurements of DNA Hybridization with Alkylated Nonoxidized Silicon Nanowires in Electrolyte Solution." *Journal of the American Chemical Society*, **128**(50):16323–16331, December 2006.

[BTZ03] S. Boussaad, N. J. Tao, R. Zhang, T. Hopson, and L. A. Nagahara. "In situ detection of cytochrome c adsorption with single walled carbon nanotube device." *Chemical Communications*, (13):1502–1503, June 2003.

[CF71] R. W. Cattrall and Henry Freiser. "Coated wire ion-selective electrodes." *Analytical Chemistry*, **43**(13):1905–1906, November 1971.

[CFS11] R.A. Chapman, P.G. Fernandes, O. Seitz, H.J. Stiegler, Huang-Chun Wen, Yves J. Chabal, and Eric M. Vogel. "Comparison of Methods to Bias Fully Depleted SOI-Based MOSFET Nanoribbon pH Sensors." *IEEE Transactions on Electron Devices*, **58**(6):1752–1760, June 2011.

[Col86] J. Colinge. "Subthreshold slope of thin-film SOI MOSFET's." *IEEE Electron Device Letters*, **7**(4):244–246, April 1986.

[CWE06] Yu Chen, Xihua Wang, Shyamsunder Erramilli, Pritiraj Mohanty, and Agnieszka Kalinowski. "Silicon-based nanoelectronic field-effect pH sensor with local gate control." *Applied Physics Letters*, **89**(22):223512, November 2006.

[CWG12] Patricia Casal, Xuejin Wen, Samit Gupta, Theodore Nicholson, Yuji Wang, Andrew Theiss, Bharat Bhushan, Leonard Brillson, Wu Lu, and Stephen C. Lee. "ImmunoFET feasibility in physiological salt environments." *Philosophical Transactions of the Royal Society of London A: Mathematical, Physical and Engineering Sciences*, **370**(1967):2474–2488, May 2012.

[CWP01] Yi Cui, Qingqiao Wei, Hongkun Park, and Charles M. Lieber. "Nanowire Nanosensors for Highly Sensitive and Selective Detection of Biological and Chemical Species." *Science*, **293**(5533):1289–1292, August 2001.

[CXY08] Yi Cheng, P. Xiong, C. Steven Yun, G. F. Strouse, J. P. Zheng, R. S. Yang, and Z. L. Wang. "Mechanism and Optimization of pH Sensing Using SnO2 Nanobelt Field Effect Transistors." *Nano Letters*, **8**(12):4179–4184, December 2008.

[DC09] Edmund J. F. Dickinson and Richard G. Compton. "Diffuse Double Layer at Nanoelectrodes." *The Journal of Physical Chemistry C*, **113**(41):17585–17589, October 2009.

[DD54] A. Distche and M. Dubuisson. "Transient Response of the Glass Electrode to pH Step Variations." *Review of Scientific Instruments*, **25**(9):869–875, September 1954.

[DSR06] M. J. Deen, M. W. Shinwari, J. C. Ranurez, and D. Landheer. "Noise considerations in field-effect biosensors." *Journal of Applied Physics*, **100**(7):074703, October 2006.

[Eis62] George Eisenman. "Cation Selective Glass Electrodes and their Mode of Operation." *Biophysical Journal*, **2**(2, Part 2):259–323, March 1962.

[EJB08] Oguz H. Elibol, Bobby Reddy Jr, and Rashid Bashir. "Nanoscale thickness double-gated field effect silicon sensors for sensitive pH detection in fluid." *Applied Physics Letters*, **92**(19):193904, May 2008.

[EJS07] Niklas Elfström, Robert Juhasz, Ilya Sychugov, Torun Engfeldt, Amelie Eriksson Karlström, and Jan Linnros. "Surface Charge Sensitivity of Silicon Nanowires: Size Dependence." *Nano Letters*, **7**(9):2608–2612, September 2007.

[EKL08] Niklas Elfström, Amelie Eriksson Karlström, and Jan Linnros. "Silicon Nanoribbons for Electrical Detection of Biomolecules." *Nano Letters*, **8**(3):945–949, March 2008.

[FL06] Zhiyong Fan and J.G. Lu. "Chemical sensing with ZnO nanowire field-effect transistor." *IEEE Transactions on Nanotechnology*, **5**(4):393 –396, July 2006.

[Gon10] Jian-Ru Gong. "Label-Free Attomolar Detection of Proteins Using Integrated Nanoelectronic and Electrokinetic Devices." *Small*, **6**(8):967–973, 2010.

[GRN91] G. Ghibaudo, O. Roux, Ch. Nguyen-Duc, F. Balestra, and J. Brini. "Improved Analysis of Low Frequency Noise in Field-Effect MOS Transistors." *Physica Status Solidi (a)*, **124**(2):571–581, April 1991.

[GSK89] Masao Gotoh, Masayasu Suzuki, Izumi Kubo, Eiichi Tamiya, and Isao Karube. "Immuno-FET sensor." *Journal of Molecular Catalysis*, **53**(3):285–292, August 1989.

[GZJ15] Ning Gao, Wei Zhou, Xiaocheng Jiang, Guosong Hong, Tian-Ming Fu, and Charles M. Lieber. "General Strategy for Biodetection in High Ionic Strength Solutions Using Transistor-Based Nanoelectronic Sensors." *Nano Letters*, **15**(3):2143–2148, March 2015.

[GZL10] Xuan P. A. Gao, Gengfeng Zheng, and Charles M. Lieber. "Subthreshold Regime has the Optimal Sensitivity for Nanowire FET Biosensors." *Nano Letters*, **10**(2):547–552, February 2010.

[Hin59] J. a. M. Hinke. "Glass Micro-Electrodes for Measuring Intracellular Activities of Sodium and Potassium." *Nature*, **184**(4694):1257–1258, October 1959.

[HK09] Fritz Haber and Zygmunt Klemensiewicz. "ber elektrische phasengrenzkrfte." *Z. phys. Chem*, **67**:385–431, 1909.

[HL04] Jong-in Hahm and Charles M. Lieber. "Direct Ultrasensitive Electrical Detection of DNA and DNA Sequence Variations Using Nanowire Nanosensors." *Nano Letters*, **4**(1):51–54, January 2004.

[Jac75] John David Jackson. *Classical electrodynamics*. Wiley, New York, 1975.

[Jan75] Jiri Janata. "Immunoelectrode." *Journal of the American Chemical Society*, **97**(10):2914–2916, May 1975.

[JN99] C.G. Jakobson and Y. Nemirovsky. "1/f noise in ion sensitive field effect transistors from subthreshold to saturation." *IEEE Transactions on Electron Devices*, **46**(1):259–261, January 1999.

[JPV10] Christopher B. Jacobs, M. Jennifer Peairs, and B. Jill Venton. "Review: Carbon nanotube based electrochemical sensors for biomolecules." *Analytica Chimica Acta*, **662**(2):105–127, March 2010.

[KCM13] Jee-Yeon Kim, Kyungyong Choi, Dong-Il Moon, Jae-Hyuk Ahn, Tae Jung Park, Sang Yup Lee, and Yang-Kyu Choi. "Surface engineering for enhancement of sensitivity in an underlap-FET biosensor by control of wettability." *Biosensors and Bioelectronics*, **41**:867–870, March 2013.

[LAM05] D. Landheer, G. Aers, W. R. McKinnon, M. J. Deen, and J. C. Ranuarez. "Model for the field effect from layers of biological macromolecules on the gates of metal-oxide-semiconductor transistors." *Journal of Applied Physics*, **98**(4):044701, 2005.

[LHL10] Ming-Pei Lu, Cheng-Yun Hsiao, Wen-Tsan Lai, and Yuh-Shyong Yang. "Probing the sensitivity of nanowire-based biosensors using liquid-gating." *Nanotechnology*, **21**(42):425505, 2010.

[LNS09] Kangho Lee, Pradeep R. Nair, Adina Scott, Muhammad A. Alam, and David B. Janes. "Device considerations for development of conductance-based biosensors." *Journal of Applied Physics*, **105**(10):102046, May 2009.

[LSD08] Yang Liu, Jon Sauer, and Robert W. Dutton. "Effect of electrodiffusion current flow on electrostatic screening in aqueous pores." *Journal of Applied Physics*, **103**(8):084701, 2008.

[LZT11] Jason Li, Yanliang Zhang, Steve To, Lidan You, and Yu Sun. "Effect of Nanowire Number, Diameter, and Doping Density on Nano-FET Biosensor Sensitivity." *ACS Nano*, **5**(8):6661–6668, August 2011.

[McL77] Stuart McLaughlin. "Electrostatic Potentials at Membrane-Solution Interfaces." In Felix Bronner and Arnort Kleinzeller, editor, *Current Topics in Membranes and Transport*, volume 9, pp. 71–144. Academic Press, 1977.

[MJH07] Ethan D. Minot, Anne M. Janssens, Iddo Heller, Hendrik A. Heering, Cees Dekker, and Serge G. Lemay. "Carbon nanotube biosensors: The critical role of the reference electrode." *Applied Physics Letters*, **91**(9):093507, 2007.

[NA07] Pradeep R. Nair and Muhammad A. Alam. "Design Considerations of Silicon Nanowire Biosensors." *IEEE Transactions on Electron Devices*, **54**(12):3400–3408, 2007.

[NJK09] Miloslav Ni, Ji Jirt, Bedich Koata, Aubrey Jenkins, and Alan McNaught, editors. *IUPAC Compendium of Chemical Terminology: Gold Book*. IUPAC, Research Triagle Park, NC, 2.1.0 edition, June 2009.

[PCC13] A. Pan, Songtao Chen, and Chi On Chui. "Electrostatic Modeling and Insights Regarding Multigate Lateral Tunneling Transistors." *IEEE Transactions on Electron Devices*, **60**(9):2712–2720, September 2013.

[PCI05] A. Poghossian, A. Cherstvy, S. Ingebrandt, A. Offenhusser, and M.J. Schöning. "Possibilities and limitations of label-free detection of DNA hybridization with field-effect-based devices." *Sensors and Actuators B: Chemical*, **111-112**:470–480, November 2005.

[PLP07] Inkyu Park, Zhiyong Li, Albert P. Pisano, and R. Stanley Williams. "Selective Surface Functionalization of Silicon Nanowires via Nanoscale Joule Heating." *Nano Letters*, **7**(10):3106–3111, October 2007.

[PLP10] Inkyu Park, Zhiyong Li, Albert P. Pisano, and R. Stanley Williams. "Top-down fabricated silicon nanowire sensors for real-time chemical detection." *Nanotechnology*, **21**(1):015501, 2010.

[PT70] Ernö Pungor and Klra Tth. "Ion-selective membrane electrodes. A review." *Analyst*, **95**(1132):625–648, January 1970.

[RBR12] Joseph E. Reiner, Arvind Balijepalli, Joseph W. F. Robertson, Jason Campbell, John Suehle, and John J. Kasianowicz. "Disease Detection and Management via Single Nanopore-Based Sensors." *Chemical Reviews*, **112**(12):6431–6451, December 2012.

[RHR11] Jonathan M. Rothberg, Wolfgang Hinz, Todd M. Rearick, Jonathan Schultz, William Mileski, Mel Davey, John H. Leamon, Kim Johnson, Mark J. Milgrew, Matthew Edwards, Jeremy Hoon, Jan F. Simons, David Marran, Jason W. Myers, John F. Davidson, Annika Branting, John R. Nobile, Bernard P. Puc, David Light, Travis A. Clark, Martin Huber, Jeffrey T. Branciforte, Isaac B. Stoner, Simon E. Cawley, Michael Lyons, Yutao Fu, Nils Homer, Marina Sedova, Xin Miao, Brian Reed, Jeffrey Sabina, Erika Feierstein, Michelle Schorn, Mohammad Alanjary, Eileen Dimalanta, Devin Dressman, Rachel Kasinskas, Tanya Sokolsky, Jacqueline A. Fidanza, Eugeni Namsaraev, Kevin J. McKernan, Alan Williams, G. Thomas Roth, and James Bustillo. "An integrated semiconductor device enabling non-optical genome sequencing." *Nature*, **475**(7356):348–352, July 2011.

[SB12] Deblina Sarkar and Kaustav Banerjee. "Proposal for tunnel-field-effect-transistor as ultra-sensitive and label-free biosensors." *Applied Physics Letters*, **100**(14):143108, April 2012.

[SBK90] R.B.M. Schasfoort, P. Bergveld, R.P.H. Kooyman, and J. Greve. "Possibilities and limitations of direct detection of protein charges by means of an immunological field-effect transistor." *Analytica Chimica Acta*, **238**:323–329, January 1990.

[SC12] K. Shoorideh and Chi On Chui. "Optimization of the Sensitivity of FET-Based Biosensors via Biasing and Surface Charge Engineering." *IEEE Transactions on Electron Devices*, **59**(11):3104–3110, 2012.

[SC14] Kaveh Shoorideh and Chi On Chui. "On the origin of enhanced sensitivity in nanoscale FET-based biosensors." *Proceedings of the National Academy of Sciences*, **111**(14):5111–5116, April 2014.

[Sch10] Fritz Scholz. "Nikolskys ion exchange theory versus Bauckes dissociation mechanism of the glass electrode." *Journal of Solid State Electrochemistry*, **15**(1):67–68, August 2010.

[se] "Synopsys' Sentaurus Device vG-2012.06.".

[SKR07] Eric Stern, James F. Klemic, David A. Routenberg, Pauline N. Wyrembak, Daniel B. Turner-Evans, Andrew D. Hamilton, David A. LaVan, Tarek M. Fahmy,

and Mark A. Reed. "Label-free immunodetection with CMOS-compatible semiconducting nanowires." *Nature*, **445**(7127):519–522, February 2007.

[sLC83] J. van der spiegel, I. Lauks, P. Chan, and D. Babic. "The extended gate chemically sensitive field effect transistor as multi-species microprobe." *Sensors and Actuators*, **4**:291–298, 1983.

[SMB07] Martin Hedegrd Sørensen, Niels Asger Mortensen, and Mads Brandbyge. "Screening model for nanowire surface-charge sensors in liquid." *Applied Physics Letters*, **91**(10):102105, September 2007.

[SV99] James R. Sandifer and Jacob J. Voycheck. "A Review of Biosensor and Industrial Applications of pH-ISFETs and an Evaluation of Honeywells DuraFET." *Microchimica Acta*, **131**(1-2):91–98, June 1999.

[SWS07] Eric Stern, Robin Wagner, Fred J. Sigworth, Ronald Breaker, Tarek M. Fahmy, and Mark A. Reed. "Importance of the Debye Screening Length on Nanowire Field Effect Transistor Sensors." *Nano Letters*, **7**(11):3405–3409, November 2007.

[SZD10] M. Waleed Shinwari, David Zhitomirsky, Imran A. Deen, P. R. Selvaganapathy, M. Jamal Deen, and D. Landheer. "Microfabricated Reference Electrodes and their Biosensing Applications." *Sensors*, **10**(3):1679–1715, March 2010.

[TS91] K. Tokunaga and J.C. Sturm. "Substrate bias dependence of subthreshold slopes in fully depleted silicon-on-insulator MOSFET's." *IEEE Transactions on Electron Devices*, **38**(8):1803–1807, August 1991.

[TV80] G. M. Torrie and J. P. Valleau. "Electrical double layers. I. Monte Carlo study of a uniformly charged surface." *The Journal of Chemical Physics*, **73**(11):5807–5816, December 1980.

[VKM11] Oshri Vaknin, Bassam Khamaisi, Mordechay Mizrahi, and Nurit Ashkenasy. "Controlling Field-Effect Transistor Biosensor Electrical Characteristics Using Immunosorbent Assay." *Electroanalysis*, **23**(10):2327–2334, 2011.

[VSI11] Luca De Vico, Martin H. Sørensen, Lars Iversen, David M. Rogers, Brian S. Sørensen, Mads Brandbyge, Jesper Nygrd, Karen L. Martinez, and Jan H. Jensen. "Quantifying signal changes in nano-wire based biosensors." *Nanoscale*, **3**(2):706–717, February 2011.

[Wan06] Joseph Wang. "Electrochemical biosensors: Towards point-of-care cancer diagnostics." *Biosensors and Bioelectronics*, **21**(10):1887–1892, April 2006.

[WP11] Hainan Wang and Laurent Pilon. "Accurate Simulations of Electric Double Layer Capacitance of Ultramicroelectrodes." *The Journal of Physical Chemistry C*, **115**(33):16711–16719, August 2011.

[YAY10] S.K. Yoo, J.Y. An, S. Yang, and J.H. Lee. "Subthreshold operation of Schottky barrier silicon nanowire FET for highly sensitive pH sensing." *Electronics Letters*, **46**(21):1450–1452, October 2010.

[YLH74] David E. Yates, Samuel Levine, and Thomas W. Healy. "Site-binding model of the electrical double layer at the oxide/water interface." *Journal of the Chemical Society, Faraday Transactions 1: Physical Chemistry in Condensed Phases*, **70**(0):1807–1818, January 1974.